Shallow magmatic recharge in an intraplate volcanic complex, Akaroa, Banks Peninsula, New Zealand

A Senior Thesis presented to
The Faculty of the Department of Geology

Bachelor of Arts

Emily Beckham
The Colorado College
May 2016

i

Table of Contents

List of Figures

List of Tables

Abstract

Lava flows of the intraplate Miocene Akaroa Volcanic Complex (AVC), Banks Peninsula, New Zealand, display a cyclical geochemical trend from picrite to benmoreite. When observed within a single stratigraphic section, flows reveal repeating patterns, or batches, of primitive to evolved magmas. Primitive flows are generally porphyritic, while the more evolved flows are consistently aphyric. Previous studies have led to a model for the AVC in which a deep reservoir (lithospheric detachment sourced) fed and replenished multiple shallow magma chambers, which then fractionated individually to produce several independently evolving magma batches. The purpose of this research is to test that model and extend it spatially across the eastern flanks of the AVC, as well as to characterize magma chamber dynamics using geochemistry and petrography.

Sixty-nine samples were taken from six stratigraphically controlled transects across the eastern AVC for XRF analysis. Based on rock type and composition, samples were separated into individual batches within their respective transects. Distinct geochemical variations were observed in samples ranging from 43-59 wt. % SiO_2, 0.5-7 wt. % MgO, 1-4 wt. % TiO_2, and 0-270ppm V. The distinction between batches were drawn where element concentrations varied significantly within stratigraphy, further supported by petrographic distinctions (plagioclase resorbtion and sieved cores, and skeletal textures). Eleven of the sixty-nine original samples were selected for microprobe analysis of individual plagioclase, clinopyroxene, and olivine crystals. Anorthite composition in plagioclase ranged from 0.15-0.77, with both reverse and normal zoning patterns observed from core to rim.

By correlating the crystallinity and textures of each flow with the bulk-rock geochemistry, this study argues that the shallow magma chambers underlying the AVC experienced cycles of magma evolution punctuated by magmatic recharge from depth. As each batch evolved, the hawaiite, benmoreite, and mugearite flows would experience crystal separation in the chamber forming a crystal mush while the residual liquid erupted aphyrically. The more primitive picrite flows, however, erupted with their phenocrysts without experiencing crystal separation, resulting in the initial, most primitive flow(s) of each cycle containing the greatest degree of crystallinity. Reverse zoning patterns coupled with resorbtion and sieve textures in the plagioclase phenocrysts within the picrite flows suggest that either the erupted flow experienced several recharge events prior to eruption, or incorporated pieces of the previous batch's crystal mush. As such, the phenocrysts contained within the picrite flows record complex geochemical process occurring in the shallow magma chambers below the AVC.

Chapter I: Introduction

Banks Peninsula, New Zealand, sits on the east coast of New Zealand's South Island. The peninsula is composed of two Miocene volcanic complexes: Lyttelton and Akaroa. These volcanic systems formed from intraplate volcanism associated with lithospheric detachment that caused asthenosphere upwelling (Timm et al., 2009). The Akaroa Volcanic Complex comprises several vents and related flows on the eastern portion of the peninsula. Recent studies (Johnson 2012, Crystal 2013, and Patel 2013) suggest that the Akaroa Volcanic Complex was supported by a main deep reservoir that fed and replenished multiple shallow magma chambers; these shallow chambers could then have fractionated individually to produce several independently evolving magma batches. This study tests this multiple shallow magma chamber model across six bays in the eastern sector of the volcanic complex, and investigates magma dynamics in the shallow chambers.

This project builds upon past fieldwork conducted by undergraduate students in Frontiers Abroad field camps. These field camps have established a large geochemical and petrographic database, however very little work has been done analyzing this database. As such, this study utilizes the available data, while also conducting additional fieldwork to add to the dataset. By correlating the geochemistry and petrography of consecutive flows within six individual stratigraphic sections, this project tests the nature of the interaction between rejuvenation events and shallow magma chamber dynamics.

New Zealand is one of the most tectonically active countries in the world, yet little is known about the volcanism that formed the Akaroa Volcanic Complex. Moreover, Akaroa has only recently been the topic of detailed geochemical and

petrographic study, therefore there is still much work to be done. This study tests the previously developed hypotheses about the magma chambers by specifically correlating the geochemistry and petrography. These correlations provide insight into magma origin, pre-eruptive magmatic processes and dynamics, and intraplate volcanics.

Chapter II: Background

Brief Overview of the New Zealand Geology

New Zealand comprises a North and South Island in the South Pacific Ocean. During the Early Cretaceous, these islands formed the microcontinent, Zealandia, which was located on the eastern margin of Gondwana. During this time, the Pacific Plate was subducting to the west under Gondwana's east coast in a compressive stress regime. This subduction metamorphosed the shallow marine sediment along Gondwana's coast, thus creating Zealandia's bedrock, the Torlesse greywacke. At ~100Ma, the tectonic regime switched from compression to extension, and around 84Ma, Zealandia started to break off from Gondwana. The subsequent northeastern land drift, caused by rifting, opened the Tasman Sea (**Figure 2.1**). The following aggradation of land in Zealandia due to compressional uplift and volcanism placed the microcontinent in the middle of the South Pacific Ocean (Sutherland,1999, Timm et al., 2009).

Currently, 90% of Zealandia is submerged (**Figure 2.2**) (Timm et al., 2010). The two islands of New Zealand sit on the edge of the Australian Plate and the Pacific Plate. Off the southern coast of the South Island, the Australian Plate is subducting under the Pacific Plate. Just off the east coast of the North Island, the Pacific Plate is subducting under the Australian Plate (**Figure 2.3**). As such, the South Island rests in between the two oppositely directed subduction zones and is split by the Alpine Fault, an oblique strike-slip fault. The South Island contains a record of the separation from Gondwana with exposures of the metamorphic core complex on the west coast transitioning into bedrock of the Torlesse Supergroup, which underlies the entire island.

The North Island is dominated by subduction-generated volcanism (such as the

130 million years ago

Uplifted plain

GONDWANA

LITHOSPHERE

ASTHENOSPHERE Magma

100 million years ago

Rift valley

← Faults →

80 million years ago

Narrow sea

Sediment

AUSTRALIA ←

→ ZEALANDIA

Mid-ocean ridge

present

Australian Alps

TASMAN SEA

AUSTRALIA

Oceanic lithosphere   Extinct mid-ocean ridge   Submerged continent
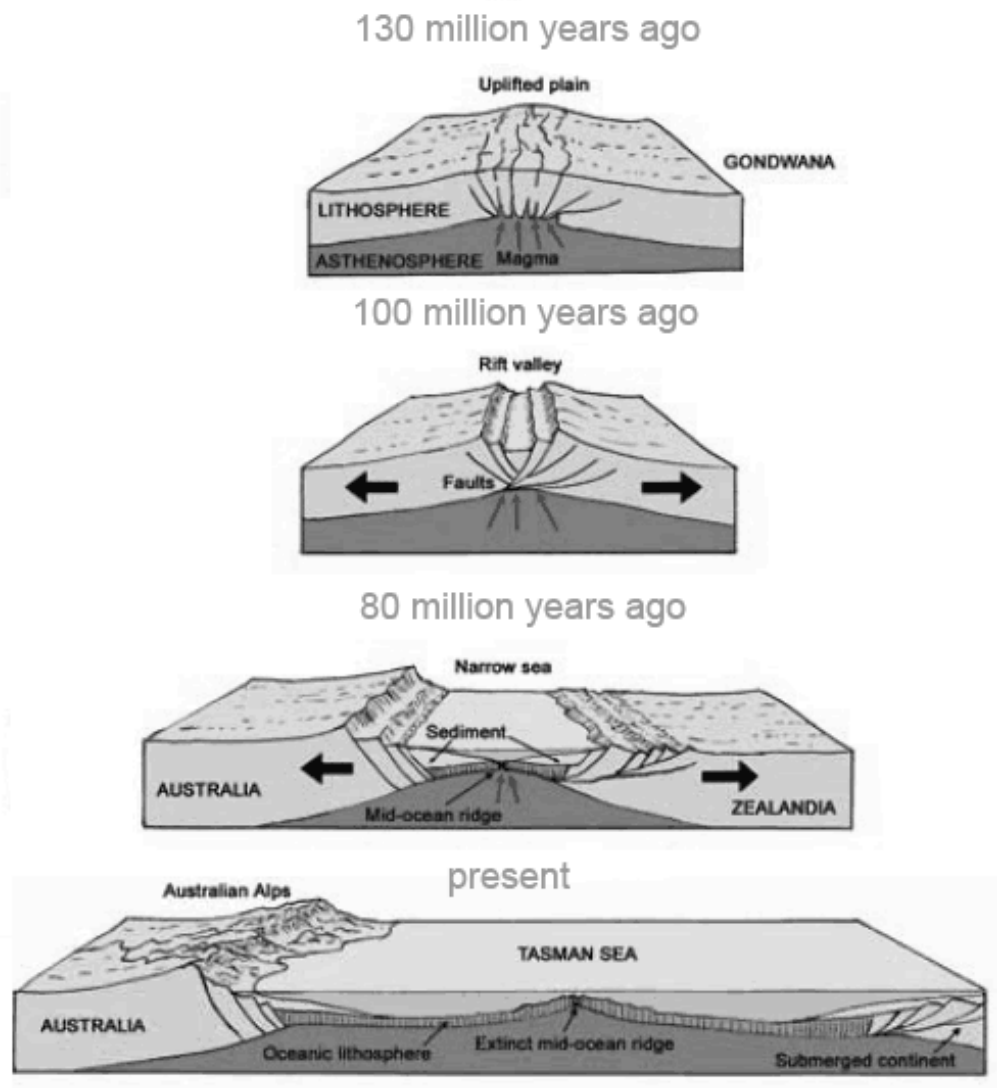
Figure 2.1: Schematic representation of the separation of Zealandia from Gondwana and the opening of the Tasman Sea (Geology, 2013).
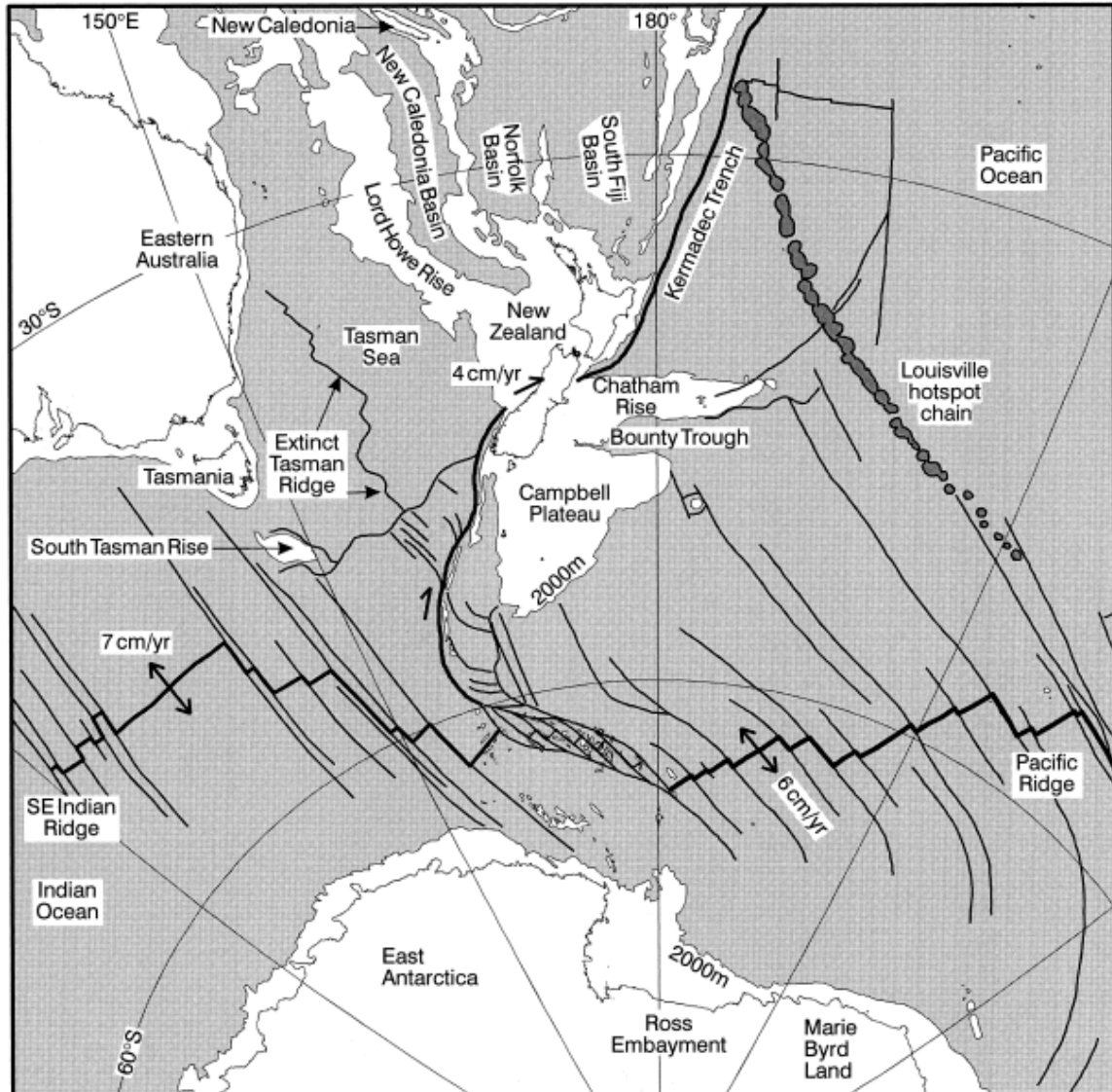
Figure 2.2: Figure depicting the tectonic setting of New Zealand, Australia, and Eastern Antarctica. The white area around New Zealand (Lord Howe Rise, Chatham Rise, and Campbell Plateau) represents the submerged continental crust of Zealandia. The line between the white and grey areas off the coast of New Zealand represents 2000m of water depth (Sutherland, 1999).
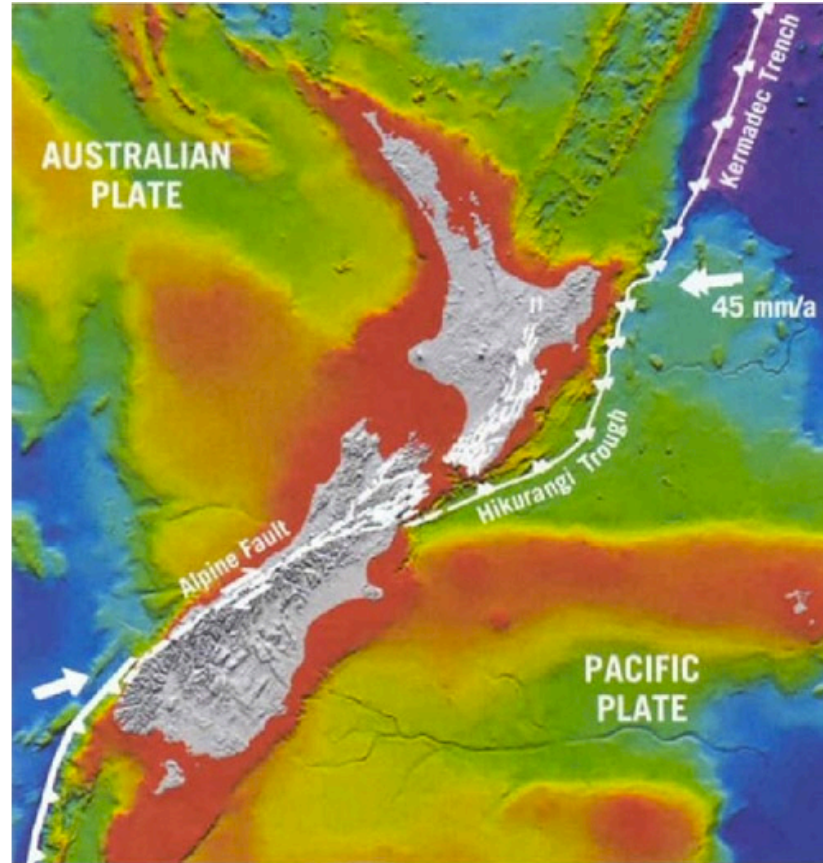
Figure 2.3: Map of the plate boundaries and their relation to New Zealand. Notice the subduction of the Pacific plate in the North and the Australian Plate in the South, separated by the Alpine Fault on the South Island. The warm colors surrounding the grey New Zealand mainland represent higher topography, thus show the submerged Zealandia continental crust (Davies and McSaveny, 2007).

Taupo Volcanic Zone and the Auckland Volcanic Field) from the Pacific plate

subducting under the Australian plate, while Cenozoic intraplate volcanism is the primary

volcanic expression on the South Island (**Figure 2.4**) (Hoernle et al., 2006, Timm et al.,

2009, Timm et al., 2010). Intraplate volcanism is defined by melt generation that is

unrelated to plate boundaries—the volcanism occurs within the plate.

In New Zealand, intraplate volcanism expresses itself in the form of monogenetic

fields and large volcanic centers (Hoernle et al., 2006, Timm et al., 2009, Timm et al.,

2010). New Zealand's location at the Australian and Pacific plate boundaries place the

intraplate volcanism near plate margins. However, the volcanism of the South Island is

unrelated to the nearby plate convergence (Hoernle et al., 2006, Timm et al., 2009). Large

volcanic centers, such as the Dunedin Volcano (active 16-10Ma) in Otago, and the

Lyttelton and Akaroa Volcanic Complexes (active 12-5Ma) in Canterbury, are the most

prominent volcanic features on the South Island (Hoernle et al., 2006). The latter two

complexes are located on Banks Peninsula (**Figure 2.5**), and represent the final stages of

the South Island's Cenozoic volcanism (Timm et al., 2009).

Traditionally, mantle plumes were thought to be the main cause of intraplate

volcanism (Hoernle et al., 2006). Timm et al. (2009, 2010), however, postulate that due

to the low silica and high trace element concentrations, coupled with a lack of volcanism

lining up with plate migration around Banks Peninsula, the Lyttelton and Akaroa

Volcanic Complexes were formed from two successive lithospheric detachment events

(**Figure 2.6**). Hoernle et al. (2006) hypothesize that these detachment events could have

been caused by an increase in density of the deepest portions of the lithosphere (relative

to the asthenosphere) due to the exposure and enrichment of Zealandia's lower
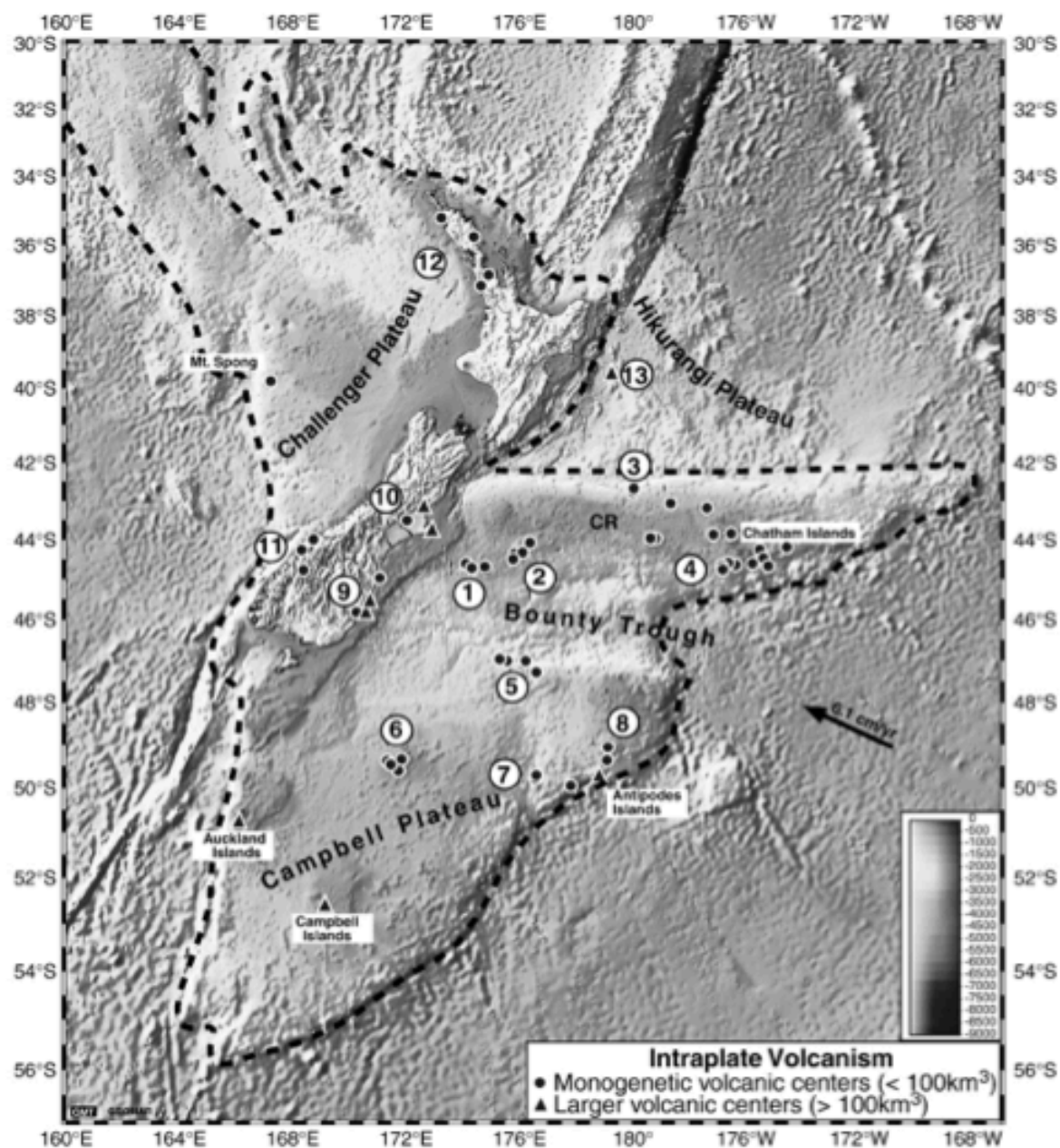
Figure 2.4: Figure depicting the various locations of Cenozoic intraplate volcanism (Timm et al., 2010). Numbers one through eleven are sampling locations of Timm et al. (2010).
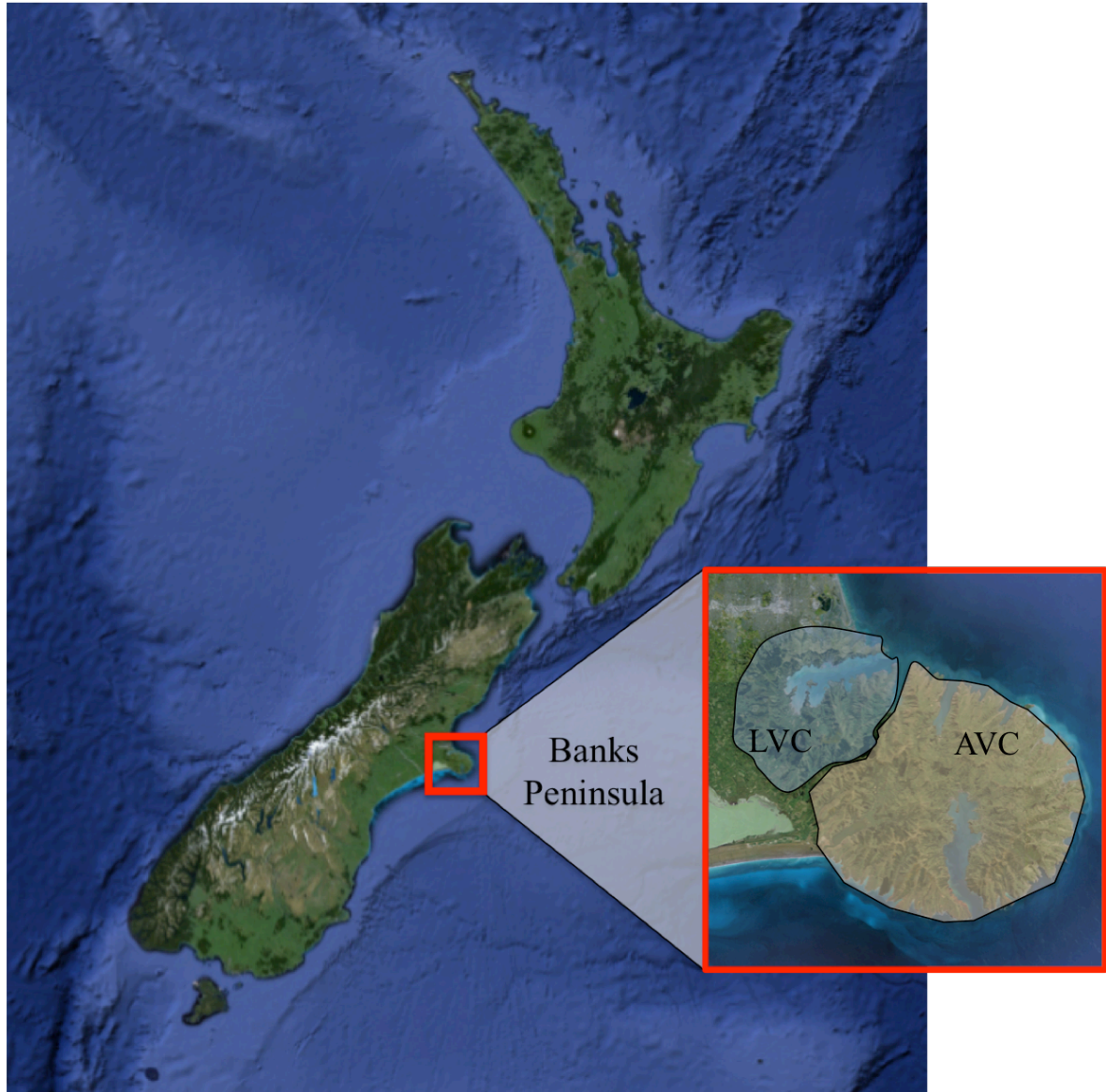
Figure 2.5: Satellite image and location of Banks Peninsula on the east coast of the South Island. The two harbors on Banks Peninsula are the volcanic centers of the Lyttelton and Akaroa volcanic complexes. The Lyttelton Volcanic Complex (LVC) is shaded in blue, and the Akaroa Volcanic Complex (AVC) is shaded in orange. Satellite images provided by Google Earth Pro (2015).
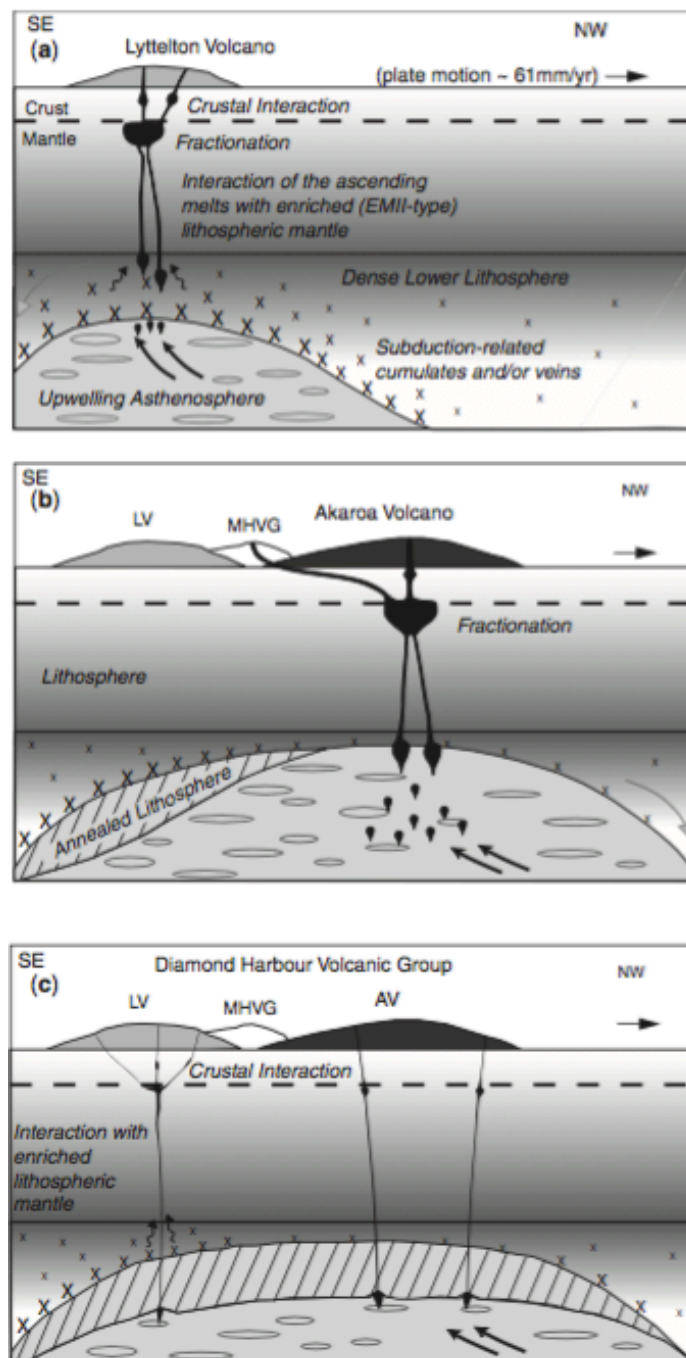
Figure 2.6: Schematic of the two lithospheric detachment events causing asthenospheric upwelling and the formation of the Lyttelton and Akaroa volcanic complexes. Notice the larger scale of the second detachment event forming the Akaroa Volcanic Complex (Timm et al., 2009).

lithosphere to the subduction-related fluids while it was still a part of Gondwana during the Mesozoic. This model assumes that the lower lithosphere was the only area affected with increased density due to enrichment from subduction-related fluids, and furthermore that it did not detach until the Miocene. If this model is accurate, then the density difference between the enriched lower lithosphere and the asthenosphere would have formed an unstable layer in the lithosphere, causing a detachment along Rayleigh-Taylor instabilities. This detachment would have occurred when the lower lithosphere exceeded the density of the underlying asthenosphere, thus causing instability and detachment of the more-dense lower lithosphere. Following the detachment, the asthenosphere would partially melt due to decompression and rise, and therefore produce the mafic rocks seen on Banks Peninsula (Hoernle et al., 2006).

The Geologic Setting of Banks Peninsula

Banks Peninsula sits on the eastern coast of the South Island, and is composed of five different volcanic groups: Pre-Lyttelton Volcanics, Lyttelton Volcano, Mt Herbert Volcanic Group, The Akaroa Volcanic Complex, and the Diamond Harbor Volcanic Group (**Figure 2.7**). These volcanic groups express themselves through features such as scoria cones, trachyte domes, lava flows, ash beds, dikes, and sills (Hampton and Cole, 2009). Volcaniclastic and lahar flows are also common features on the peninsula.

During the active phases of volcanism, the peninsula was a volcanic island separated from the mainland. The sea between the volcanic island and the mainland was subsequently filled in by the erosion of the rising Southern Alps, creating the Canterbury region of which Banks Peninsula is a part. Sewell et al. (1992) mapped the general
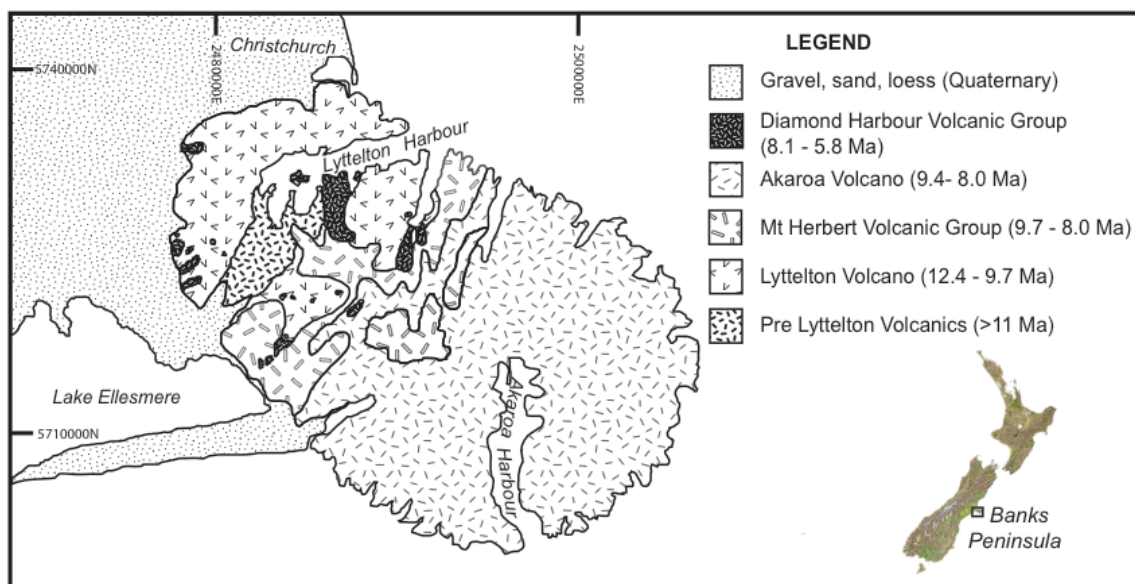
Figure 2.7: Simplified geologic map of Banks Peninsula, based on Sewell (1992), from Hampton and Cole (2009).

geology of the peninsula. The two dominating features of the peninsula are the Lyttelton and the Akaroa Volcanic Complexes.

The first record of volcanism on Banks Peninsula is the Pre-Lyttelton Volcanic Group, exposed on the southwestern edge of the peninsula and dating at >11Ma. This group is predominantly composed of the rhyolitic Mount Somers Group and various volcaniclastic sedimentary rocks. The Mount Somers Group lies on the Torlesse Supergroup. Compared to the other volcanic groups making up the peninsula, the Mount Somers Group is small in exposure (Hampton, 2010).

The Lyttelton Volcanic Complex is located on the western side of Banks Peninsula, and was active from 12.4-9Ma. This feature is a basaltic-dominated complex and comprises roughly one-third of the peninsula. Prior to the work undertaken by Hampton and Cole (2009), Sewell et al. (1992) mapped this feature as a simple shield volcano. However, Hampton and Cole (2009) mapped multiple eruptive vents, proving the feature was a large volcanic complex. This feature has since been subject to differential erosion along highly altered regions around the various vents and along valleys created by overlapping flows. This erosion caused the creation of the Lyttelton Harbor (Suggate, 1978, Hampton, 2010).

The Mt. Herbert Volcanic Group was active from 9.7-8Ma, and erupted from the already deeply eroded center of the Lyttelton Volcanic Complex. The center of volcanism then migrated southeast (Hampton, 2010, Sewell, 1985). This group is smaller in scale than the Lyttelton and Akaroa Volcanic Complexes that it lies between, and includes alkaline basaltic plugs and flows and epiclastic and pyroclastic deposits (Sewell, 1985).

The Akaroa Volcanic Complex, the subject of this study, lies on the eastern half of the peninsula, dates from 9.4-8.0Ma, and was active at roughly the same time as the Mt. Herbert Volcanic Group. Similar to the Lyttelton Volcanic Complex, the Akaroa Volcanic Complex was previously hypothesized to be a homogeneous shield volcano (Sewell, 1992, Hoernle et al., 2006, Timm et al., 2009). But, Hampton (2010) postulated that if the geomorphic features seen on the Lyttelton Volcanic Complex are indicative of vent locations, the Akaroa volcano might also be a volcanic complex built from multiple vents. A study of dike orientation and erosional valleys indicated that, like Lyttelton, Akaroa does indeed have multiple vents (Hampton, 2010). Furthermore, recent geochemical work undertaken on the eastern portion of the complex suggests that the complex is not composed of one continuously evolving magma, but rather the product of more intricate evolutionary cycles (Johnson, 2012, Crystal, 2013, and Patel, 2013).

The Diamond Harbor Group represents the final phase of volcanism, active from 8.1-5.8Ma. This group is located on southern flanks of the Lyttelton Volcanic Complex (Suggate et al., 1978, Hampton, 2010). The volcanism on Banks Peninsula was cut off at the onset of a compression stress regime. The compression effectively plugged the magmatic conduits feeding the peninsula, thus ending intraplate volcanism of Banks Peninsula (Ring and Hampton, 2012).

Previous Work on Banks Peninsula

Despite the prominence of the features comprising Banks Peninsula, little work has been conducted on their history. As previously mentioned, Sewell et al. (1992) produced the only geologic map of the area. This map, however, at a scale of 1:100000 is

highly simplified. Furthermore, this map was created under the hypothesis that the Lyttelton and Akaroa Volcanic Complexes were continuously evolving, single vent shield volcanoes. Even so, while Sewell et al. (1992) may have been incorrect on the interpretation of the units, their study successfully maps out the geographic location of the various volcanic groups. Using primary volcanic landforms and geomorphic features such as volcanic dikes and erosional valleys, Hampton and Cole (2009) mapped seven different vents for the Lyttelton volcanic complex, thus rebutting the interpretation of Sewell et al. (1992). Moreover, through a similar study of geomorphic features, Hampton (2010) indicated that, like Lyttelton, Akaroa contains multiple vents.

Timm et al. (2009) focuses primarily on the source for the volcanism on Banks Peninsula. Through geochemical sampling of both the Lyttelton and Akaroa complexes, Timm et al. (2009) attribute the source of intraplate magmatism to two lithospheric detachment events (one for each complex). Based on the Hoernle et al. (2006) study on the intraplate Dunedin Volcano south of Banks Peninsula in Otago, the delamination of the lower lithosphere could have caused an upwelling of the underlying asthenosphere into the crust. The basaltic flows in the Lyttelton Volcanic Complex contain a higher silica content, and lower trace element concentrations, than the Akaroa Volcanic Complex. Thus, this first detachment may have been smaller in scale. A smaller, or incomplete, detachment of the lithosphere would cause less partial melting and upwelling of the asthenosphere, thus creating a higher ratio of lithospheric to asthenosphere partial melt. Timm et al. (2009) hypothesize that the higher silica concentration and trace element signature in the Lyttelton flows are indicative of a pyroxenitic magma formed largely from crustal assimilation. The second detachment event that created the Akaroa

basaltic flows would have been larger in scale, causing a greater volume of asthenospheric upwelling (**Figure 2.6**). This larger volume would produce the low silica, high trace element signatures characteristic of a peridotite parent magma with smaller percentages of crustal assimilation.

Ring and Hampton (2012) hypothesize that the controls on magma ascent and vent location could be a function of inherited Cretaceous faults (**Figure 2.8**). These NE-SW trending faults were originally normal, and are the relicts of a pull apart basin formed during the separation of Zealandia from Gondwana. These normal faults were then reactivated as oblique reverse and dextral strike slip faults in the Late Miocene as the stress regime switched from extensional to compressional. This switch coincides with the onset of the Southern Alps orogeny, whose erosion would later fill the sea between the Banks Peninsula island and the mainland of New Zealand. The conduits through which the lithospheric detachment melt could rise and erupt are through these reactivated faults. In a similar manner, the termination of volcanic activity roughly coincides with an increase in transpressive rate in which the reverse faults would have been effectively sealed (Ring and Hampton, 2012).

Johnson (2012), Crystal (2013), and Patel (2013) analyzed the geochemical stratigraphy of various sections within the Akaroa Volcanic Complex, noting bulk rock geochemical cycles from picrite to benmoreite that repeated across the lava flows. These geochemical cycles were grouped into magma batches, with each batch defining a single continuous trend of melt. Johnson (2012), Crystal (2013), and Patel (2013) noted several batches within a single stratigraphic section, thus disproving Sewell's (1992) hypothesis that the Akaroa flows are all one formation and sourced from a single, continuously
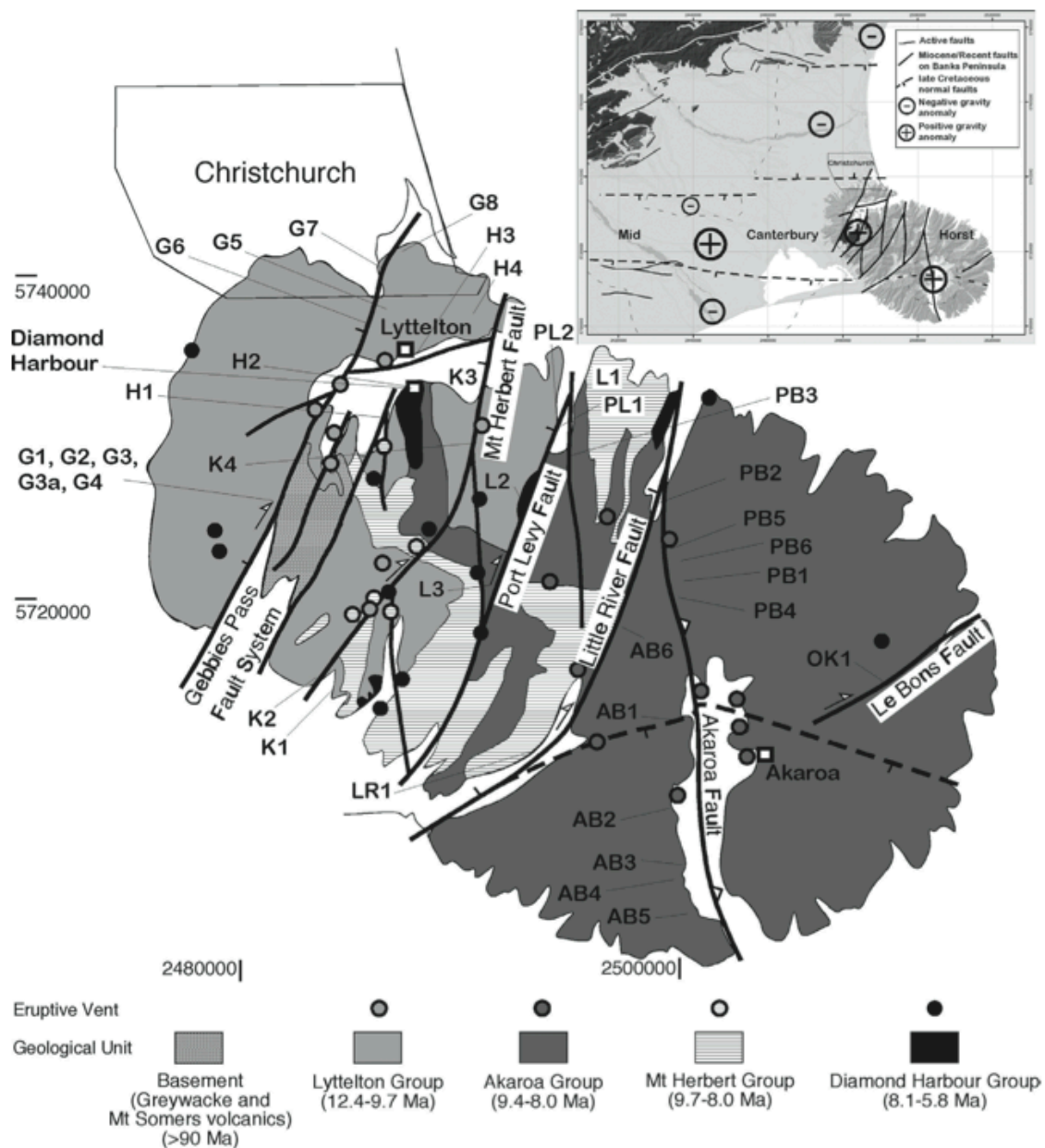
Figure 2.8: Note the various faults on Banks Peninsula. The bold solid lines represent

the Cretaceous normal faults reactivated as oblique reverse faults in the late Miocene,

and the dashed line represents a Cretaceous normal fault (Ring and Hampton, 2010).

evolving vent. Johnson (2012) correlated geochemical sequences with spatial distribution around the volcanic complex, suggesting a model of various eruptive vents (like Hampton and Cole, 2009) rising from multiple shallow magma chambers (**Figure 2.9**). These shallow magma chambers were fed by a deep reservoir derived through intraplate processes (Timm et al., 2009). Shallow chambers would allow primitive magma to undergo slightly different evolutionary trends, which upon eruption would be recorded and localized to a particular area of the volcanic complex (Johnson, 2012). Johnson (2012) also suggests that these shallow magma chambers were subject to magma replenishment from depth, thus starting the evolutionary cycle within the shallow chambers over and allowing for the observed repeating compositional pattern. Each batch represents the evolutionary pathway that occurs within specific shallow chamber between magma replenishment episodes.

Due to the recent nature of Johnson's (2012) shallow chamber magma recharge model, there has not been much research done on the specifics of the Akaroa Volcanic Complex. Crystal (2013) supports Johnson's model through analysis of repeating geochemical trends in Lavericks Bay. By organizing the geochemical data into a stratigraphic section and evaluating the various trends of both bulk geochemistry and trace element signatures, Crystal (2013) was able to verify that there is magma replenishment occurring, thus producing the evolved to primitive transition seen between batches. Furthermore, her findings support Johnson's (2012) idea that fractional crystallization is the driving force for batch evolution. Crystal (2013) notes that a scoria cone or ash deposit often separates the magma batches, representing the start or end of one evolutionary package.
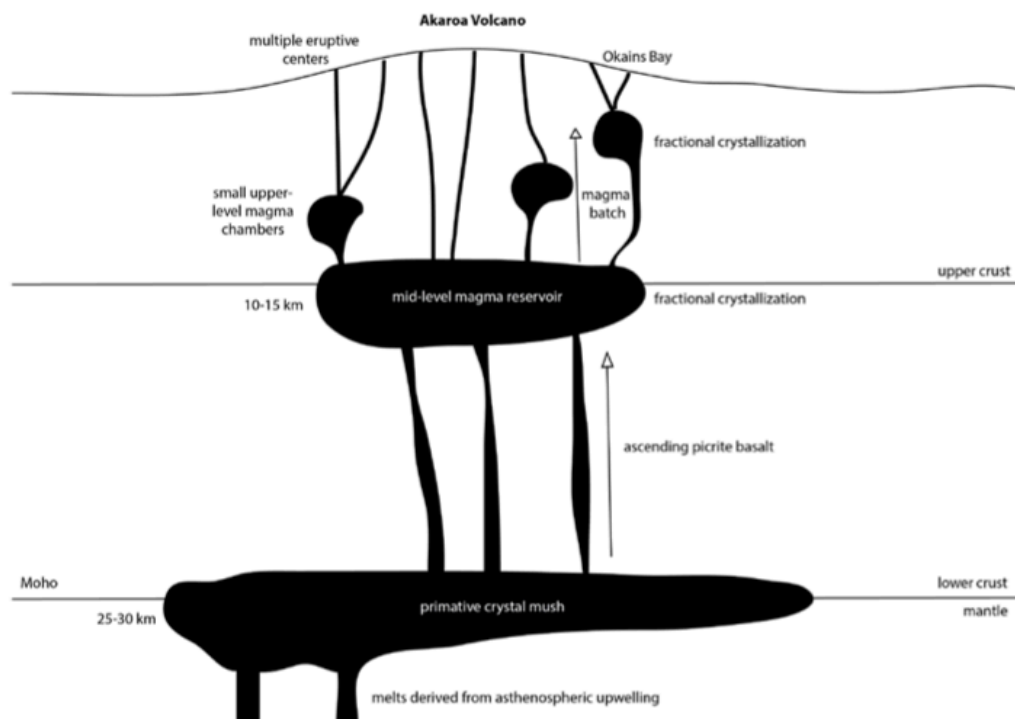
Figure 2.9: Subsurface model of the Akaroa Volcanic Complex created by Johnson
(2012). It is in the small upper level magma chambers that Johnson (2012), Crystal
(2013), and Patel (2013) postulate that recharge driven geochemical evolutional cycle
is occurring.

Similarly, Patel (2013) correlates the geochemical trends to petrographic textural observations of plagioclase phenocrysts, noting specific core and zone patterns that support ascent from a deep source, fractional crystallization, magma mixing, and magma replenishment. Based on Vicarro et al. (2010), Patel (2013) hypothesizes that through sieved, resorbed, and patchy textures one can reconstruct some of the mechanisms occurring within Johnson's (2012) shallow magma chambers.

Mount Etna, Italy, displays similar conditions in which smaller magma chambers interact with primitive melt replenishment from depth (Johnson 2012, Patel 2013). Mount Etna is composed of several dikes and sills, which are fed by a deep magma reservoir. The textural study undertaken by Viccaro et al. (2010) shows that, within theses dikes and sills, a complex magmatic interaction between primitive and evolved magma is taking place outside normal fractionation. These processes can be traced by the various textures seen in plagioclase. Due to the similar nature of the model put forth by Johnson (2012), Patel (2013) applied Viccaro et al.'s (2010) plagioclase textures to lava flows observed in Stony Bay, supporting the existence of shallow magma chambers.

Plagioclase textures similar to the classifications assigned by Viccaro et al. (2010) have been utilized in other volcanic areas as a proxy for magmatic dynamics and cooling and ascent rates in alkali magmas. Work undertaken at Volcán Tatara-San Pedro uses textural observations, along with trace element geochemistry to ascertain magmatic evolution, magma chamber dynamics, and magma cooling rates (Singer et al. 1995). While the geologic setting is not as closely related to Banks Peninsula as Mount Etna, the processes shaping the phenocrysts are very similar. Moreover, Singer et al. (1995) uses trace element geochemistry in combination with the plagioclase textures, thus taking a

more comprehensive approach to magmatic evolution. The conclusions put forth by Singer et al. (1995) suggest the magma was subject to significant undercooling coupled with fast crystal growth rates, similar to the conclusions drawn by Patel (2013).

The Akaroa Volcanic Complex has only recently been the topic of detailed geochemical and petrologic study, therefore there is still much work to be done. Furthermore, the past geochemical studies (Johnson 2012, Crystal 2013, Patel 2013) were focused within single bays within the Akaroa Volcanic Complex. This study tests Johnoson's (2012) magma chamber model across six bays comprising 15km in the eastern section of the 100km circumference of the Akaroa Volcanic Complex circumference. Insight into magma origin, intraplate volcanics, and pre-eruptive magma chamber dynamics for the Akaroa Volcanic Complex are investigated by implementing the plagioclase textural analysis used by Viccaro et al. (2010) and Patel (2013) in conjunction with the stratigraphically constrained geochemical analysis used by Johnson (2012), Crystal (2013) and Patel (2013).

Chapter III: Fieldwork and Sample Collection

In order to test and extend the shallow chamber model of Johnson (2012) across the entire Akaroa Volcanic Complex, fieldwork was conducted in six bays (Menzies Bay, Little Akaloa, Stony Bay, Lebons Bay, Lavericks Bay, and Ducksfoot Bay) stretching across eastern Banks Peninsula (**Figure 3.1**). Fieldwork was undertaken in February 2015 in Menzies Bay and Little Akaloa, while preexisting data were analyzed from Stony, Lebons, Lavericks, and Ducksfoot Bay. This preexisting dataset was provided from fieldwork conducted in past Frontiers Abroad field camps. In order to obtain a spatially representative dataset, these bays were purposely selected because they cover a laterally extensive area across the eastern flanks of the Akaroa Volcanic Complex where there are both geochemical data and thin sections available.

In Menzies Bay and Little Akaloa, three field days were spent where two mapping groups from the Frontiers Abroad 2015 Geology Field Camp took samples along transects starting at shore platforms and extending to the ridgelines. These transects were chosen due to the excellent outcrop exposure along bay walls (**Figures 3.2**, **3.3**). Samples and detailed field observations were taken at each lava flow. Individual flows ranged from .5-5m thick, separated by .5-8m thick layers of breccia. In some cases, a thin red ash horizon separated consecutive flows (**Figure 3.4**). The units themselves were highly weathered dark grey to black aphyric massive lava flows. The primary variability between successive flows was whether the units were completely aphyric or contained some crystals. A total of thirty-three samples were taken at these two bays.

For Stony, Lebons, Lavericks, and Ducksfoot Bay, preexisting geochemical data from thirty-seven samples were matched with GPS points mapped on ArcGIS in order to
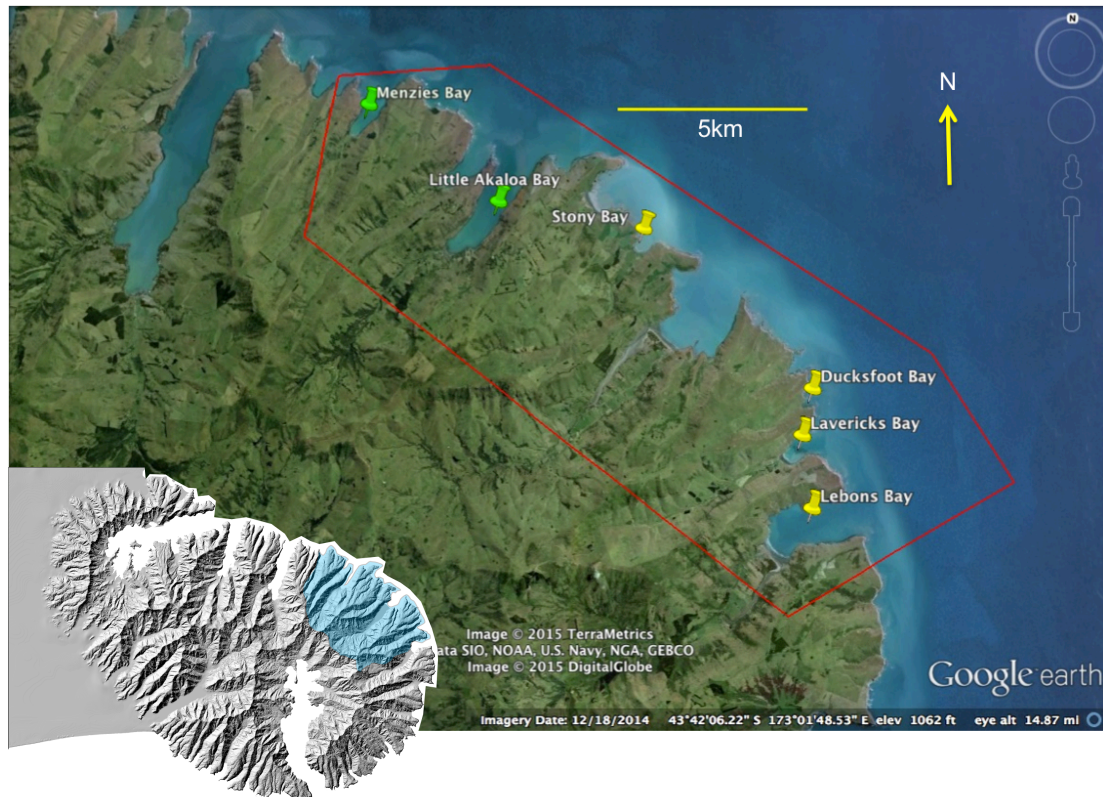
Figure 3.1: Map of the field sites relative to the rest of the Peninsula. The blue shading on the DEM is the location of the study area on the peninsula. The satellite image shows the six bays studied. The green pins are bays in which fieldwork was done in 2015, the yellow pins are bays in which past data was available from previous years' field seasons. Satellite image from Google Earth 2015.

Figure 3.2: Picture of an exposed section of lava flows in Menzies Bay.

Figure 3.3: Picture of an exposed set of lava flows in Menzies Bay. Transects were planned in the field by exploring and sketching the various areas within the individual bays.
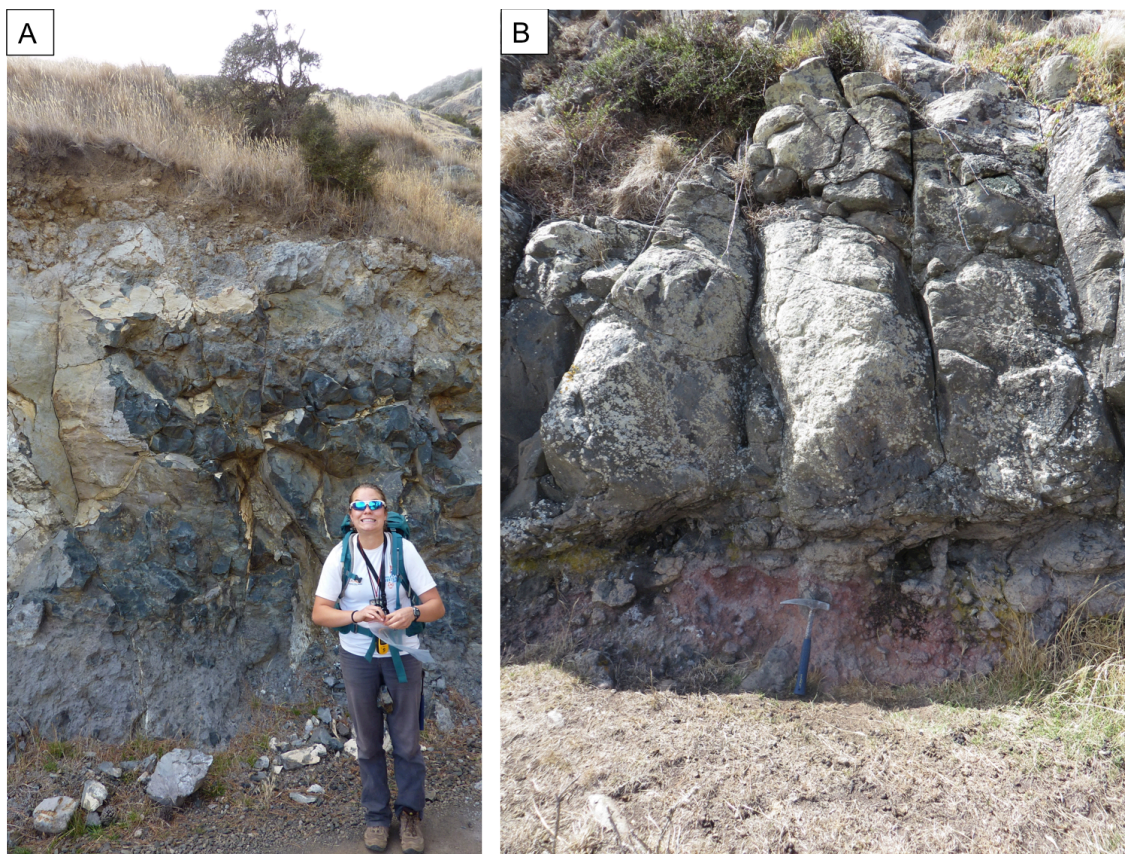
Figure 3.4: Field pictures of the units sampled. **A)** 1.5m thick massive lava flow sitting on top of a .5m thick breccia layer. Geologist, Laura Stamp, for scale. **B)** Red ash horizon below a .7m thick massive lava unit.

identify complete stratigraphic geochemical transects from shore platforms to ridgelines. Both field photographs and notes from the Frontiers Abroad field camp database at the University of Canterbury, New Zealand, were consulted in conjunction with the ArcGIS maps and the geochemical data. Furthermore, thin sections were matched with the geochemical data in order to create a complete dataset for the study.

Chapter IV: Petrography

Methods

Sixty-six hand samples were cut into thin section blanks and submitted to the University of Canterbury geology labs for the cutting and mounting of thin sections. The number of samples was contingent upon the number of exposed flows within each bay for a single stratigraphic section. Transects ranged from eight to eighteen samples. Multiple hand samples were taken for each unit, however only one sample was prepared and submitted for thin section mounting. Using a Leica optical microscope, basic petrographic observations were made on sixty-six thin sections to understand general crystallinity trends, phenocryst populations, and mineral textures. Particularly important are estimations of percent phenocrysts (crystallinity), and percent plagioclase, olivine, clinopyroxene, and opaque populations. Groundmass composition and crystal texture were also noted. Initial research led to the selection of eleven representative samples for point counting, the preparation of polished thin sections, and electron microprobe analysis.

Nine of the eleven polished thin section samples were selected for modal analysis (Appendix I, Table 1A). At least one sample from each bay was chosen to represent the lateral extent of the study area. Due to the aphyric nature of the lava flows, the modal analysis focused on the more crystalline samples. In each section, an average of 1,200 points were counted moving in lengthwise transects on the section by .5mm increments. Each transect was spaced 1mm apart along the width of each section. Points counted in the groundmass were counted separately from phenocrysts in order to understand variability in the groundmass with respect to the phenocrysts. Minerals were identified

primarily through crystal habit, angle of extinction, birefringence, and fractures within the crystal (**Table 4.1**).

Petrographic data were organized by and viewed in light of the stratigraphically constrained bulk rock geochemistry described in Chapter 5 (see also Appendix I, Tables 2A-7A). As such, the rock type classifications below are drawn from the geochemical data in Chapter 5.

Rock Description and Composition

Picrite-Basalts

From general petrographic observations, it is evident that picrites within each transect contain the highest percent crystallinity, on average ranging from 8-20% crystalline (Appendix I, Table 8A). Even so, there is variability between the bays in average picrite crystallinity. Ducksfoot Bay, for instance, does not exceed 3% crystallinity, whereas every other bay exceeds 10% crystallinity in at least one flow.

Modal analysis of six different picrites (**Figure 4.1**, **Table 4.2**) revealed that the primary phenocryst population is plagioclase at an average of 79%, followed by olivine (11%), opaque minerals (5%), and clinopyroxene (3%). Phenocrysts ranged from 0.2mm-6.0mm in length. Anorthite proportion determined from the microprobe analysis described in Chapter 5 averaged 0.61. The groundmass population is also primarily plagioclase at 49%, followed by opaque minerals (22%), clinopyroxene (17%), olivine (7%), and glass (4%). The groundmass was composed both of plagioclase laths and microlites.
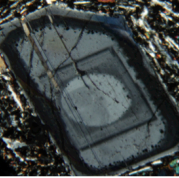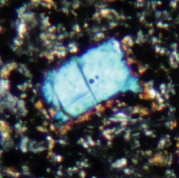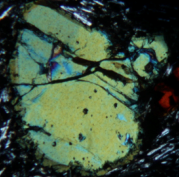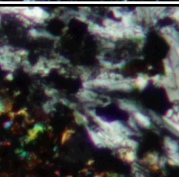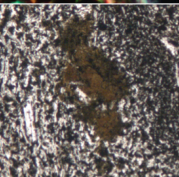
Mineral	Crystal Habit	Cleavage	Extinction	Max Birefringence	PP Color	Comments	Picture
Plagioclase	Subhedral-Euhedral: rectangular, or lath Anhedral: plates	Perfect	Varies with composition	1st order	White-grey to pale yellow	Crystals display range of textures.	
Clinopyroxene	Subhedral-Euhedral: rectangular or eight sided crystals	Good	Inclined	Middle 2nd order	White-grey to pale yellow	Often weathered to clay, with secondary hematite/magnetite infilling the crystal.	
Olivine	Subhedral: six sided polygon Anhedral	Rarely seen in thin section	Parallel	Upper 2nd order	White-grey to pale yellow	Conchoidal fracturing. Many crystals iddingzitized, but still counted as olivine due to crystal habit.	
Opaques	Euhedral: square-amorphous Anhedral	None	N/A	N/A	Black	Opaques mostly in groundmass, with cubic or circular shapes.	
Glass (groundmass only)	Anhedral: interstitial	None	N/A	N/A	Black-brown	Glass has devitrified appearance and is highly weathered.	

Table 4.1: This table presents the classification criteria used when point counting. Criteria were selected based on point counting observations, and cross-referenced with Perkins and Henke (2004).
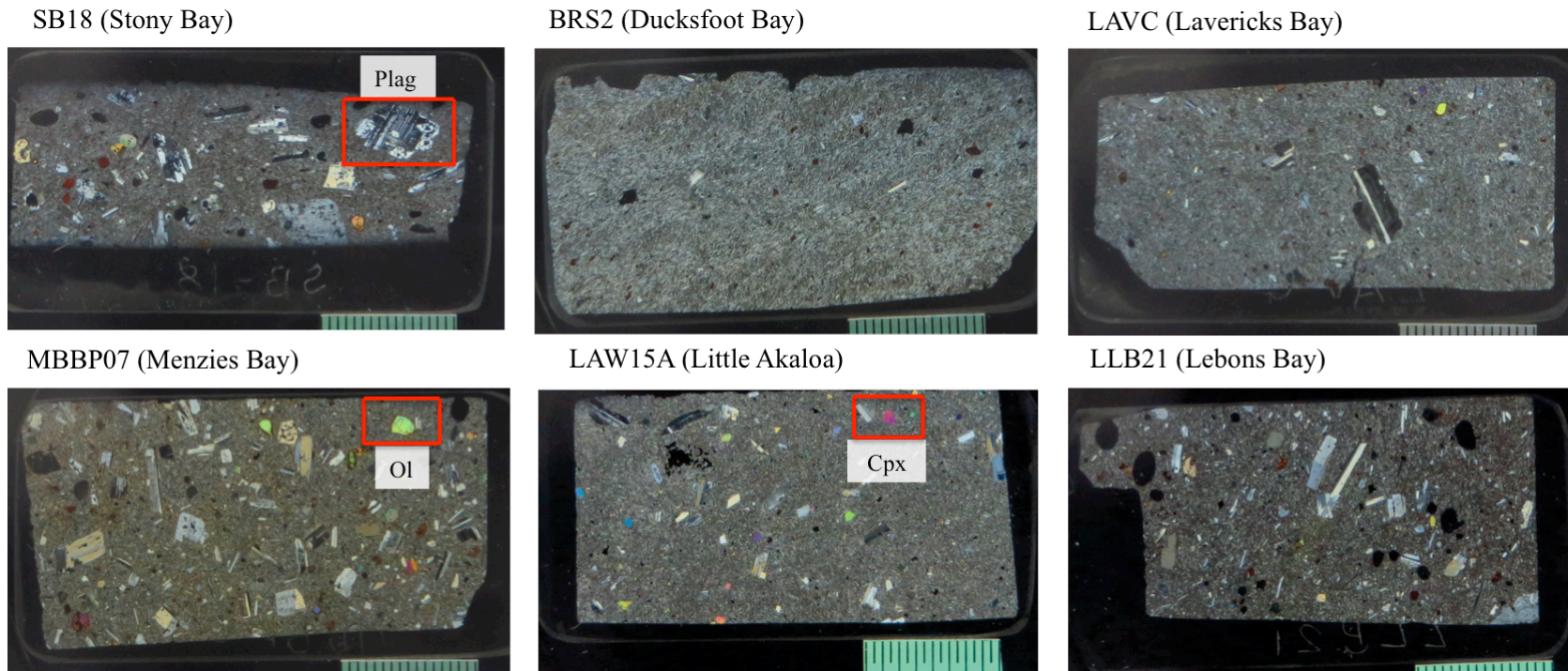
Figure 4.1: Cross polar images of the picrite thin sections. Representative plagioclase (Plag), olivine (Ol) and clinopyroxene (Cpx) boxed in red.

Phenocrysts						Groundmass						
	rock type	plag	cpx	ol	opaques	open space inside plag	plag	cpx	ol	opaques	glass	vesicle/hole
SB18	picrite	70.9	0.8	20.5	1.2	6.6	43.3	29.3	6.3	13.8	4.3	3.0
MBBP07	picrite	65.9	9.3	21.3	3.5	0.0	55.7	18.0	10.1	16.2	0.0	0.0
BRS2	picrite	100.0	0.0	0.0	0.0	0.0	54.5	7.8	8.3	24.3	4.6	0.6
LAW15A	picrite	71.8	3.2	5.6	19.4	0.0	45.5	28.7	8.5	15.6	0.9	0.8
LAVC	picrite	85.4	3.3	11.3	0.0	0.0	52.7	7.4	5.1	29.0	5.5	0.4
LLB21	picrite	81.6	2.8	10.6	5.0	0.0	41.9	9.0	4.3	30.9	11.0	3.0
AVERAGE:		**79.3**	**3.2**	**11.5**	**4.9**	**1.1**	**48.9**	**16.7**	**7.1**	**21.6**	**4.4**	**1.3**
LAV10EA	hawaiite	77.6	2.6	4.2	1.0	14.7	35.5	15.9	0.7	20.9	8.4	18.6
LAVJ	mugearite	86.0	3.0	5.0	6.0	0.0	56.5	3.2	2.6	29.4	7.9	0.4
SB34	benmoreite	87.5	10.4	0.0	2.1	0.0	56.2	19.9	0.0	16.0	7.7	0.1

Table 4.2: Tabulated modal analyses for both the phenocrysts and groundmass. Numbers represent percent surface area of each phase in the thin section for both the phenocrysts and the groundmass.

Hawaiites

Hawaiites are predominantly aphyric, ranging on average from <1%-4% crystallinity. There are a few samples (LAWBP5A, PAB32, LAV10EA) that range from 7-25% crystallinity, however these are outliers compared with the majority of the twenty-two hawaiites (Appendix I, Table 9A).

LAV10Ea (**Figure 4.2**, **Table 4.2**) was selected for modal analysis due to its more porphyritic composition. Similar to the picrites, the predominant phenocryst phase is plagioclase at 78%. There are very few other phases represented, containing olivine (4%), clinopyroxene (3%) and opaque minerals (1%). Within this sample, plagioclase often contains open spaces within its structure, having 15% open space. Phenocrysts ranged from 0.2mm-4mm in length. Anorthite proportion determined from the microprobe analysis described in Chapter 5 averaged 0.54. The groundmass was predominantly plagioclase (35%), followed by opaque minerals (21%), clinopyroxene (17%), and glass (4%). Similar to open spaces inside plagioclase phenocrysts, 19% of the groundmass is open space due to the presence of vesicles.

Mugearite

Mugearite flows are aphyric, with all but one sample (Lav-J) between 0%-1% crystallinity. Lav-J has 12% crystallinity (Appendix I, Table 10A). Due to the aphyric nature of every other mugearite, Lav-J was selected for modal analysis.

In Lav-J (**Figure 4.2**, **Table 4.2**), plagioclase is the most common phenocryst at 86%. Plagioclase is followed in population by opaque minerals (6%), olivine (5%), and clinopyroxene (3%). Phenocrysts ranged from 0.2mm-4.0mm in length. Anorthite proportion determined from the microprobe analysis described in Chapter 5 averaged

LAV10EA (Lavericks Bay)   LAVJ (Lavericks Bay)   SB34 (Stony Bay)
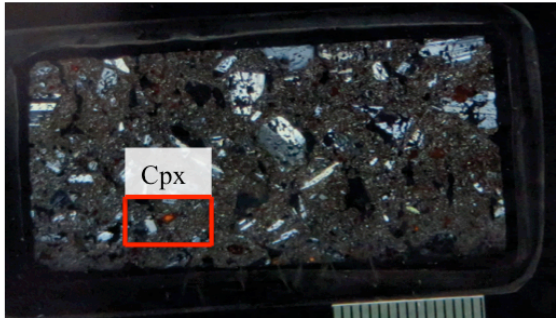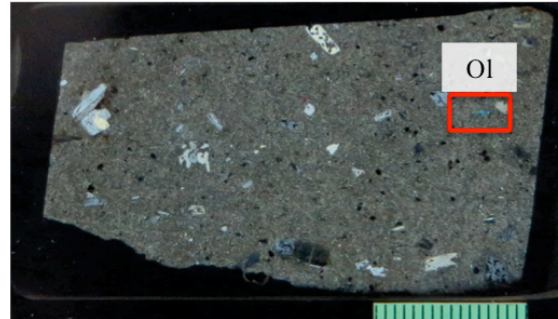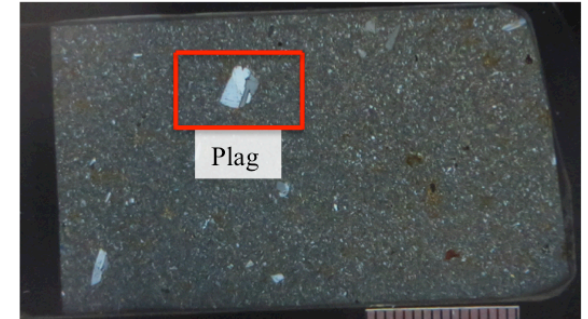
Figure 4.2: Cross polar images of the hawaiite (LAV10EA), mugearite (LAVJ), and benmoreite (SB34). Representative

plagioclase (Plag), olivine (Ol) and clinopyroxene (Cpx) boxed in red.

0.36. The groundmass is mostly plagioclase (56%), followed by opaque minerals (29%), clinopyroxene (3%) and olivine (3%).

Benmoreite

There are only two benmoreite flows within the study area, both contained within the Stony Bay transect (SB-34 and SB-15). Both flows are crystal poor and highly weathered; SB-34 contains 6% crystallinity, and SB-15 has 2% crystallinity (Appendix I, Table 11A). Because SB-34 is the more crystalline of the two samples, SB-34 was chosen for modal analysis (**Figure 4.2**, **Table 4.2**).

The primary phenocryst in SB-34 is plagioclase at 88%, followed by clinopyroxene (10%) and opaque minerals (2%). Olivine was not identified in this sample. Phenocrysts ranged from 0.2mm-3.0mm in length. Anorthite proportion determined from the microprobe analysis described in Chapter 5 averaged 0.25. The groundmass is composed predominantly of plagioclase (56%), again followed by clinopyroxene (20%) and opaque minerals (16%), and glass (8%).

Textural Observations

Mineral textures act as windows into pre-eruptive magmatic processes (Cashman, 1993, Singer et al., 1995, Viccaro et al., 2010, Patel, 2013). Specifically, plagioclase textures have been utilized in many volcanic areas as a proxy for magmatic dynamics and cooling and ascent rates in alkali magmas (Singer et al., 1995, Viccaro et al., 2010). Specific textures observed in this project were catalogued and interpreted according to the Petrographic Guide (**Figure 4.3**), based on Viccaro et al. (2010). Viccaro et al. (2010) classified plagioclase mineral textures of Mount Etna lava flows into seven different
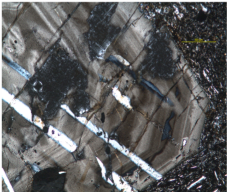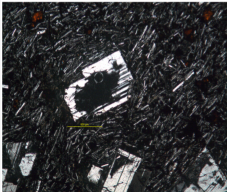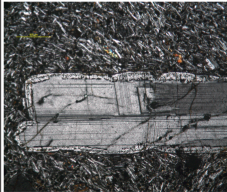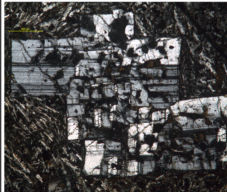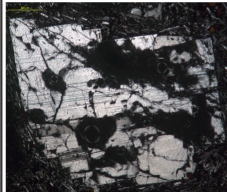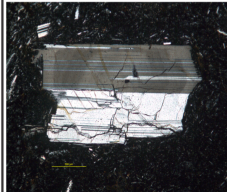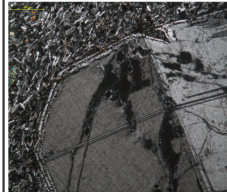
Petrographic Guide						
Texture						
Zoned	Resorbed Core	Resorbed Rim	Sieved Core	Patchy Core	Swallow Tail	Melt Inclusions
Interpretation						
Magma chamber convection	Fast decompression, magma recharge	Magma recharge	Decompression, magma recharge	Slow decompression	Fast decompression	Rapid crystal growth with decompression, undercooled

Figure 4.3: Petrographic Guide of observed plagioclase textures and their interpretation. The classification is based on plagioclase textural analysis in Viccaro et al. (2010) and Singer et al. (1995).

categories: sieved core, resorbed rim, resorbed core, patchy, swallow tail, zoned, and melt inclusions. Each texture implies specific information about magma ascent rate prior to eruption, volcanic plumbing, shallow chamber dynamics and replenishment, magma mixing, and fractional crystallization. Sixty-six thin sections from the six different bays were observed and categorized with respect to these classifications.

In all the samples, groundmass textures range from felty to trachytic. All the samples containing phenocrysts, regardless of rock type, displayed some of the textures listed in **Figure 4.3**. Due to the more crystalline nature of the picrite flows and aphyric nature of the hawaiites, mugearites, and benmoreites, the majority of crystal textures seen are in picrite flows.

Mineral textures are most easily visible in plagioclase, however clinopyroxene displays similar textures to that of the plagioclase. Primary textures observed are zoning, sieved cores, and resorbed cores and rims (**Figure 4.4**). Melt inclusions, skeletal dissolution (swallow tail), and patchy cores were also observed to a lesser extent within the transects. In some phenocrysts, multiple rings of inclusion trains, surrounded by zoning patterns can be seen (**Figure 4.5**). See Appendix I, Tables 2A-7A for a description of each sample's observed mineral textures.
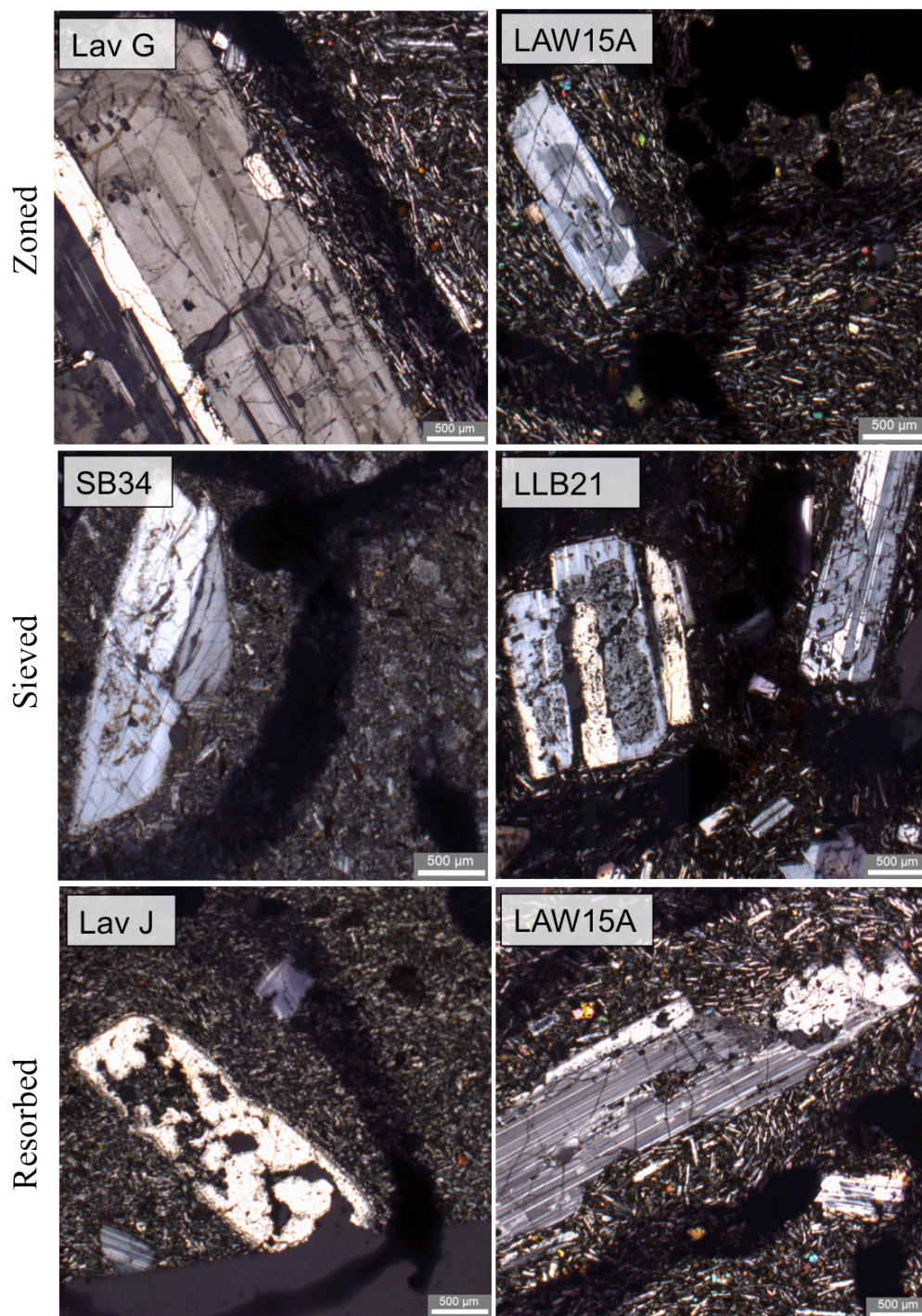
Figure 4.4: Photomicrographs of the primary plagioclase textures observed. Lav G and LAW15A (top) contain representative zoning textures, SB34 and LLB21 are representative sieved textures, and Lav J and LAW15A (bottom) contain representative resorbed cores and rims.
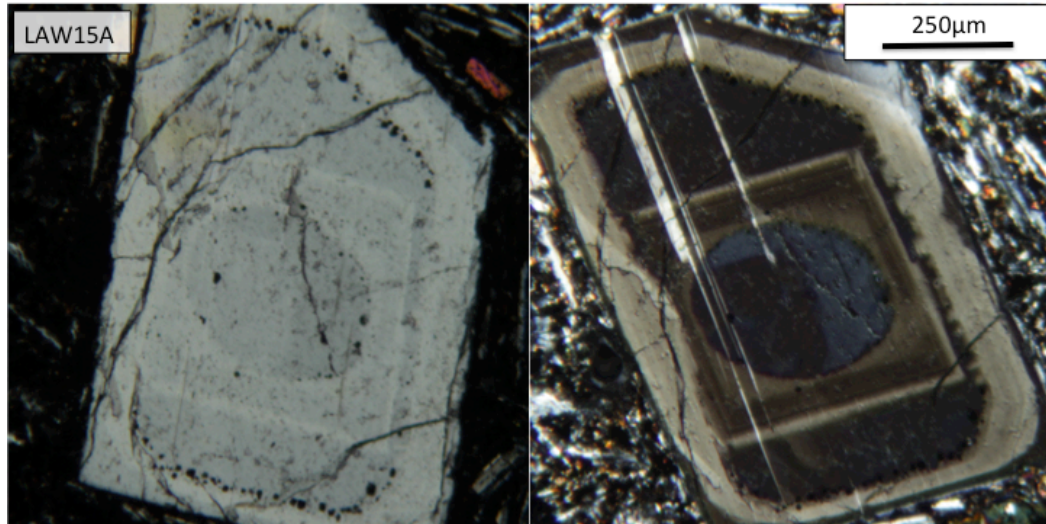
Figure 4.5: This phenocryst in LAW15A contains two distinct inclusion trains as well as unique zoning patterns and an abnormally shaped core. The inner inclusion train surrounds a circular core of the plagioclase, and marks the transition from the circular core to a square zoning pattern. The outer inclusion train is polygonal, and marks the transition to a rectangular/polygonal zoning pattern.

Chapter V: Geochemistry

Bulk Rock Geochemistry

Sample Preparation

Field samples of each of the initial seventy lava flows were prepared for bulk rock geochemistry. Samples were cut with a diamond-edged saw to remove weathered surfaces, dried in an oven for twenty-four hours, and then crushed into powder for x-ray fluorescence analysis (XRF). The resulting powders (20-100g) were pressed into pellets for trace element analysis, and fused into glass disks for major element analysis. These samples were then analyzed on the University of Canterbury's XRF. Fifteen powdered samples from the Menzies Bay transect were also analyzed with the Colorado College Geology Department's XRF for a comparative trace element geochemistry analysis. These powders were pressed into pellets and analyzed on the CC XRF.

Standards from both XRF analyses are given in Appendix II. There are two potential sources of error with the data: machine precision and alteration of the rocks. Individual error calculations for the bulk rock geochemistry data provided by the University of Canterbury are not available, however the data were analyzed in conjunction with international standards (Appendix II, Table 1B). The error for the CC XRF trace element data is between 1-3%, based on comparison with international standards.

Bulk rock geochemical data were then organized in stratigraphic order and divided into individual evolutionary batches according to geochemical trends and rock type. Batches were defined by one continuous phase of magmatic evolution. Specifically, SiO_2, TiO_2, MgO, FeO, Zr, V, Sr were used to define the boundaries of each batch. These

elements were chosen because they show the geochemical trends associated with magma evolution most clearly. The data were plotted using IgPet2013 to look at specific geochemical trends and variations between batches and between bays.

Bulk Rock Results

Geochemical data from the University of Canterbury XRF were sorted into transects according to their specific bay and plotted in a Total Alkali-Silica diagram (**Figures 5.1**). Rock types range from picritic basalt to benmoreite. Stony Bay was the only transect that contained benmoreite flows.

These data were sorted into stratigraphic order within single bays, individual batches were delineated by identifying geochemical patterns in both the major and trace elements. Specifically, batches within each bay were recognized by discontinuities of rock type (identified through TAS diagrams and stratigraphic position) and by uncharacteristic jumps, or regressions in element concentrations. Each geochemical transect within the six bays shows several repeating patterns of rock types. Each repetition constitutes a magma batch, and is punctuated by a more primitive lava flow, which starts the geochemical evolution over again (**Figures 5.2, 5.3, 5.4, 5.5, 5.6, 5.7**). These trends are reflected in both rock type and specific elements in the flows. Of the elements observed, specific attention was paid to increasing SiO_2, K_2O, and Zr, with decreasing MgO, FeO, P_2O_5, and V. These negatively correlated elements are indicative of fractionation driven evolution; as plagioclase, olivine, pyroxene, and iron oxides crystallize, the compatible elements will decrease in percentage, while silica, alkalis, and incompatible elements will increase. Multiple batch cycles were observed within each transect, but those showing the most prominent trends are in Stony Bay (**Figure 5.2**) and
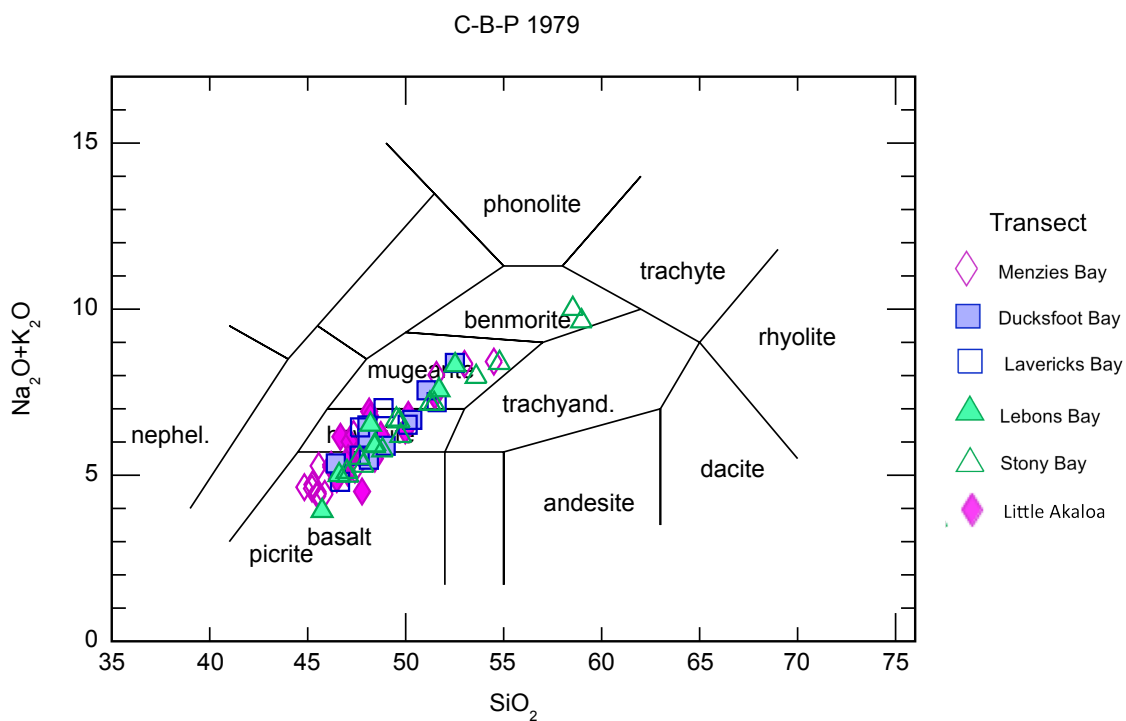
Figure 5.1: Total Alkali Silica diagram plotted by transect. Each transect displays a

similar range in rock type (Cox et al., 1979).
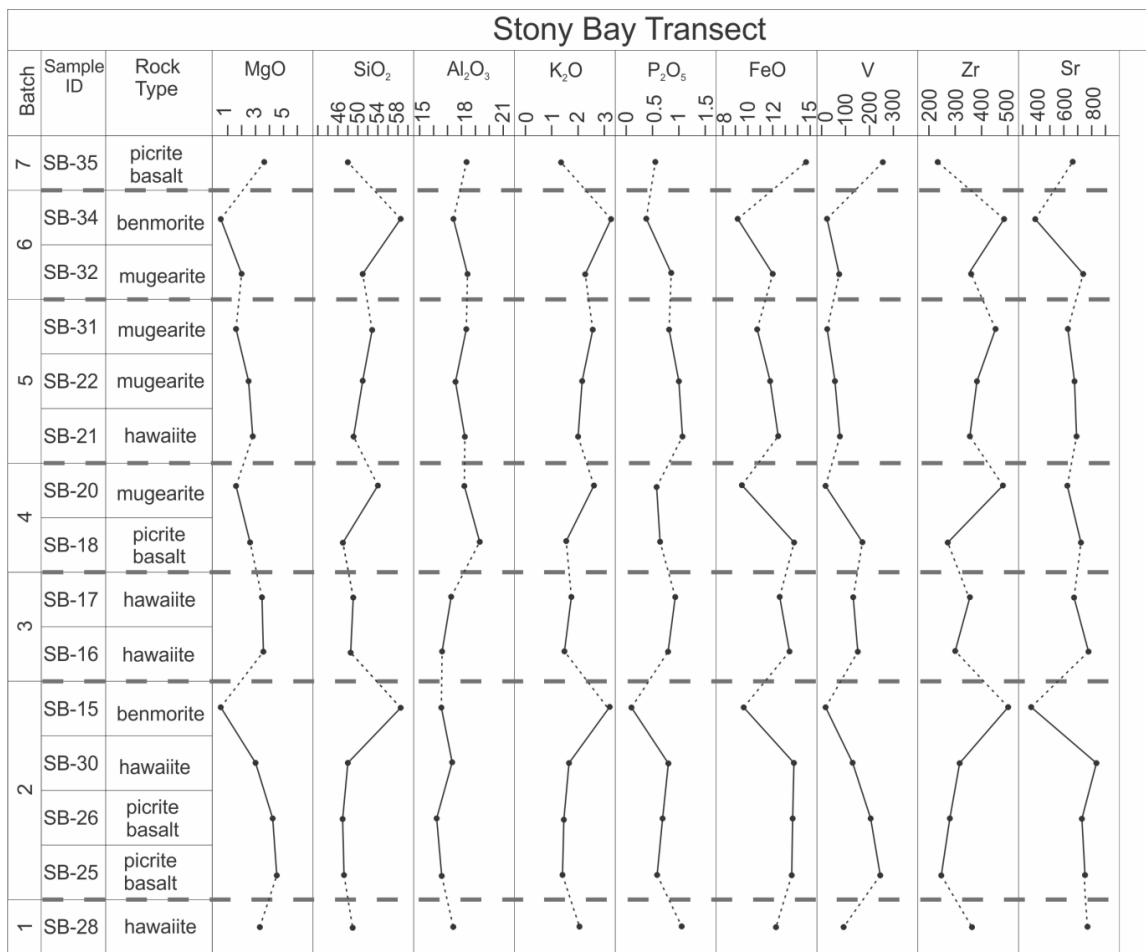
Figure 5.2: Stony Bay stratigraphic geochemical plot. Horizontal dashed lines divide batches, vertical solid lines relate flows within single batches, and vertical dashed lines show unrelated flows between two batches.
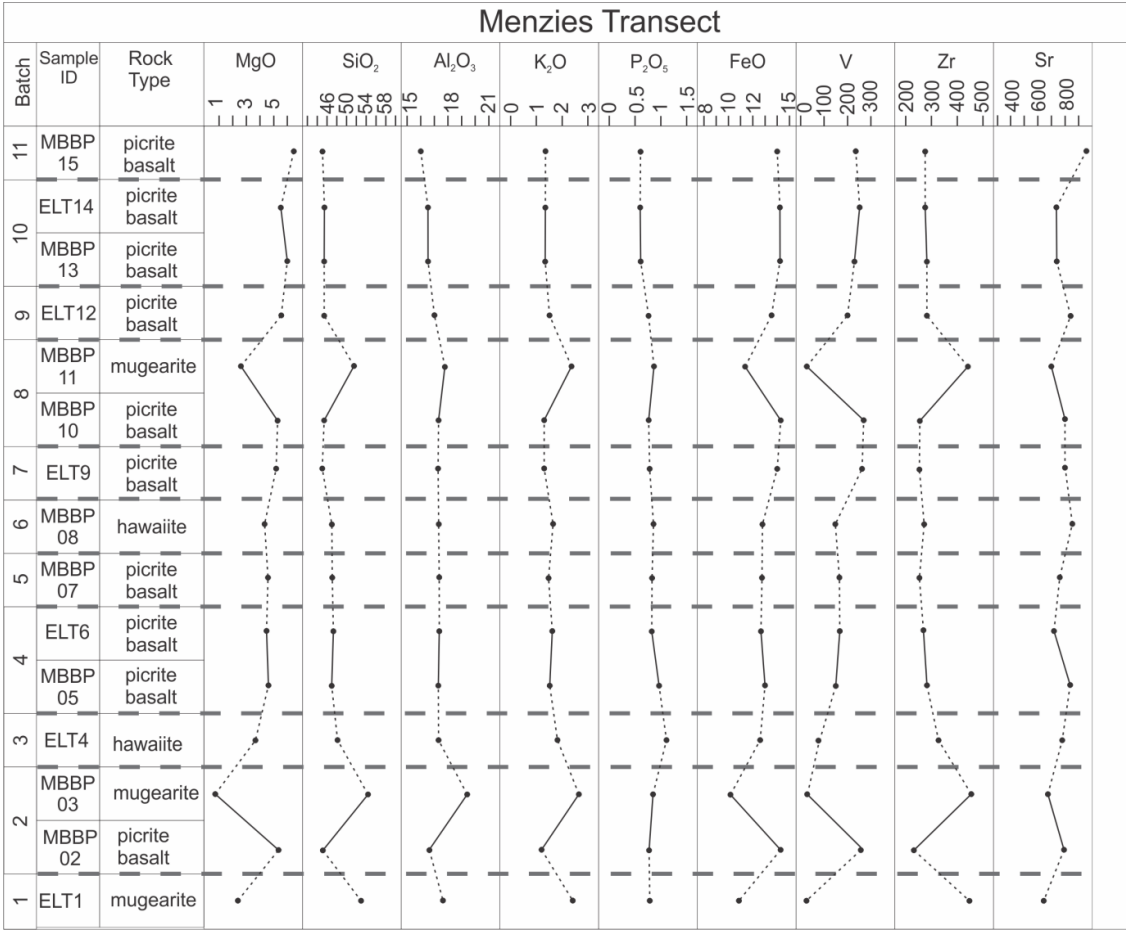
Figure 5.3: Menzies Bay stratigraphic geochemical plot. Horizontal dashed lines divide batches, vertical solid lines relate flows within single batches, and vertical dashed lines show unrelated flows between two batches.
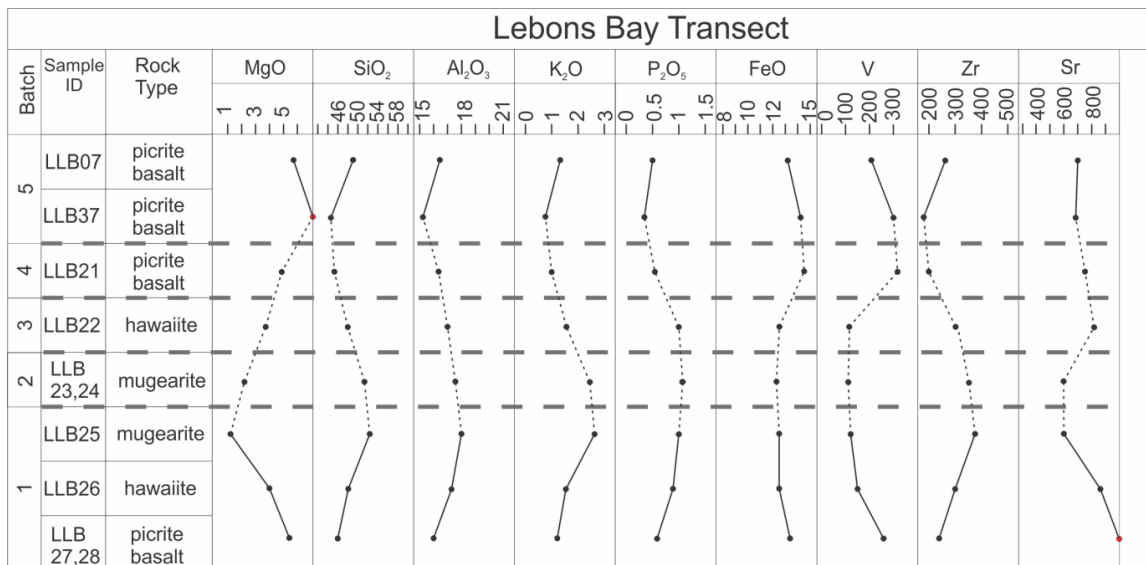
Figure 5.4: Lebons Bay stratigraphic geochemical plot. Horizontal dashed lines divide batches, vertical solid lines relate flows within single batches, and vertical dashed lines show unrelated flows between two batches.
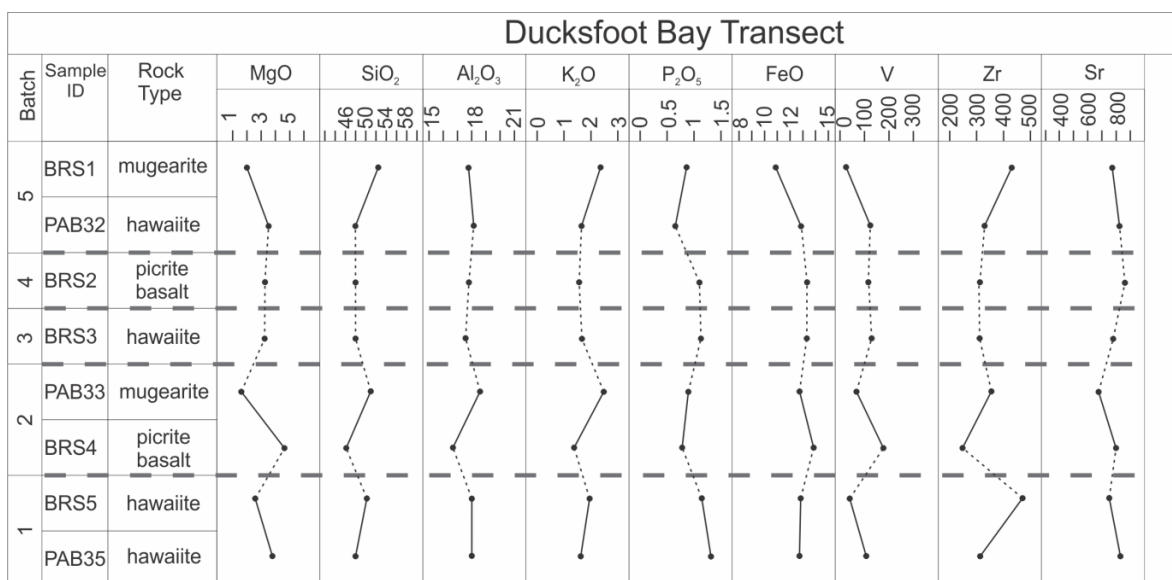
Figure 5.5: Ducksfoot Bay stratigraphic geochemical plot. Horizontal dashed lines divide batches, vertical solid lines relate flows within single batches, and vertical dashed lines show unrelated flows between two batches.
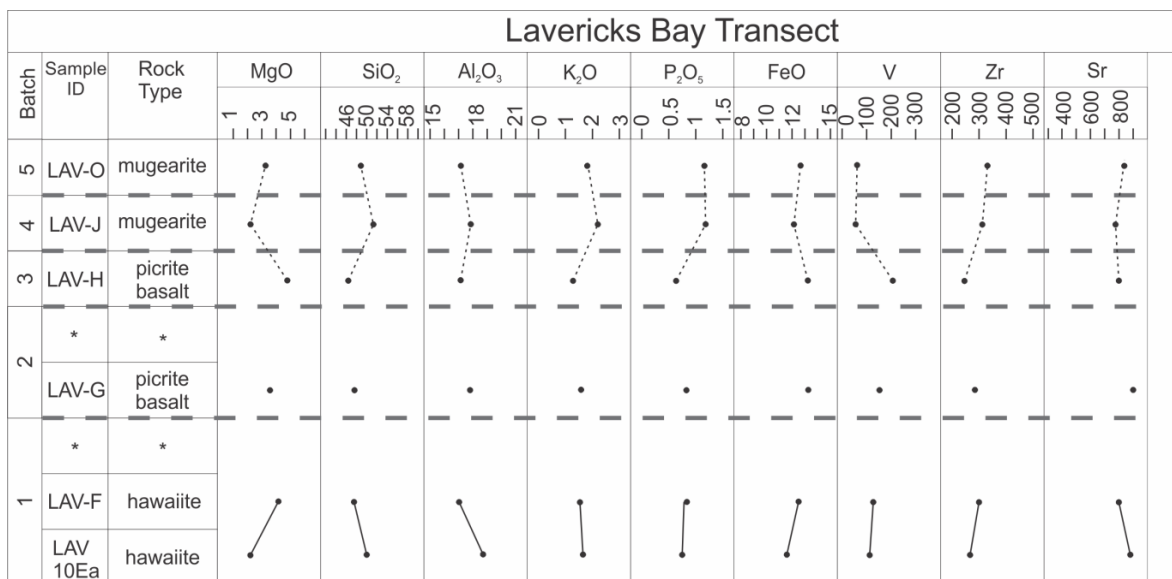
Figure 5.6: Lavericks Bay stratigraphic geochemical plot. Horizontal dashed lines divide batches, vertical solid lines relate flows within single batches, and vertical dashed lines show unrelated flows between two batches. Asterisks symbolize flows that are present in the stratigraphic sections but lack geochemical data.
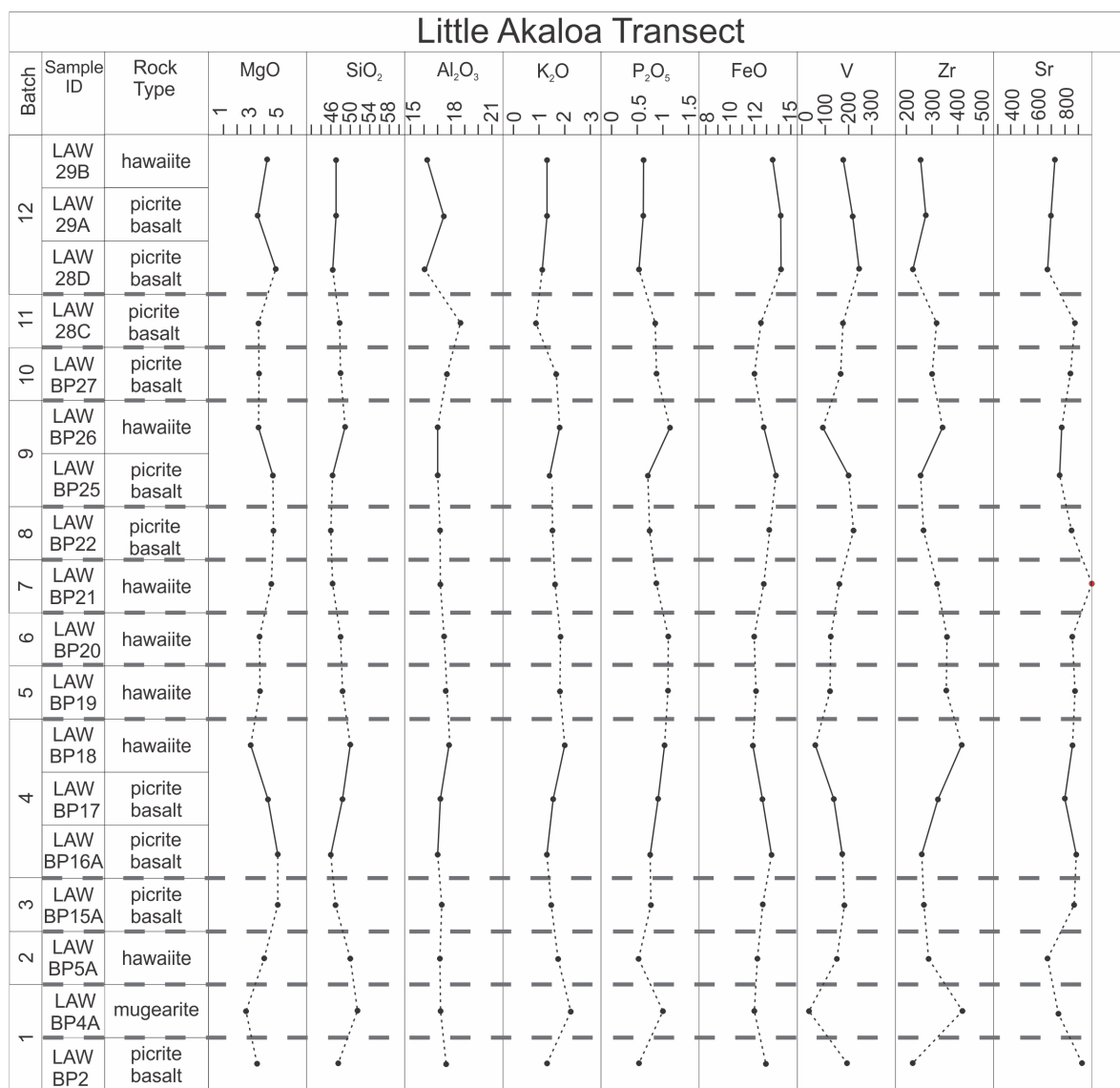
Figure 5.7: Little Akaloa Bay stratigraphic geochemical plot. Horizontal dashed lines divide batches, vertical solid lines relate flows within single batches, and vertical dashed lines show unrelated flows between two batches.

Menzies Bay (**Figure 5.3**).

Stony Bay (**Figure 5.2**) contains fifteen flows, and seven batches. Of the batches, only batch 2, 4, and 7 start with picrite basalt flows, the others start with hawaiites and mugearites. Batches are on average composed of two flows, however, batch 2 contains four flows, and batch 5 has three flows. These larger batches show the decreasing compatible elements, and increasing incompatible elements. Menzies Bay (**Figure 5.3**) contains fifteen flows and eleven batches. Most batches contained only one flow, with batch 2, 4, 8, and 10 consisting of two flows. Furthermore, batches 2 and 8 record a melt evolution of picrite basalt directly to mugearite. Lebons Bay (**Figure 5.4**) is composed of eight flows and five batches. Batch 1 is the most continuous, and is composed of three flows evolving from picrite to mugearite. The majority of the other batches are single flows, similar to Menzies Bay. Ducksfoot Bay (**Figure 5.5**) contains eight flows and five batches. Most of the batches are composed of two flows, however three of the batches (1, 3, and 5) start with hawaiite flows. Lavericks Bay (**Figure 5.6**) has eight flows, however only six flows were taken as samples during field work due to the missing two samples being too weathered. As such, batch 1 with two flows is the longest continuous batch represented by the data. Other batches are composed of single flows. Little Akaloa (**Figure 5.7**) contains eighteen flows and twelve batches. Only batches 4, 9 and 12 show continuous evolution between two or more flows, with the rest of the batches containing only one flow.

Common to all of the bays are the single flow batches, and none of the batches contain every rock type. Batches do not always start with a picrite, nor do they always

show a continuous evolution from picrite to hawaiite and mugearite flows. Rather, the batches jump from picrite to mugearite, or start with a hawaiite or mugearite flow.

Slight geochemical differences were observed between batches, however the UC XRF data does not provide the necessary trace elements for detailed comparison between individual flows. The comparative Menzies transect analyzed on the CC XRF, however, provides a more detailed selection of trace element geochemistry. As such, REE plots revealed that while flows within single transects are very similar geochemically, each batch has a unique range of REE concentration (**Figures 5.8, 5.9**).

Similarities and differences in geochemical ranges are observed for each bay transect. When comparing elements against SiO_2, the transects all fall within the same range of silica and the compared element (**Figure 5.10**, **5.11**). On the Total Alkali-Silica diagram, each bay seems to have a different slope on the evolutionary path it takes through the rock types. Within each rock type, however, the individual transects exhibit broadly similar geochemical values between transects, suggesting similar starting geochemical composition (**Figure 5.12**, **5.13**, **5.14**, **5.15**).

Electron Microprobe

Sample Preparation

The CAMECA SX50 Electron Microprobe at the University of Wisconsin-Madison was used to obtain mineral chemistries. Standards used are listed in Appendix II, Table 3B. The probe was calibrated to measure Si, Al, Na, Ca, K, Fe, and Sr for plagioclase, and Na, Mg, Cr, Mn, Ca, Ti, Si, Al, Fe, and Ni for olivine and pyroxene. The beam spot size was defocused at 10μm, with a beam intensity of 15kHz.
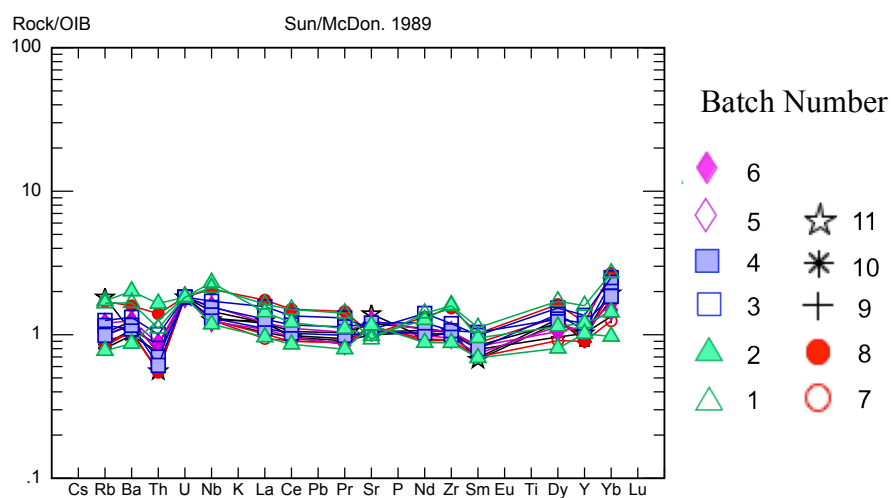
Figure 5.8: Spider diagram for Menzies Bay, plotted by individual magma batches (Sun and McDonough, 1989).
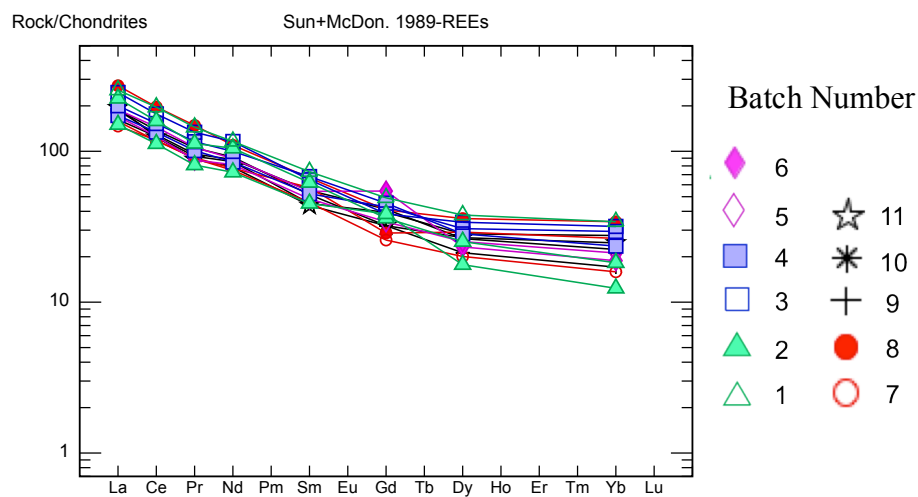
Figure 5.9: REE spider diagram for Menzies Bay, plotted by individual magma batches. The batches are mostly parallel to each other, with some variation in Gd and Dy, but total amount of elements are defined in each batch (Sun and McDonough, 1989).
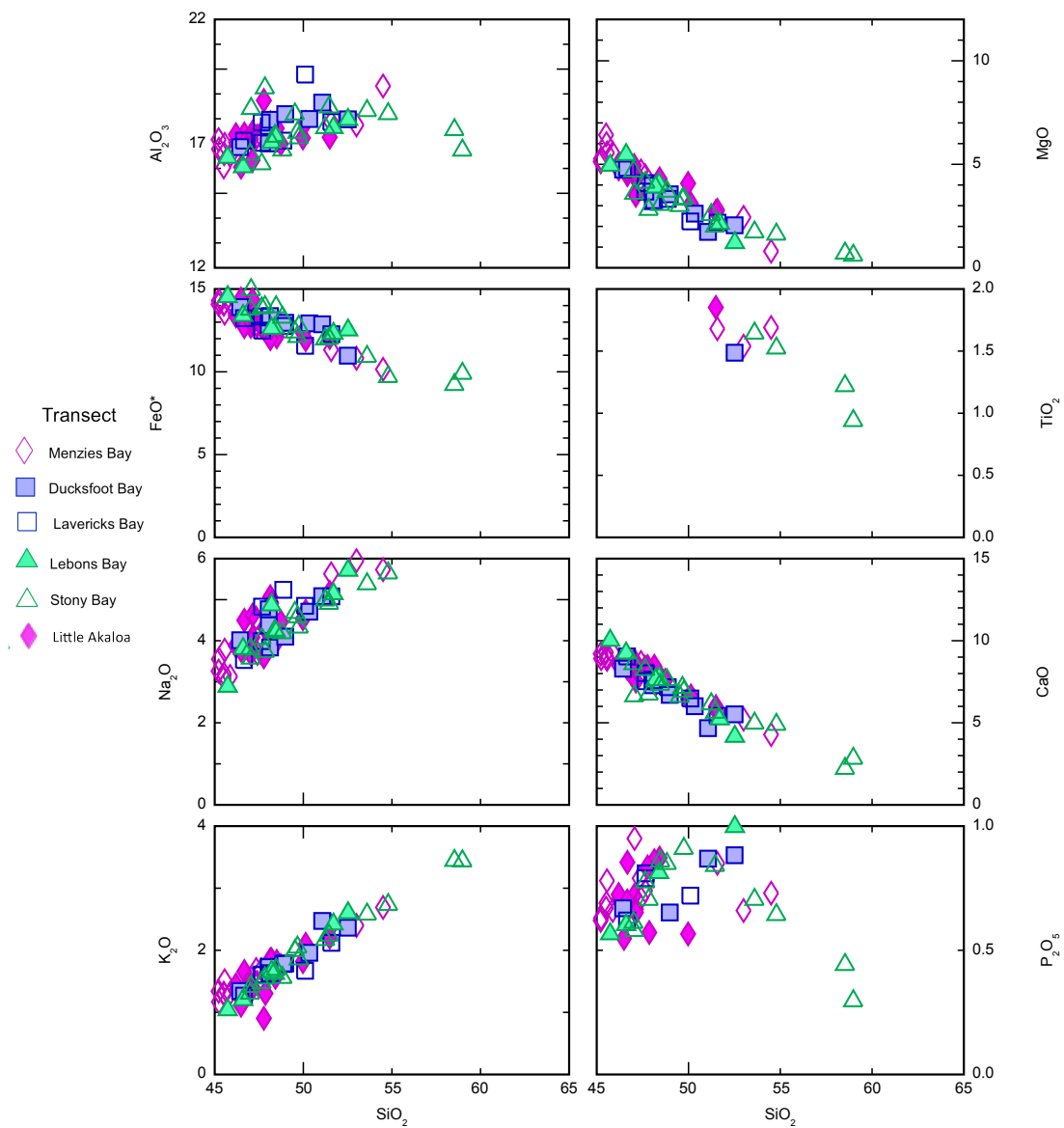
Figure 5.10: Harker Diagrams plotted by transect for all samples' bulk rock geochemistry.
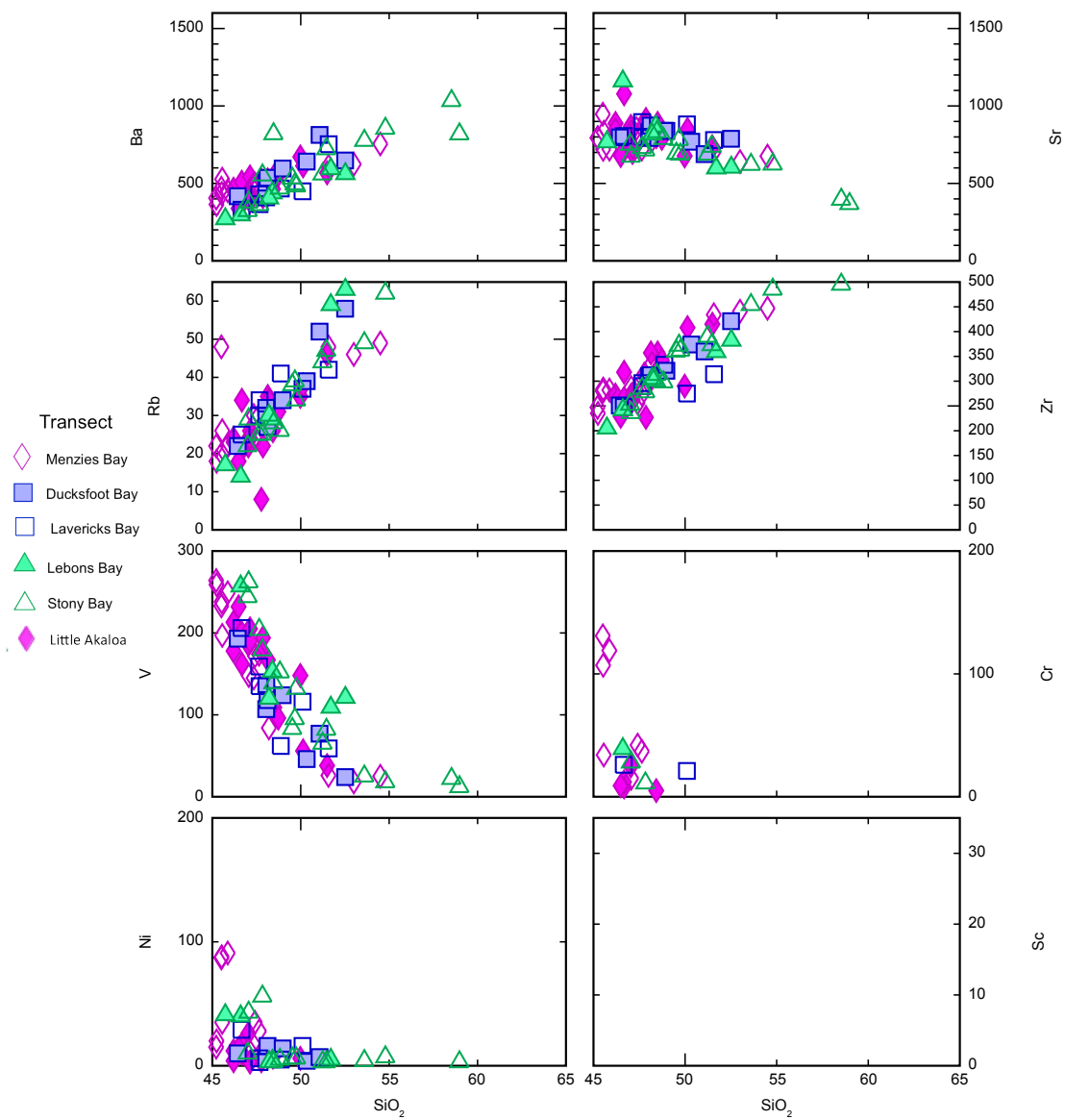
Figure 5.11: Harker Diagrams plotted by transect for all samples' bulk rock geochemistry. Sc was not recorded by the University of Canterbury XRF.
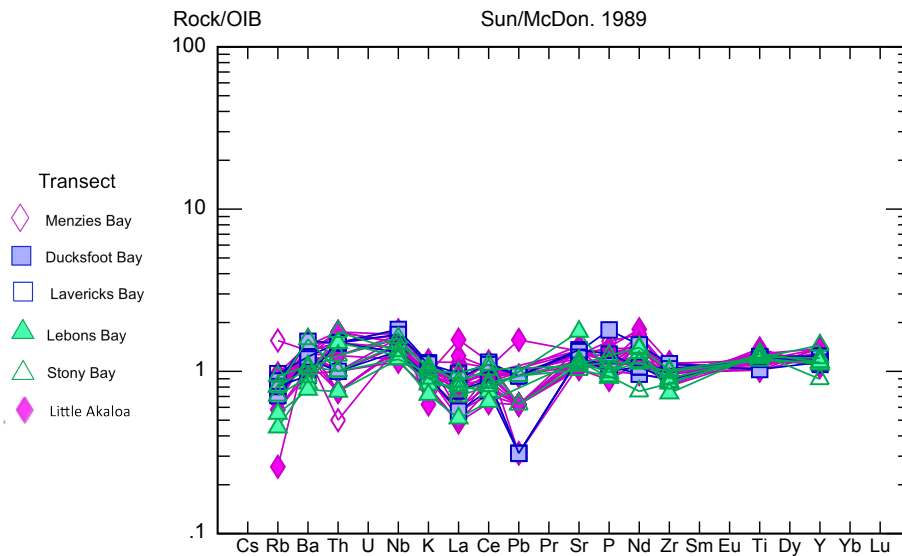
Figure 5.12: Spider diagram for every picrite flow, plotted by transect for all

samples' bulk rock geochemistry (Sun and McDonough, 1989).
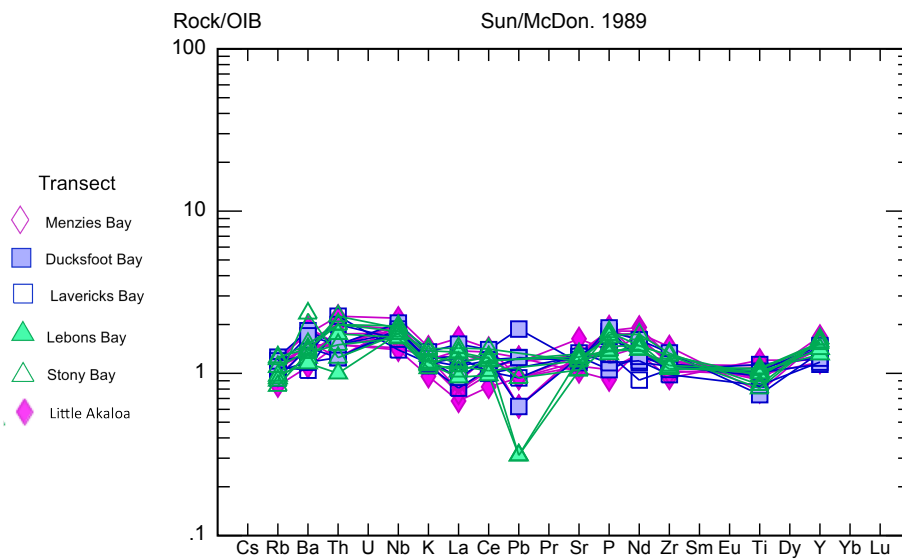
Figure 5.13: Spider diagram for every hawaiite flow, plotted by transect for all

samples' bulk rock geochemistry (Sun and McDonough, 1989).
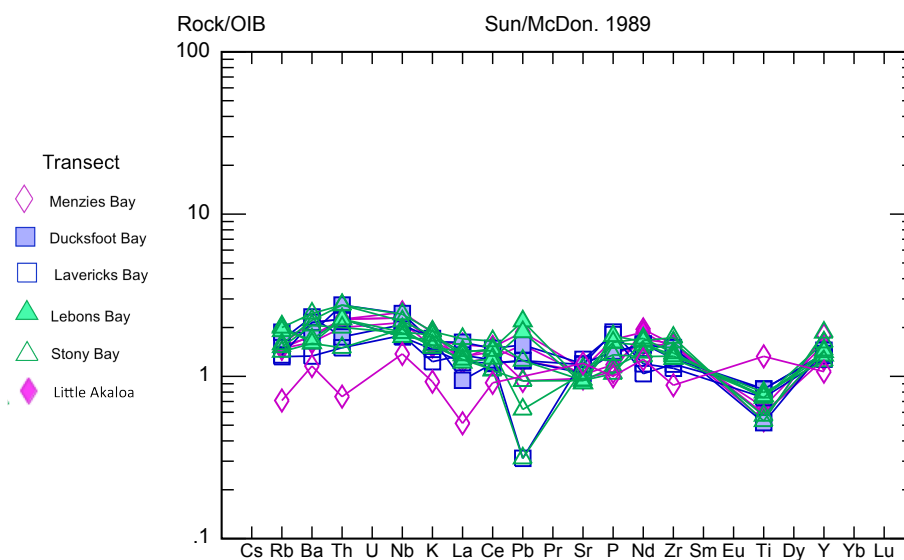
Figure 5.14: Spider diagram for every mugearite flow, plotted by transect for all samples' bulk rock geochemistry (Sun and McDonough, 1989).
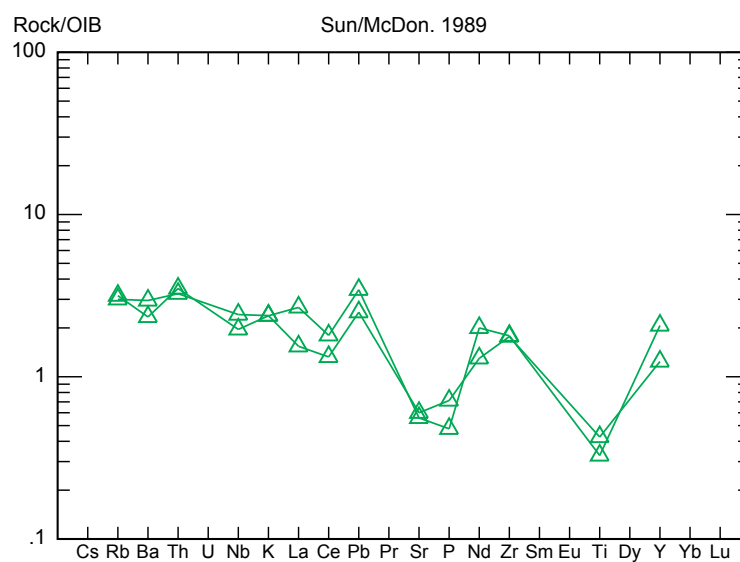
Figure 5.15: Spider diagram for every benmoreite flow (all from Stony Bay), plotted by transect for all samples' bulk rock geochemistry (Sun and McDonough, 1989).

Eleven samples were analyzed on the microprobe; eight picrites, and one representative hawaiite, mugearite, and benmoreite (**Table 5.1**). One picrite from each bay was chosen to investigate lateral changes in geochemistry between bays, and two additional picrites were chosen from the Little Akaloa transect to represent stratigraphic, or temporal, changes in geochemistry. While the selected hawaiite, mugearite, and benmoreite were chosen as the most representative samples of their chemistries, the samples are relatively more crystalline compared to others of the same rock type. This is due to needing phenocrysts for probe analysis, rather than groundmass.

Crystals were selected for probe analysis on the basis of phase, size, morphology, and mineral texture. Due to plagioclase displaying the most prominent textural features, the focus of the probe work was on plagioclase within the thin sections, however, selected samples were chosen for olivine and clinopyroxene analysis (**Table 5.1**). Furthermore, plagioclase was of special importance due to the ability to measure anorthite content in various places within the crystal, and relate this to magma evolution and fractionation trends. Olivine and clinopyroxene were analyzed to provide data for investigating the source magma, and the selected samples were chosen in order to represent the different rock types within the study area. Three points on each crystal were analyzed. Individual spots within the identified crystals were placed on the core of every crystal, and if size allowed, on the rim and halfway between the rim and the core. More point analyses were taken on crystals displaying prominent zoning patterns.

Similar to the bulk rock geochemistry, potential sources of error are sample alteration from weathering and machine error. The resulting data were sorted according to the total oxide percentages—data that did not fall within 1.5% of 100% of oxide totals

Flow	Rock type	Phenocryst %	Mineral Texture	Plag Analysis	Mafic Analysis
SB-34	Benmorite	6%	Sieved core, resorbed rim and melt inclusions	Yes	No
SB-18	Picrite	15-20%	Resorbed and patchy core	Yes	Yes
MBBP02	Picrite	10%	Zoned, sieved core, swallow tail, some melt inclusions	Yes	No
LAWBP28C	Picrite	12%	Zoned, sieved core, swallow tail	Yes	No
LAWBP15A	Picrite	10%	Sieved core, zoning, swallow tail	Yes	Yes
LAWBP2	Picrite	10%	Zoned, swallow tail	Yes	No
BRS2	Picrite	1-2%	Swallow tail, some resorbed core, melt inclusions	Yes	No
LLB21	Picrite	20%	Sieved, zoned, some resorbtion	Yes	No
Lav-J	Mugearite	12%	Sieved and patchy cores, inclusion trains, resorbed rim	Yes	Yes
Lav-C	Picrite	7%	Zoned, sieved cores, resorbtion and melt inclusions	Yes	Yes
Lav-10Ea	Hawaiite	25%	Sieved and patchy cores, zoning, melt inclusion, resorbtion	Yes	Yes

Table 5.1: List of the samples analyzed with the CAMECA SX50 microprobe. Phenocryst

percent and mineral textures were ascertained from microscopy.

(compared to the listed standards in Appendix II) were not used. Machine error depended on the microprobe count time. Generally, however, typical error in elemental analyses for feldspar was <1.5% for Na, Ca, Al, Si, and <15% for K and Fe, and +/-0.09 for An. For pyroxene, error was typically <3.0% for Si, Fe, Mg, <20% for Mn and Na, and >100% for Cr and Ni. For olivine, error was <1.5% for Si, Fe, Mg, <50% for Al, Ti, Mn, Ni, Cr, and ~100% for Na (Appendix II, Tables 4B-6B). Table 7B in Appendix II lists the sample name and points used according to the error listed.

Plagioclase Results

Data were initially recorded as oxide percentages, which were then converted into element weight percent and anorthite (An) content. Anorthite concentration is reflective of magma evolution. As a magma evolves in a closed system, it will decrease in anorthite and increase in albite. The resulting dataset was organized into three different categories for interpretation: 1) comparing points on all of the samples, thus comparing different bays and rock types represented by the samples; 2) comparing points only within a single sample to study the different crystal populations within a representative single thin section; and 3) comparing points within individual crystals.

Initially the data were plotted by rock type (**Figures 5.16, 5.17, 5.18**). These plots show a clustering of the analyses taken for anorthite content on the picrites, to hawaiites, mugearites, and benmoreites (**Tables 5.2**, **5.3**). Plagioclase crystals analyzed in picrites consistently have the highest concentration of iron (**Figure 5.17**) and the lowest of potassium (**Figure 5.18**). More evolved rock types (hawaiite, mugearite, and benmoreite) have relatively higher concentrations of potassium and lower concentrations of iron and
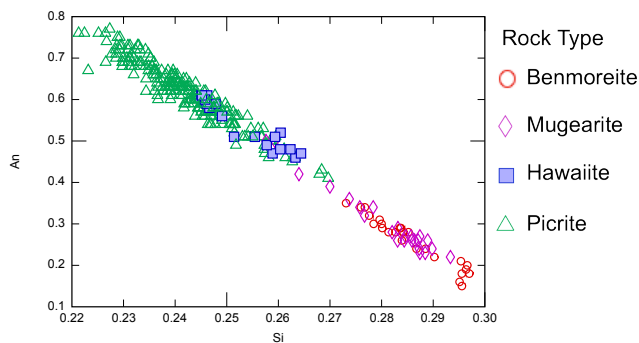
Figure 5.16: Anorthite content (An) vs Si content (wt%) of plagioclase microprobe data, plotted by rock type.
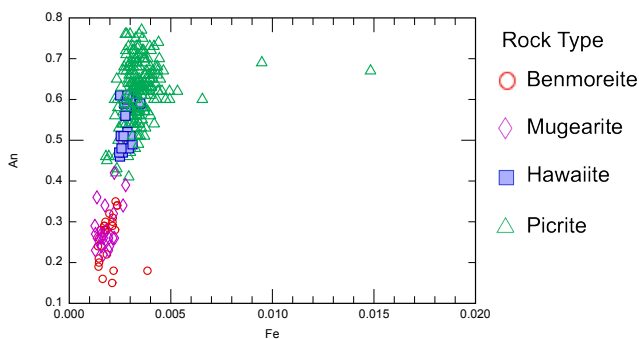
Figure 5.17: Anorthite content (An) vs Fe content (wt%) of plagioclase microprobe data, plotted by rock type.
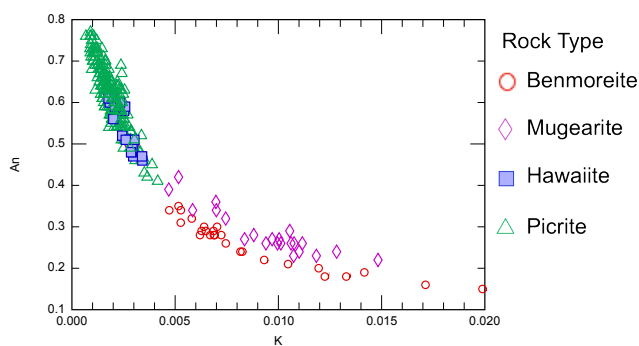
Figure 5.18: Anorthite content (An) vs K content (wt%) of plagioclase microprobe data, plotted by rock type.

Bay (sample ID)	Max An Content	Min An Content	Rock Type
Stony (SB18)	0.71	0.54	Picrite
Menzies (MBBP02)	0.72	0.46	Picrite
Ducksfoot (BRS02)	0.62	0.60	Picrite
Little Akaloa (LAW15A, LAWBP2, LAW28c)	0.77	0.41	Picrite
Lavericks (LAVC)	0.75	0.61	Picrite
Lebons (LLB21)	0.73	0.42	Picrite

Table 5.2: Anorthite content for each picrite sample.

Bay (sample ID)	Max An Content	Min An Content	Rock Type
Lavericks (LAV10EA)	0.61	0.46	Hawaiite
Lavericks (LAVJ)	0.50	0.22	Mugearite
Stony (SB34)	0.35	0.15	Benmoreite

Table 5.3: Anorthite content for the representative hawaiite, mugearite, and benmoreite samples.

anorthite. Plagioclase phenocrysts in the hawaiite flow (LAW10EA) overlap geochemically with picrite samples LLB21, MBBP07, and LAWBP2.

To investigate geochemical variations of picrites between bays, the different picrite samples were plotted against each other (**Figure 5.19**). Picrite samples plotted in **Figure 5.19** all display a negative linear trend with similar slopes of decreasing anorthite and increasing silica content. The specific range of anorthite content within the picrite samples have significant overlap, however there is some variability between the samples.

Each sample was then plotted individually to investigate geochemical processes that may be specific to individual bays. The plots are specific to individual samples, and are grouped according to the individual crystals analyzed (**Figures 5.20**, **5.21**, **5.22**, **5.23**, **5.24**, **5.25**, **5.26**, **5.27**, **5.28**, **5.29**, **5.30**).

Sample SB18 (**Figure 5.20**), which is a picrite flow of Stony Bay, contains three distinct crystals. There is limited data plotted, relative to the other samples, due to machine error and sample weathering affecting the number of acceptable data points.

Sample MBBP02 (**Figure 5.21**), representing the picrite flows of Menzies Bay, contains fifteen distinct crystals and a negative linear trend between anorthite and silica. The crystals appear to fall into two distinct groups along the negative linear trend of anorthite and silica, one group plotting in Si ranges of 0.23-0.24 and the other in Si ranges of 0.242-0.26. Many of the crystals remain segregated within these two groups, however, two crystals overlap between the two groups. This distinction between groups could be reflective of differences in evolution, or could be a product of machine error due to Si error being +/- 0.015 (1.5%) and An error being +/- 0.09.

Sample LLB21 (**Figure 5.22**), which is a picrite flow of Lebons Bay, contains
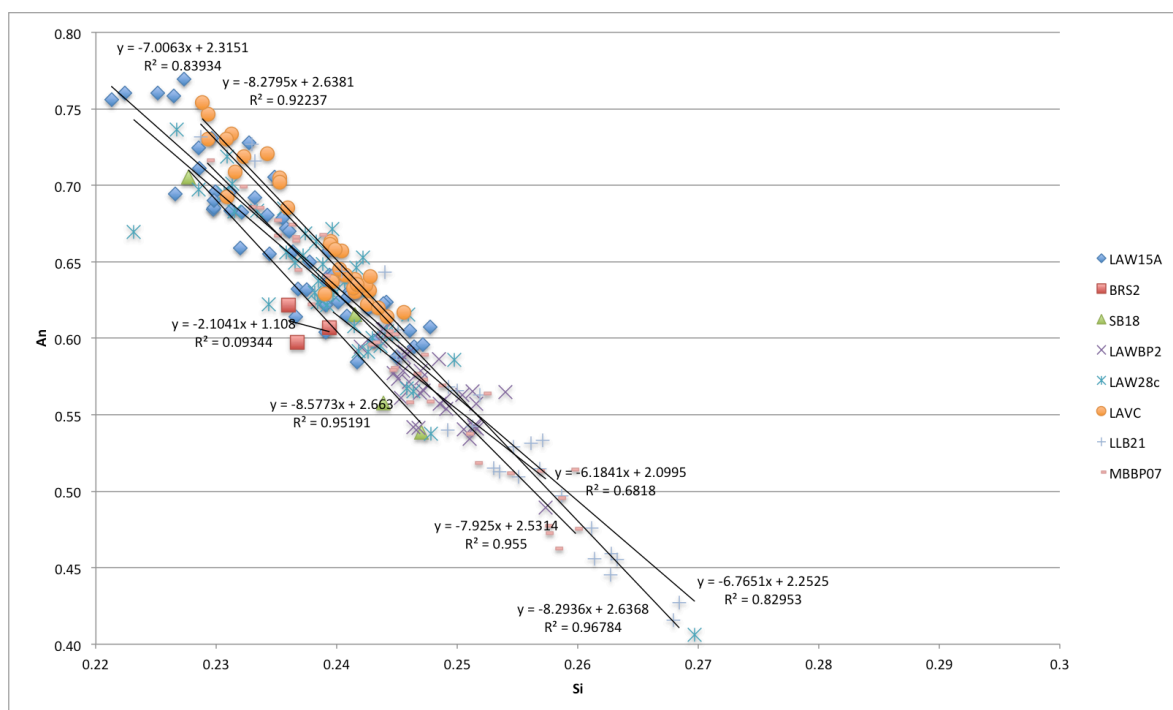
Figure 5.19: Anorthite (An) vs Si (wt%) plot for the picrite microprobe samples. Note the similar slopes of the trendlines for each of the samples, suggesting similar fractionation processes. The trendline for BRS2 is the only outlier, containing inconsistent data relative to the other samples due to the limited probe analyses.
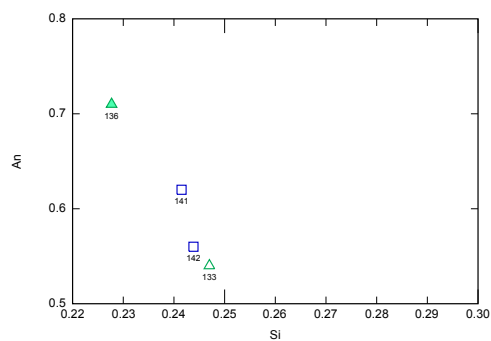
Figure 5.20: An vs Si (wt%) plot for sample SB18, a picrite from Stony Bay. Each symbol represents an individual crystal. Limited data due to microprobe error.
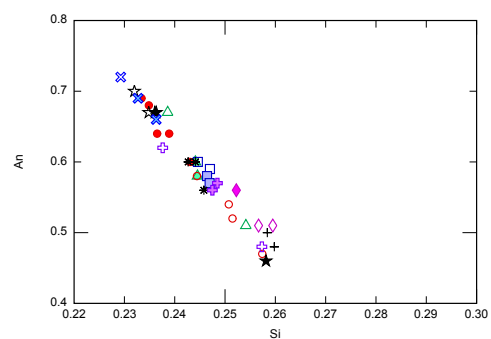
Figure 5.21: An vs Si (wt%) plot for sample MBBP02, a picrite from Menzies Bay. Each symbol represents an individual crystal.
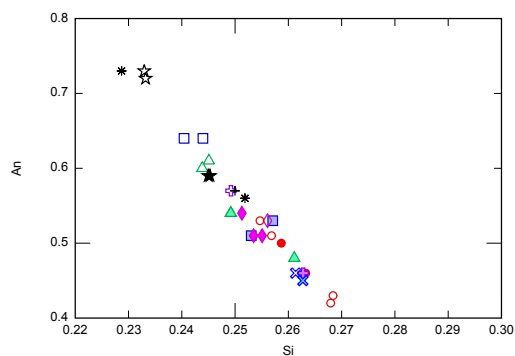
Figure 5.22: An vs Si (wt%) plot for sample LLB21, a picrite from Lebons Bay. Each symbol represents an individual crystal.
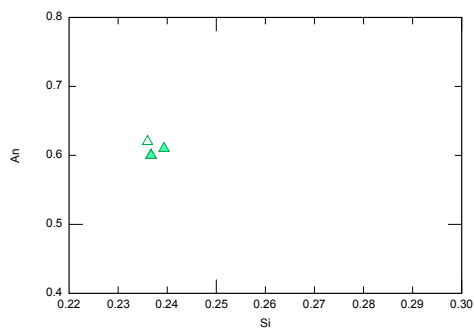
Figure 5.23: An vs Si (wt%) plot for sample BRS2, a picrite from Ducksfoot Bay. Each symbol represents an individual crystal. Limited data due to microprobe error and few crystals.
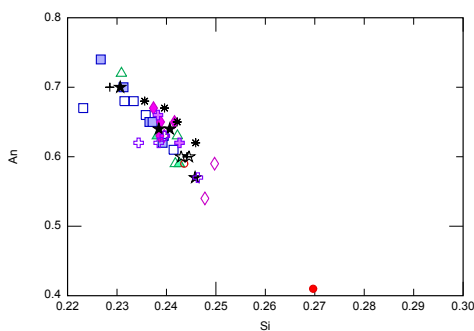
Figure 5.24: An vs Si (wt%) plot for sample LAW28c, a picrite from the top of a stratigraphic section in Little Akaloa. Each symbol represents an individual crystal within this sample.
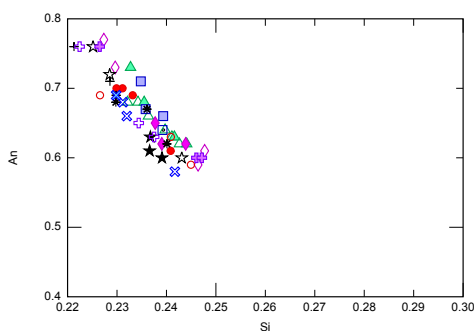
Figure 5.25: An vs Si (wt%) plot for sample LAW15A, a picrite from the middle of a stratigraphic section in Little Akaloa. Each symbol represents an individual crystal within this sample.
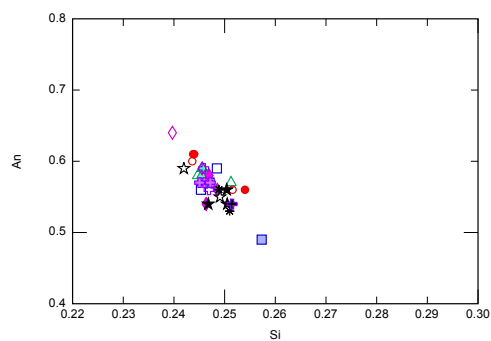
Figure 5.26: An vs Si (wt%) plot for sample LAWBP2, a picrite from the bottom of a stratigraphic section in Little Akaloa. Each symbol represents an individual crystal within this sample.
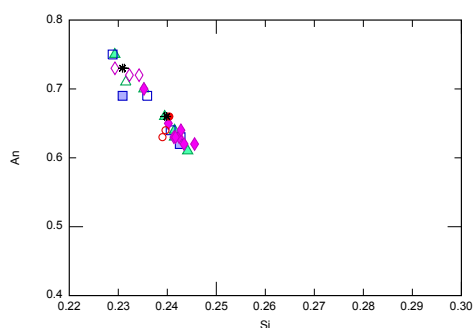
Figure 5.27: An vs Si (wt%) plot for sample LAVC, a picrite from Lavericks Bay. Each symbol represents an individual crystal.
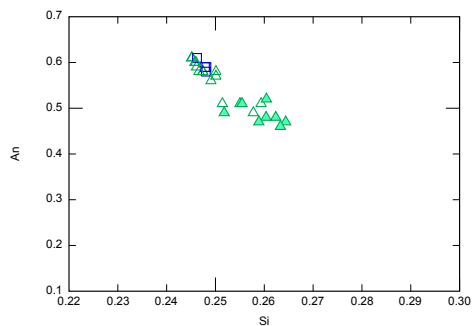
Figure 5.28: An vs Si (wt%) plot for sample LAV10EA, a hawaiite from Lavericks Bay. Each symbol represents an individual crystal.
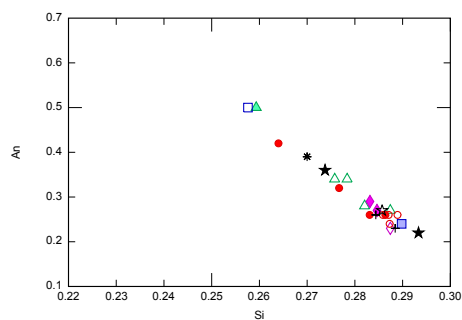
Figure 5.29: An vs Si (wt%) plot for sample LAVJ, a mugearite from Lavericks Bay. Each symbol represents an individual crystal.
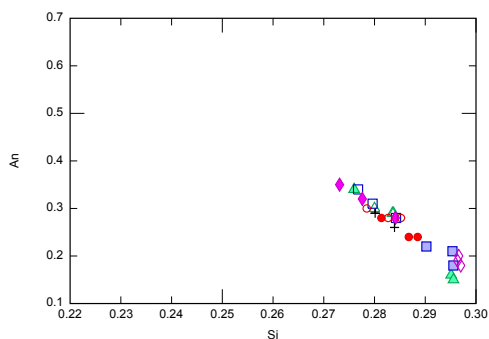
Figure 5.30: An vs Si (wt%) plot for sample SB34, a benmoreite from Stony Bay. Each symbol represents an individual crystal.

fourteen individual crystals along a negative linear trend between anorthite and silica. The trend is fairly continuous, however two crystals contain uncommon high anorthite, low silica geochemistry.

Sample BRS2 (**Figure 5.23**), which is a picrite flow of Ducksfoot Bay, contains two analyzed crystals. Like SB18 (**Figure 5.20**), machine error and weathering reduced the number of acceptable data points, however both crystals display a range of anorthite and silica.

Samples LAW28c (**Figure 5.24**), LAW15A (**Figure 5.25**), and LAWBP2 (**Figure 5.26**) are all picrite samples taken from the top, middle and bottom (respectively) of the stratigraphic section within Little Akaloa. These samples all plot within a similar anorthite range. Individually, each sample plots crystals in a continuous, geochemically overlapping group. The samples do not show significant distinctions between different crystals.

Sample LAVC (**Figure 5.27**), representing the picrite flows of Lavericks Bay, has ten crystals within two distinct groups. One group plots between Si content 0.225-0.235, and the other Si content of 0.239-0.248, similar to MBBP02 (**Figure 5.21)**. Again, these two groups could be reflective of differences in evolution, or could be a product of machine error.

Sample LAV10EA (**Figure 5.28**), representing the hawaiite flows, plots fourteen crystals in two geochemical groups along the anorthite vs silica graph. These groups plot in between Si concentrations of 0.24-0.25 and 0.26-0.27. Like MBBP02 and LAVC, these groups could be indicative of differences in evolution, or could be reflective of machine error.

Sample LAVJ (**Figure 5.29**), representative of the mugearite flows, plots twelve crystals in a fairly continuous linear trend on the anorthite vs silica graph. Along this continuous trend, some crystals show geochemical variation within their individual structure.

Sample SB34 (**Figure 5.30**), representative of the benmoreite flows, plots fifteen crystals all of lower anorthite and higher silica concentration. The specific crystals within this sample show a continuous range of anorthite and silica within their structure.

Specific crystals that showed a range of geochemical composition were then plotted separately to investigate geochemical processes recorded within the individual mineral chemistries. In order to plot this data, there had to be multiple points existing for the crystal in question. Due to machine error reducing the number of acceptable data points, only six crystals contain sufficient mineral chemistry transects (**Table 5.4**). These phenocrysts were then plotted to show spatial geochemical variations from rim to core of the crystal (**Figures 5.31**, **5.32**, **5.33**, **5.34**, **5.35**, **5.36**). Phenocrysts expressed both normal zoning and reverse zoning (**Table 5.4**). Data is presented and discussed here under the assumption that the machine error did not significantly alter the results, however the data should be viewed skeptically due to each analysis containing a +/-0.09 An error. All data points fall within an overlapping range when considered with the An error.

Crystal MBBP02-15 (**Figure 5.31**) displays reverse zoning from core to rim, showing a reverse pattern between probe spot 511 and 510. Crystal MBBP02-23 (**Figure 5.32**) displays reverse zoning from core to rim, containing a reverse zoning pattern from probe spot 523 and 522. Crystal LAW15A-10 (**Figure 5.33**), displays normal zoning

Bay	Sample ID-Crystal #	Zoning
Menzies	MBBP02-15	Reverse
Menzies	MBBP02-23	Reverse
Little Akaloa	LAW15A-10	Normal
Little Akaloa	LAW15A-12	Reverse
Lebons	LLB21-22	Reverse
Lavericks	LAVC-12	Reverse

Table 5.4: Table of the samples containing mineral geochemical transects from rim to core, and the zoning that they display.
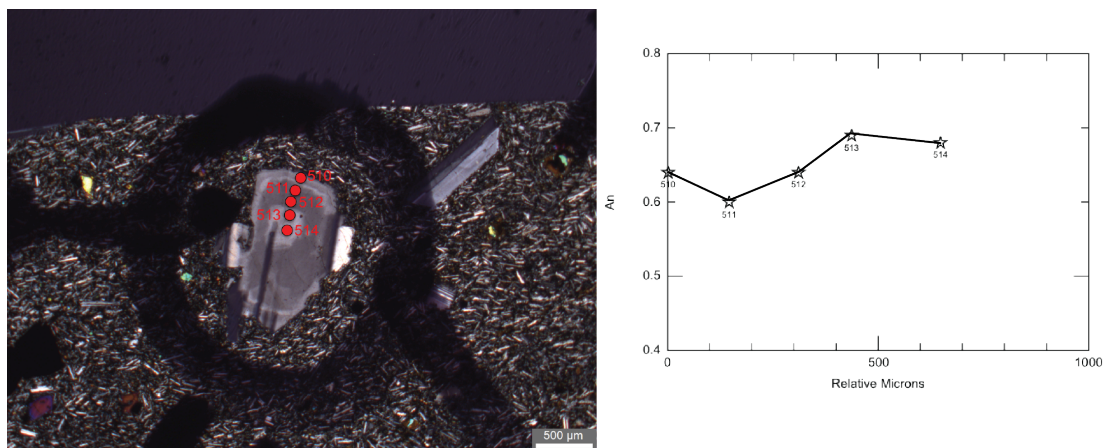
Figure 5.31: MBBP02-15 crystal transect from rim to core. Relative Microns starts at the rim.
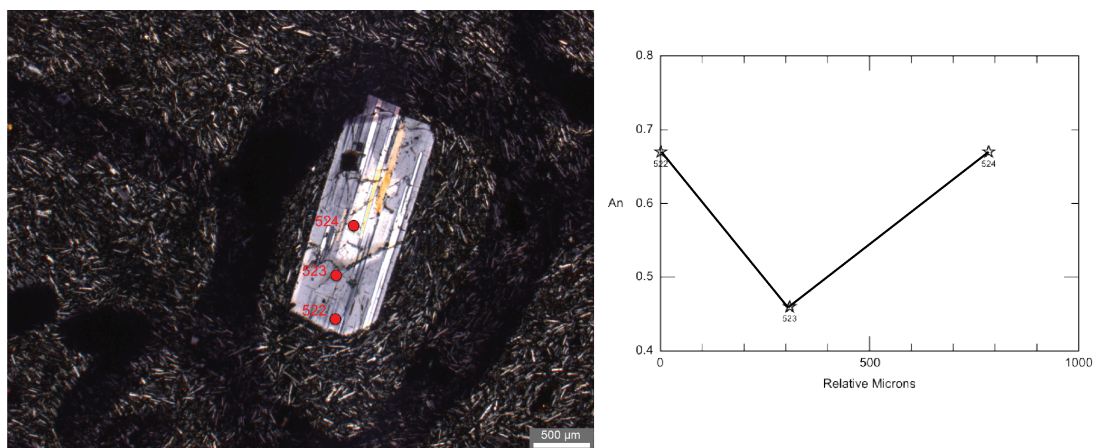
Figure 5.32: MBBP02-23 crystal transect from rim to core. Relative Microns starts at the rim.
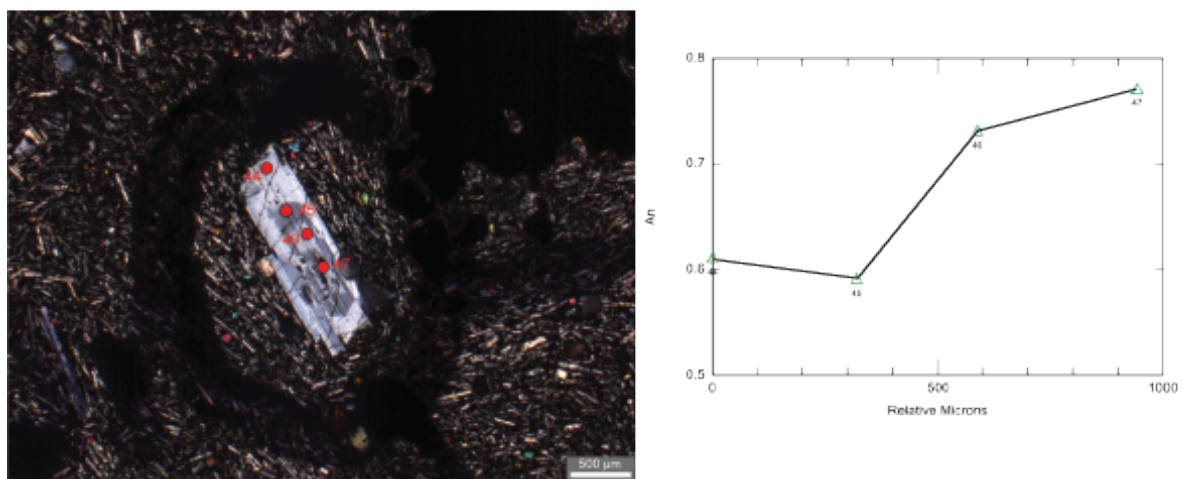
Figure 5.33: LAW15A-10 crystal transect from rim to core. Relative Microns starts at the rim.
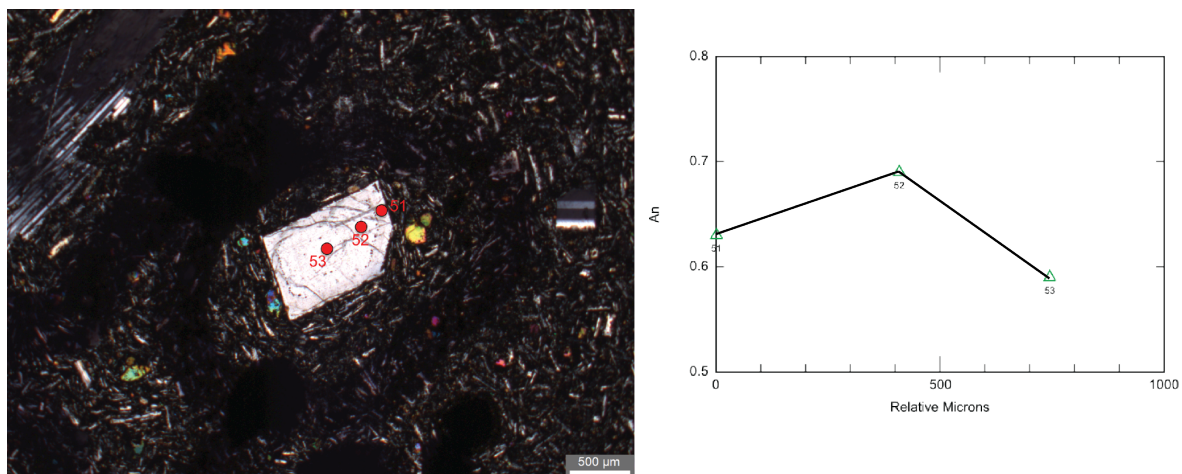
Figure 5.34: LAW15A-12 crystal transect from rim to core. Relative Microns starts at the rim.
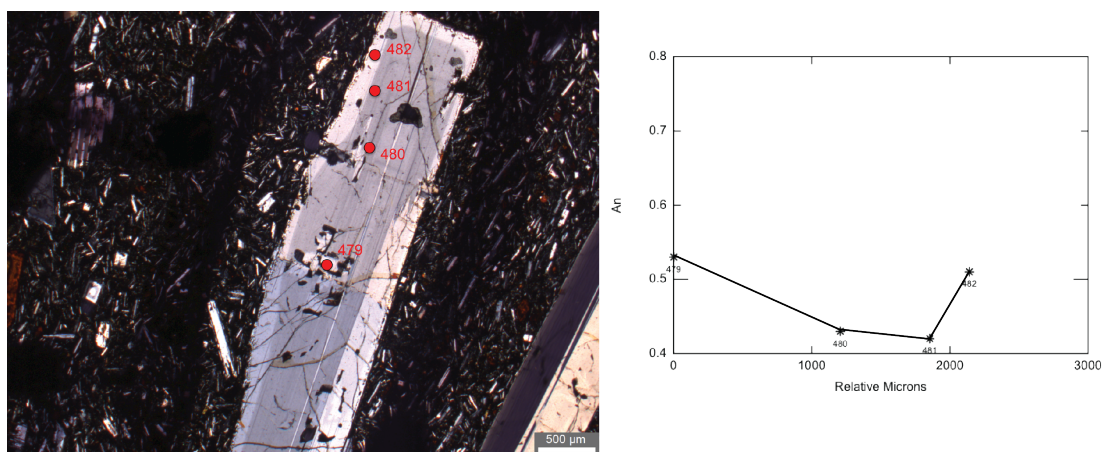
Figure 5.35: LLB21-22 crystal transect from core to rim. Relative Microns starts at the rim.
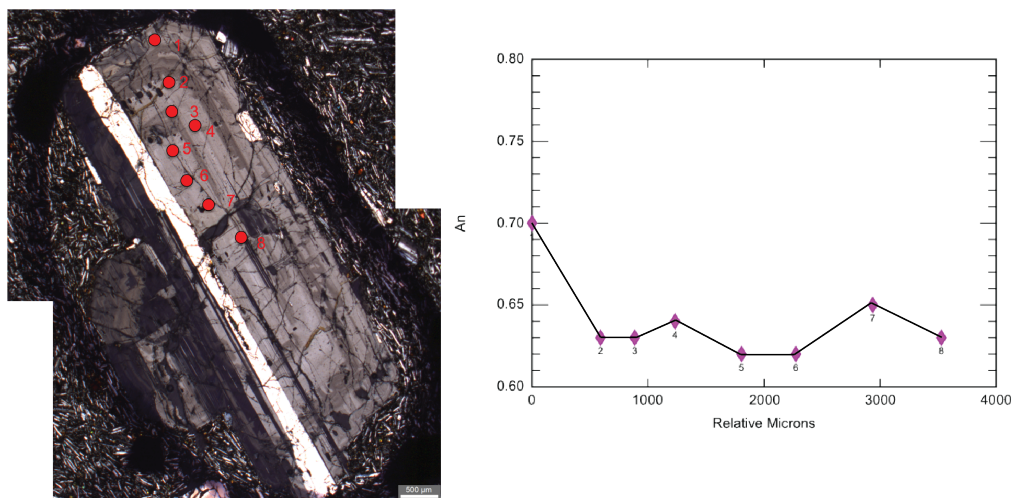
Figure 5.36: LAVC-12 crystal transect from rim to core. Relative Microns starts at the rim.

from core to rim. There is slight reverse zoning between probe spots 45 and 44, however

the anorthite composition is similar at both spots. Crystal LAW15A-12 (**Figure 5.34**)

displays reverse zoning from core to rim, showing reverse zoning patterns between probe

spots 53 and 52. These three probe spots on LAW15A-12 are also separated by inclusion

trains. Crystal LLB21-22 (**Figure 5.35**) displays oscillatory zoning from core to rim,

containing a reverse zoning pattern in between probe spots 481 and 482. Crystal LAVC-

12 (**Figure 5.36**) contains reverse zoning between probe spots 8 and 7, 5 and 4, and 2 and

1.

Mafic Mineral Results

      Mafic mineral data were categorized according to whether the probe analysis was

conducted on olivine or clinopyroxene (**Table 5.5**). Crystals were chosen solely on the

basis of weathering, selectively choosing the least iddingzitised olivines and the least

weathered clinopyroxenes. As such this data could contain a sample bias against size and

morphology. For each mafic mineral, the Mg# was calculated by the formula:

$$\frac{MgO}{MgO + FeO} \times 100$$

 Of the analyzed olivines, the phenocrysts from the picrite samples displayed Mg#

ranging from 60-77, and Mg# of 29-35 for the mugearite (**Table 5.6**). The hawaiite did

not contain any identifiable olivine phenocrysts for probe analysis. From the

clinopyroxene analysis, phenocrysts in the picrite flows yielded Mg# ranging from 60-74,

the phenocryst in the hawaiite flow yielded Mg# 56, and the phenocrysts in the mugearite

yielded Mg# 57 (**Table 5.7**). Between the olivine and clinopyroxene analyses there is

some variability in the data, specifically with the mugearite flow yielding Mg#s of 29-35

(olivine analyses) and 57 (clinopyroxene analyses). The variability could reflect error

Bay	Sample ID	Rock Type	Olivine	Clinopyroxene
Lavericks	LAV10EA-1	hawaiite	no	yes
Little Akaloa	LAW15A-1	picrite	yes	no
Little Akaloa	LAW15A-3	picrite	yes	no
Little Akaloa	LAW15A-8	picrite	no	yes
Little Akaloa	LAW15A-12	picrite	yes	no
Little Akaloa	LAW15A-13a	picrite	yes	no
Little Akaloa	LAW15A-18	picrite	yes	no
Little Akaloa	LAW15A-21	picrite	yes	no
Little Akaloa	LAW15A-23	picrite	yes	no
Lavericks	LAVJ-4	mugearite	no	yes
Lavericks	LAVJ-16	mugearite	yes	no
Lavericks	LAVJ-21	mugearite	yes	no
Stony	SB18-4	picrite	yes	no
Stony	SB18-8	picrite	no	yes
Stony	SB18-9	picrite	no	yes
Stony	SB18-16	picrite	no	yes
Stony	SB18-21	picrite	yes	no
Stony	SB18-27	picrite	no	yes
Lavericks	LAVC-7	picrite	yes	no
Lavericks	LAVC-10	picrite	yes	no
Lavericks	LAVC-16	picrite	yes	no

Table 5.5: List of all of the samples analyzed with the probe for mafic minerals.

Bay	Sample ID	Rock Type	100xMg# (phenocryst)
Little Akaloa	LAW15A-1	picrite	73.0
Little Akaloa	LAW15A-3	picrite	64.6
Little Akaloa	LAW15A-12	picrite	60.0
Little Akaloa	LAW15A-13a	picrite	60.7
Little Akaloa	LAW15A-18	picrite	66.7
Little Akaloa	LAW15A-21	picrite	57.4
Little Akaloa	LAW15A-23	picrite	63.6
Lavericks	LAVJ-16	mugearite	34.3
Lavericks	LAVJ-21	mugearite	29.9
Stony	SB18-4	picrite	72.3
Stony	SB18-21	picrite	70.9
Lavericks	LAVC-7	picrite	65.8
Lavericks	LAVC-10	picrite	60.8
Lavericks	LAVC-16	picrite	76.6

Table 5.6: List of the samples containing olivine phenocrysts, and their Mg# obtained from the probe.

Bay	Sample ID	Rock Type	100xMg# (phenocrysts)
Lavericks	LAV10EA-1	hawaiite	56.4
Little Akaloa	LAW15A-8	picrite	60.7
Lavericks	LAVJ-4	mugearite	57.1
Stony	SB18-8	picrite	61.0
Stony	SB18-9	picrite	61.0
Stony	SB18-16	picrite	61.5
Stony	SB18-27	picrite	73.4

Table 5.7: List of the samples containing clinopyroxene phenocrysts, and their Mg# obtained from the probe.

within the calculation, or it could reflect different times of fractionation between the clinopyroxene and olivine. If the latter scenario, then the Mg#s record the evolution of the magma through time relative to the other mafic minerals.

Chapter Summary

Both the bulk rock data and the microprobe data reveal geochemical similarities and differences between the six bays within the study area, as well as geochemical jumps within individual bays, samples, and minerals (**Table 5.8**). These similarities imply a common origin, while the differences imply different evolutionary history between bays, and between batches within single bays. The geochemical similarities between bays are also reflected in the mafic mineral probe data with the Mg#s yielding similar ranges. The geochemical differences between bays are also reflected in the microprobe data taken on plagioclase phenocrysts from the picrite samples of each bay. Each plagioclase probe analysis taken on a picrite flow plots similar to the other picrite plagioclase analyses, however each bay contains a specific anorthite range.

Bulk rock data reveals element concentration jumps indicative of multiple evolutionary magma batches within each bay. These geochemical jumps are also recorded on the micro scale within geochemical transects taken on individual plagioclase phenocrysts. Reverse zoning within the plagioclase crystals is similar to the geochemical jumps observed between two successive batches. These geochemical jumps, both in bulk rock and microprobe data, imply a process other than continuous magma evolution, such as a new melt with different geochemistry being introduced to the present, evolving, magma (**Table 5.9**).

Data Type	Similarities between Bays	Differences between Bays
Bulk Rock Geochemistry	• Geochemical cycles from picrite-mugearite or benmoreite within individual bay transects • Parallel trends within spider diagrams • Similar geochemistry values for each rock type • Linear trends in harker diagrams	• Geochemical cycles within bay transects evolve to different degrees within picrite-benmoreite rock types
Mineral Chemistry by Bay	• An concentration for picrites range from 0.41-0.77 • Slope of An concentration for each picrite is similar • Evolved rock types (hawaiite, mugearite, benmoreite) show consistently lower An concentrations ranging from 0.15-0.61	• An concentration for each bay is slightly different within the given range for picrites • Samples for Menzies Bay (MBBP02) and Lavericks Bay (LAVC, LAV10EA) show distinct groups of crystals, implying discontinuous evolution between crystals • Samples for Lebons (LLB21), Ducksfoot (BRS2), Stony (SB18, SB34), Little Akaloa (LAW28c, LAW15A, LAWBP2), and Lavericks (LAVJ) show continuous evolution between crystals
Mineral Chemistry by Crystal	• Reverse zoning is recorded in most individual plagioclase analysis (MBBP02-15, MBBP02-23, LAW15A-12, LLB21-22, LAVC-12) • Mg#s fall in similar ranges for picrites	• Normal zoning in LAW15A-10

Table 5.8: List of the similarities and differences between bays for each of the geochemical analyses.

Bay	Sample ID	Rock Type	Crystals	Mineral Transect?	Observation	Interpretation
Stony	SB18	Picrite	3		Each crystal contains unique An values (**Figure 5.17**).	Different populations of plagioclase.
Menzies	MBBP02	Picrite	15	MBBP02-15 (**Figure 5.28**), MBBP02-23 (**Figure 5.29**)	Crystals separate into two individual groups(**Figure 5.18**). Reverse Zoning in both crystal transects (**Figures 5.28**, **5.29**).	Different populations of plagioclase, complex magma evolutionary history.
Lebons	LLB21	Picrite	14	LLB21-22 (**Figure 5.32**)	Continuous range of An values (**Figure 5.19**). Reverse zoning in crystal transect (**Figure 5.32**).	Single population of plagioclase, but complex magma evolutionary history.
Ducksfoot	BRS02	Picrite	2		The two crystals contain unique An values (**Figure 5.20**).	Different populations of plagioclase.
Lavericks	LAVC	Picrite	10	LAVC-12 (**Figure 5.33**)	Crystals separate into two individual groups (**Figure 5.25**). Reverse zoning in crystal transect (**Figure 5.33**).	Different populations of plagioclase, and complex magma evolutionary history.
Little Akaloa	LAW15A	Picrite	16	LAW15A-10 (**Figure 5.30**), LAW15A-12 (**Figure 5.31**)	Continuous range of An values (**Figure 5.23**). Both normal (**Figure 5.30**) and reverse (**Figure 5.31**) zoning.	Single population of plagioclase, but complex magma evolutionary history.
Little Akaloa	LAWBP2	Picrite	14		Continuous range of An values (**Figure 5.24**).	Single population of plagioclase, continuous evolution.
Little Akaloa	LAW28c	Picrite	15		Continuous range of An values (**Figure 5.22**).	Single population of plagioclase, continuous evolution.
Lavericks	LAV10EA	Hawaiite	14		Crystals separate into two individual groups (**Figure 5.26**).	Different populations of plagioclase.
Lavericks	LAVJ	Mugearite	12		Continuous range of An values (**Figure 5.27**).	Single population of plagioclase, continuous evolution.
Stony	SB34	Benmoreite	15		Continuous range of An values (**Figure 5.21**).	Single population of plagioclase, continuous evolution.

Table 5.9: List of the microprobe samples, data observations, and interpretations for each sample.

Chapter VI: Discussion

Introduction

This chapter provides a discussion of petrographic and geochemical data in order to investigate the source of the Akaroa Volcanic System magma, and the processes the melt experienced pre-eruption. By considering bulk rock and microprobe geochemical data together, parent melt composition and formation depth are investigated, and four models for crustal processes are presented and discussed. There are many questions associated with each model, therefore steps regarding the future work needed to test the proposed hypotheses are also contained within this chapter.

Source

Bulk rock data (**Figure 6.1**) confirms an intraplate origin of the Akaroa lava flows (Hoernle et al., 2006, Timm et al., 2009). In the study area, picrites are the most primitive melt. As such, if it is assumed that the most primitive magma represented in the bulk rock data is the closest representation of the parent magma, then the picrites in each transect provide insight into the geochemistry of the parent melt. However, the geochemical variation in the plagioclase mineral chemistries from bay to bay suggest that crustal processes have influenced the geochemistry of each transect relative to the original source composition (**Table 5.2**, **Figure 5.19**). These variations could be due to different degrees of partial melting, crustal assimilation, and ascent rate. Due to such geochemical differences, the picrites, while most representative of the most primitive melt, are not likely the source magma. Furthermore, geochemical data from past Frontiers Abroad field camps collected outside this project's study area, but within Stony Bay, reveal the
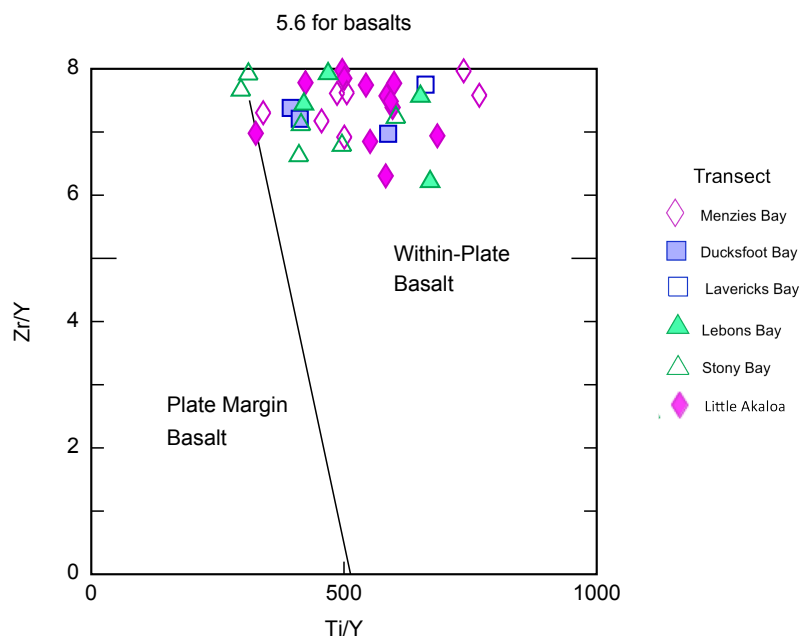
Figure 6.1: Discriminant basalt diagram of data plotted by transect. Results are congruent with other discriminant basalt diagrams, agreeing with past studies (Timm et al., 2009, Hoernle et al., 2006) identifying the Akaroa Volcanic Complex as an intraplate volcanic feature (Pearce and Gale, 1977).

presence of four nephelinite flows. These nephelinites have not been observed anywhere else on the peninsula. However active research is being conducted to investigate their origin and characteristics (Kroner, 2016). The nephelinites are geochemically much more primitive than all of the other samples within the six transects studied in this project (**Figure 6.2**, **6.3, 6.4**). The low Rb, Ba and high Ni, Cr, and Mg# within the nephelinite flows are indicative of a primitive melt, while Zr values greater than 100ppm suggests crustal assimilation within the melt. Despite crustal input, the nephelinite flows may represent the most primitive chemistry of the Akaroa Volcanic Complex. Non-linear trends in the Harker diagrams (**Figure 6.2**, **6.3**) of FeO, TiO_2, NaO_2, K_2O, Ba, Rb, Zr, and V between the nephelinites and the other rock types, however, suggest that the nephelinites are not related to the other flows. As such, the picrites are the closest proxy to the parent melt.

Based on the microprobe analysis of olivine and clinopyroxene, the mineral chemistry and the bulk rock chemistry were used together as geothermal barometers to obtain pressures and temperatures of formation. It is assumed that the minerals formed in equilibrium with the melt at that time, so by using the aphyric bulk rock data as a proxy for the liquid chemistry one can find the temperature of formation (Purtirka et al., 2003). Clinopyroxene was the only mineral used to calculate a pressure. The geothermal barometry analysis was conducted through a provided spreadsheet from the authors of Purtirka et al. (2003) and Nimis (1999), using formulas described in these papers. Within the picrites, olivine phenocrysts yielded an average formation temperature of 1069°C, and clinopyroxene a formation temperature of 1046°C and an average pressure of 6.2kbars. Not included in the above average was one measurement (LAW15A-8) on
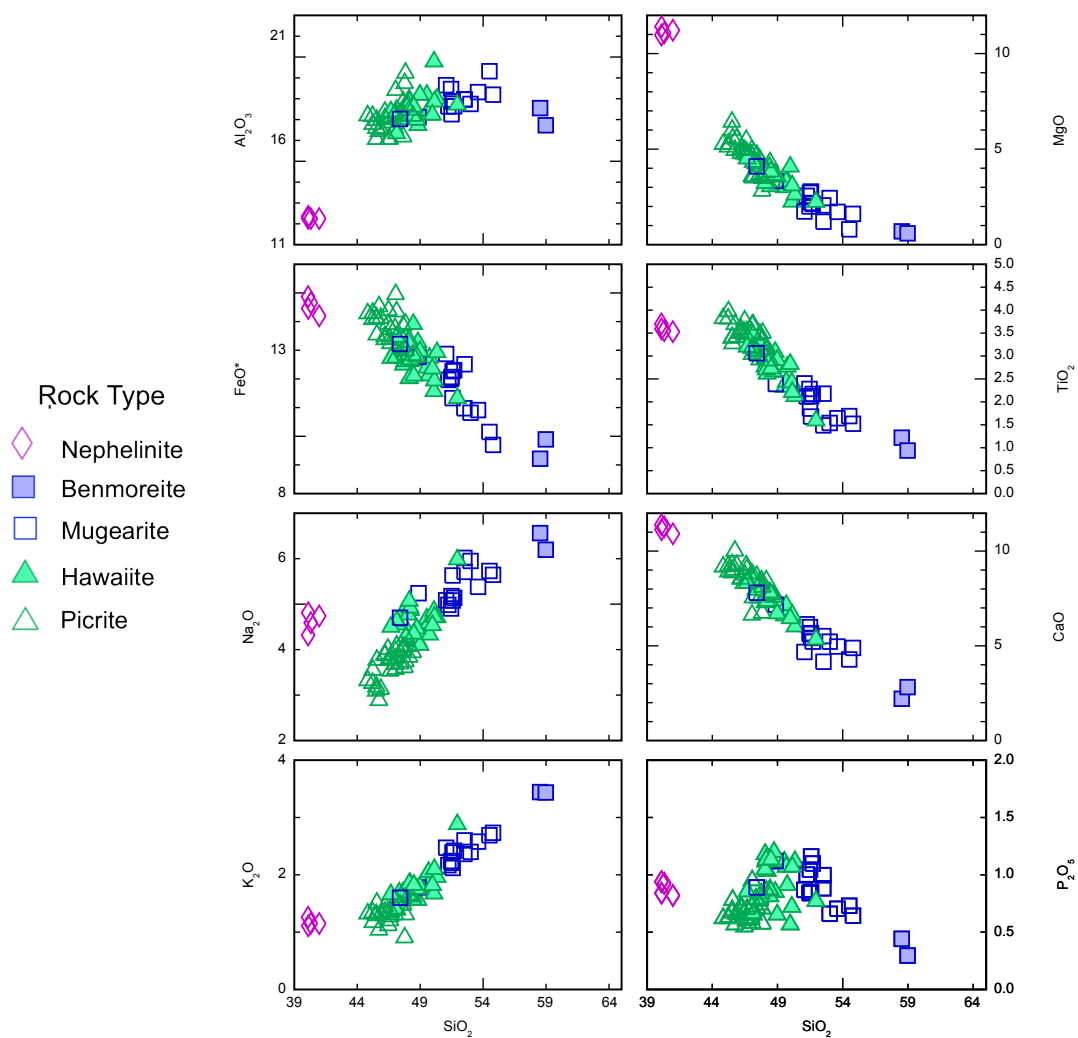
Figure 6.2: Harker Diagrams plotted by rock type for all samples. Note the clear distinction with the more primitive composition of the nephelinite flows.
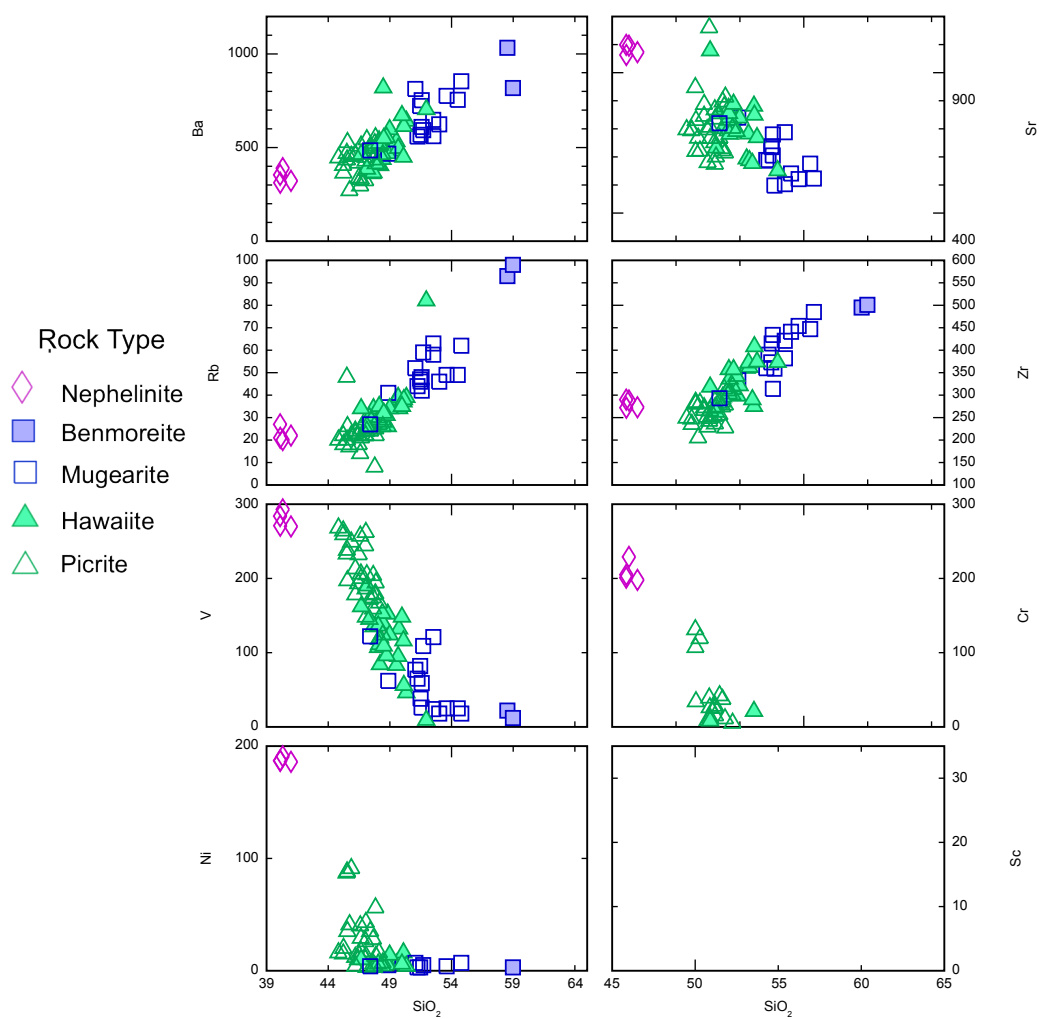
Figure 6.3: Harker Diagrams plotted by rock type for all samples. Note the clear distinction and primitive composition of the nephelinite flows, indicative of low crustal involvement. Sc was not recorded by the University of Canterbury XRF.
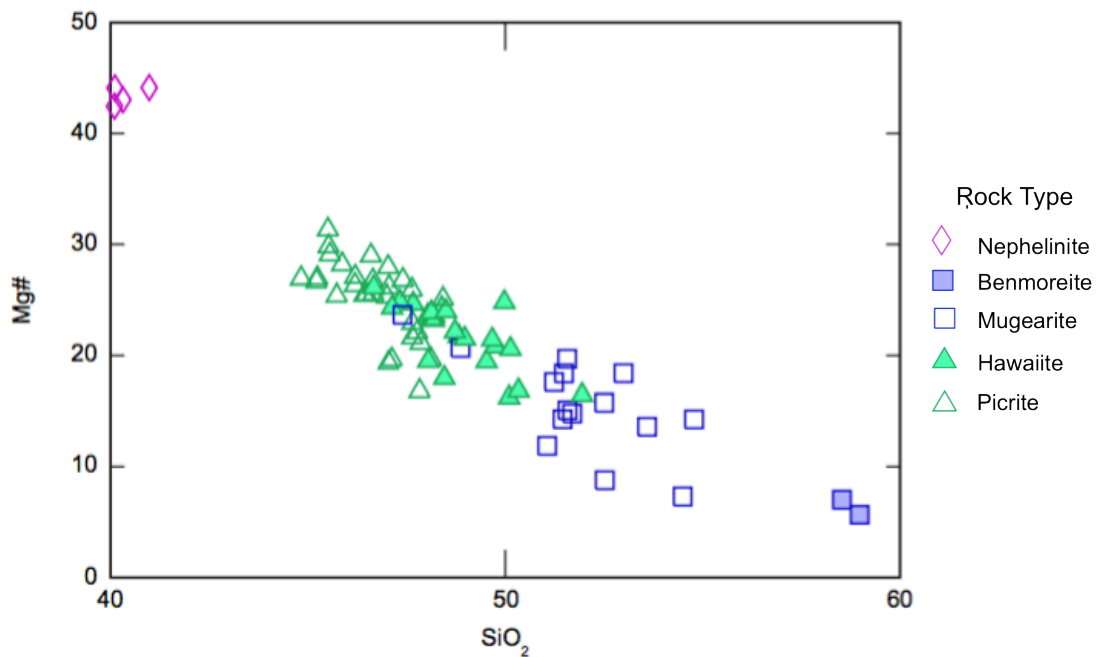
Figure 6.4: Mg# vs SiO₂ graph of bulk rock geochemical data, plotted by rock

type. Note the high Mg# for the nephelinite flows, and the low Mg#s for the

benmoreite flows. Compared to the Mg#s provided by the individual minerals,

the bulk rock Mg#s are much lower. These lower values are due to the bulk rock

data incorporating more evolved phases with low Mg and Fe concentrations into

the calculations.

a clinopyroxene in a picrite basalt that yielded 1159°C and 10kbars. Olivine phenocrysts in the mugearite yielded average formation temperatures of 995°C, and the clinopyroxene analyzed within the hawaiite and mugearite yielded an average formation temperature of 1005°C and pressure of 5.1kbars (**Tables 6.1**, **6.2**).

From this data, most of the picrites appear to have formed at similar, or slightly deeper depths, than the hawaiite and mugearite. Furthermore, due to the outlier analysis on LAW15A-8, there may be multiple geochemical populations of clinopyroxene within the picrites. The clinopyroxene analyzed in LAW15A-8 may have been carried up from a greater depth, implying that within the picrite flows, fractionation of mafic minerals was occurring both at deep and in shallow levels.

Magmatic Recharge Model

Due to the consistency of the geochemical batches and evolutionary cycles within each transect, the whole eastern bay region likely underwent similar magma recharge events, confirming Johnson's (2012) model. This is supported by bulk rock geochemical reversals in rock type and element percentages to more primitive compositions, when viewing the data in stratigraphic order. Each transect contains several batches, and thus experienced several replenishment episodes (**Figure 6.5**). Furthermore, the mineral textures, specifically resorbtion and sieved cores, suggest either disequilibrium textures due to rapid decompression pre-eruption, or the introduction of a new hot melt (**Table 6.3**). These textures generally occur in the beginning of the interpreted magma batch, and therefore are supportive of magmatic recharge.

In order to investigate the relationship of batches within a single stratigraphic

Bay	Sample ID	Rock Type	Temperature (C)
Little Akaloa	LAW15A-1	picrite	1099
Little Akaloa	LAW15A-3	picrite	1097
Little Akaloa	LAW15A-12	picrite	1097
Little Akaloa	LAW15A-13a	picrite	1096
Little Akaloa	LAW15A-18	picrite	1097
Little Akaloa	LAW15A-21	picrite	1096
Little Akaloa	LAW15A-23	picrite	1097
Stony	SB18-4	picrite	1002
Stony	SB18-21	picrite	1002
Lavericks	LAVC-7	picrite	1051
Lavericks	LAVC-10	picrite	1049
Lavericks	LAVC-16	picrite	1053
Lavericks	LAVJ-16	mugearite	991
Lavericks	LAVJ-21	mugearite	999

Table 6.1: List of the samples containing olivine phenocrysts, and their formation temperature.

Bay	Sample ID	Rock Type	Temperature (C)	Pressure (kb)
Lavericks	LAV10EA-1	hawaiite	1003	5.6
Little Akaloa	LAW15A-8	picrite	1159	10
Lavericks	LAVJ-4	mugearite	1008	4.7
Stony	SB18-8	picrite	1047	6.3
Stony	SB18-9	picrite	1050	6.6
Stony	SB18-16	picrite	1038	5.8
Stony	SB18-27	picrite	1052	6.2

Table 6.2: List of the samples containing clinopyroxene phenocrysts, and their formation temperature and pressure.
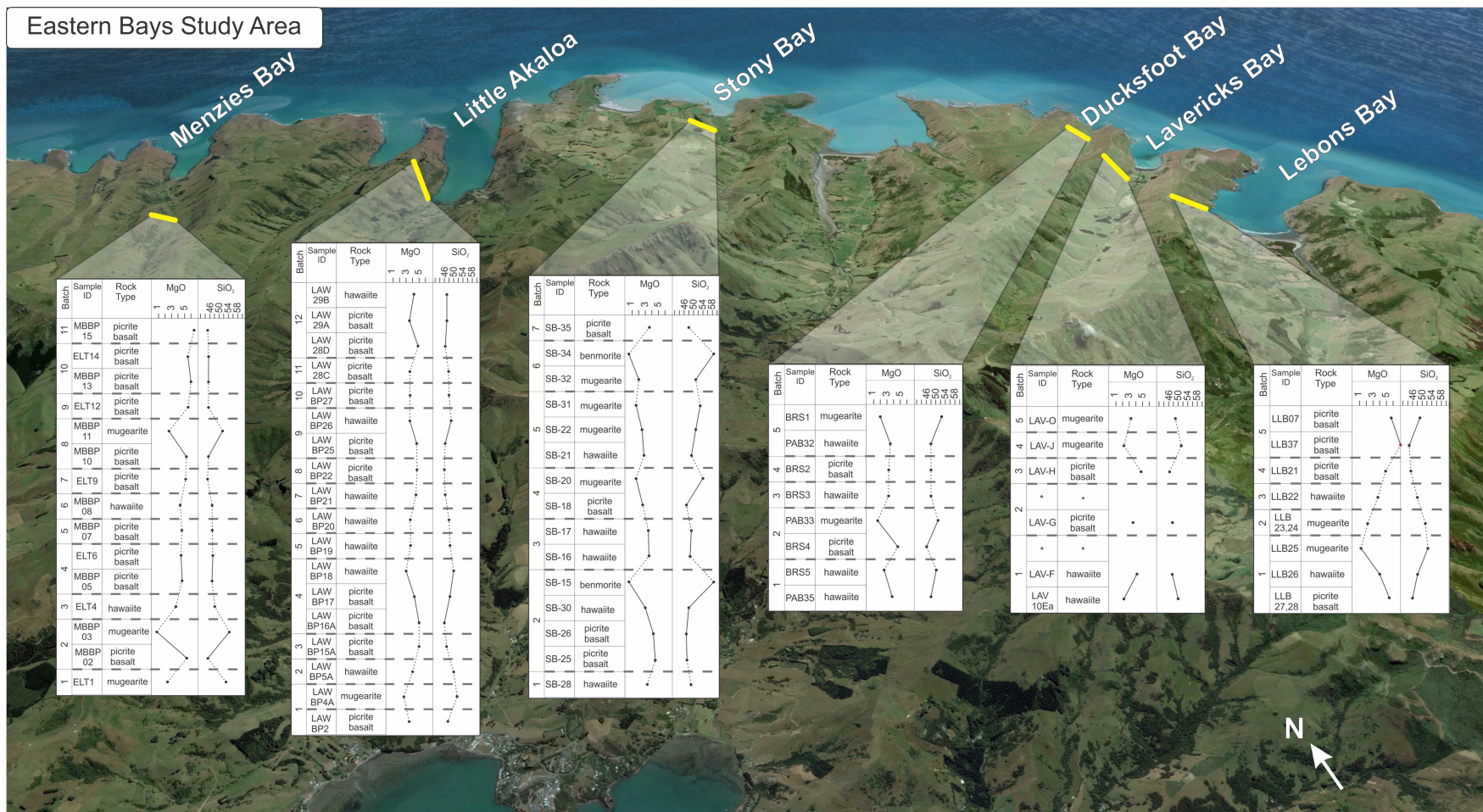
Figure 6.5: Map of the study area and transects taken (yellow lines) in eastern Banks Peninsula. Geochemical plots for each transect are shown, depicting the SiO₂ and MgO trends observed in stratigraphic sequence. Horizontal dashed lines divide batches, vertical solid lines relate flows within single batches, and vertical dashed lines show unrelated flows between two batches.

Table 6.3 (below): Collated bulk geochemical and textural interpretations for each bay transect.

Flow	Batch	Rock type	Textural Interpretation (if available)	Mineral Chemistry Interpretation (if available)
Stony Bay				
SB-35	7	Picrite	Recharge, decompression	
SB-34	6	Benmorite	Recharge, decompression, rapid crystal growth	
SB-32	6	Mugearite	Recharge, decompression	
SB-31	5	Mugearite		
SB-22	5	Mugearite		
SB-21	5	Hawaiite	Recharge, slow decompression	
SB-20	4	Mugearite		
SB-18	4	Picrite	Recharge, decompression	
SB-17	3	Hawaiite		
SB-16	3	Hawaiite	Recharge, slow decompression	
SB-15	2	Benmorite	Recharge, decompression	
SB-30	2	Hawaiite	Fast decompression	
SB-26	2	Picrite	Recharge, rapid crystal growth	
SB-25	2	Picrite	Recharge, fast decompression, convection	
SB-28	1	Hawaiite	Recharge, decompression, rapid crystal growth	
Menzies Bay				
MBBP15	11	Picrite	Recharge, decompression, convection	
ELT14	10	Picrite	Recharge, decompression, convection	
MBBP13	10	Picrite	Recharge, fast crystal growth	
ELT12	9	Picrite	Recharge, fast decompression, convection	
MBBP11	8	Mugearite	Rapid crystal growth	
MBBP10	8	Picrite	Recharge, decompression	
ELT9	7	Picrite	Rapid crystal growth	
MBBP08	6	Hawaiite	Recharge, fast decompression	
MBBP07 (MBBP02)	5	Picrite	Recharge, decompression, convection	Recharge (MBBP02-15, MBBP02-23)
ELT6	4	Picrite	Recharge, decompression, convection, rapid crystal growth	
MBBP05	4	Picrite	Recharge, fast decompression, convection, rapid crystal growth	
ELT4	3	Hawaiite		
MBBP03	2	Mugearite	Fast decompression	
MBBP02	2	Picrite	Recharge, slow decompression, convection, rapid crystal growth	
ELT1	1	Mugearite	Recharge, rapid crystal growth	
Little Akaloa				
LAWBP29B	12	Hawaiite	Recharge, decompression	
LAWBP29A	12	Picrite		
LAWBP28D	12	Picrite	Fast decompression, rapid crystal growth	
LAWBP28C	11	Picrite	Recharge, fast decompression, convection	
LAWBP27	10	Picrite	Recharge, decompression, convection, rapid crystal growth	

LAWBP26	9	Hawaiite		
LAWBP25	9	Picrite	Fast decompression, convection	
LAWBP22	8	Picrite	Recharge, rapid crystal growth	
LAWBP21	7	Hawaiite	Convection	
LAWBP20	6	Hawaiite	Recharge, convection	
LAWBP19	5	Hawaiite		
LAWBP18	4	Hawaiite	Slow decompression	
LAWBP17	4	Picrite	Recharge, decompression, convection	
LAWBP16A	4	Picrite	Recharge, decompression	
LAWBP15A	3	Picrite	Recharge, fast decompression, convection	Recharge (LAW15A-12)
LAWBP5A	2	Hawaiite	Recharge, fast decompression	
LAWBP4A	1	Mugearite	Recharge, fast decompression	
LAWBP2	1	Picrite	Fast decompression, convection	
Ducksfoot Bay				
BRS1	5	Mugearite		
PAB32	5	Hawaiite	Recharge, decompression, rapid crystal growth	
BRS2	4	Picrite	Recharge, fast decompression, rapid crystal growth	
BRS3	3	Hawaiite		
PAB33	2	Mugearite		
BRS4	2	Picrite	Recharge, decompression, rapid crystal growth	
BRS5	1	Hawaiite		
PAB35	1	Hawaiite	Recharge, fast decompression	
Lebons Bay				
LLB20	3	No geochem		
LLB21	3	Picrite	Recharge, decompression, convection	Recharge (LLB21-22)
LLB22	2	Hawaiite		
LLB23, 24	1	Mugearite		
LLB25	1	Mugearite		
LLB26	1	Hawaiite		
LLB27, 28	1	Picrite	Fast decompression, convection, rapid crystal growth	

section, data obtained from the Menzies Bay transect were plotted by incompatible element ratios (**Figure 6.6**, **6.7**, **6.8)**. If flows are related by fractionation, the ratio of incompatible elements should not change significantly until the final stages of crystallization.

Due to the similarity and consistency of ratios between successive batches (see **Figures 6.6**, **6.7**, **6.8**), the source melt replenishing each batch was likely homogenous and very large in volume. Furthermore, most of the flows, regardless of rock type, show similar incompatible element ratios. This observation suggests that while fractionation was the driving evolutionary force, the melt was not fractionating to the completeion before a recharge event interrupted its evolution. If the melt were fractionating to the final stages of crystallization, one would expect to see variation between primitive picrite flows and more evolved flows. Batch 2, in **Figures 6.6**, **6.8**, and batches 1 and 8 in **Figure 6.8** are the only outliers containing flows with greater Zr, Rb, and Ba relative to the other flows. These higher ratios suggest greater crustal assimilation in the melts producing these flows.

Crustal Processes

Once magma starts its ascent through the crust, which is suggested to be of average continental crust thickness (Hoernle, 2006), the starting composition begins to change due to crustal assimilation, ascent rate, and whether or not the magma stalls in an upper levels, undergoing fractional crystallization. As previously mentioned, each picrite has a slightly different anorthite range suggesting different processes occurring among the bays (**Table 5.2**, **Figure 5.19**). These differences suggest that there may be multiple
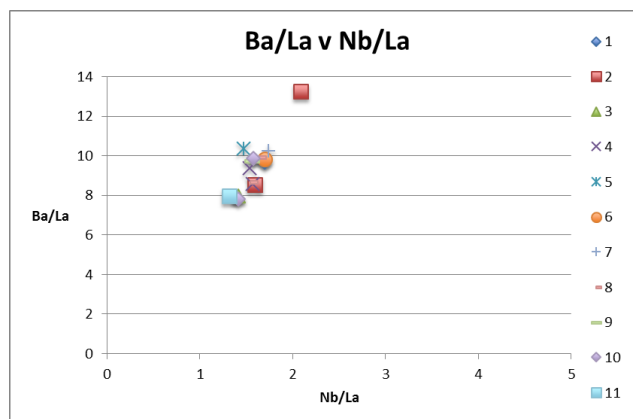
Figure 6.6: Ba/La vs Nb/La plotted by batch for the Menzies Bay.
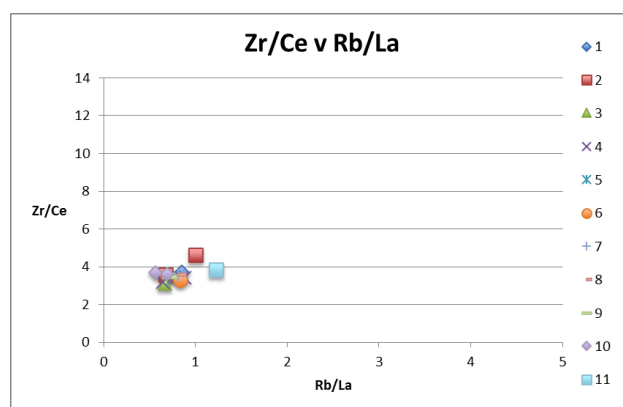
Figure 6.7: Zr/Ce vs Rb/La plotted by batch for the Menzies Bay.
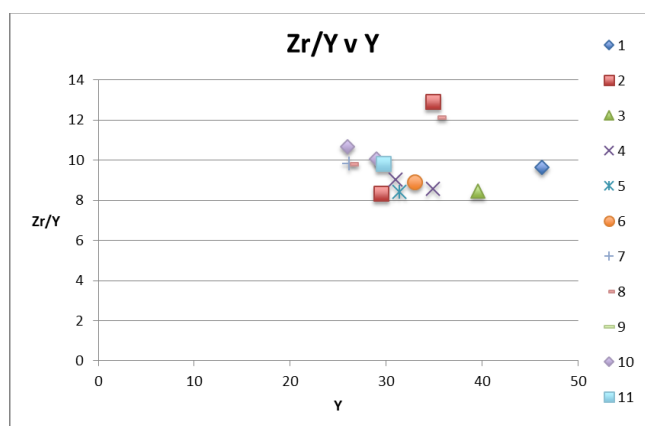
Figure 6.8: Zr/Y vs Y plotted by batch for the Menzies Bay.

shallow chambers below the Akaroa Volcanic Complex, and/or that there is a significant temporal difference between the eruption of the flows composing the different bays.

Bulk rock geochemistry supports the theory of parent magma regularly supplying shallow crustal chambers with magma, thus allowing for the fractionation of individual evolutionary batches between recharge events (**Figure 6.5**). The main question, then, is what happens to the magma on the path from source to eruption. Petrographic and geochemical data are consistent with four hypotheses:

1. Parent magma rises to a shallow chamber where it evolves, fractionates, and erupts in a continuous process.

2. Parent magma rises to a shallow chamber where it evolves, fractionates and forms a magma mush, while the residual crystal-poor liquid (hawaiite, mugearite, benmoreite) is erupting. Upon a recharge event in the shallow chamber, the previous batch's crystal mush is stirred up and erupted with the new picrite magma.

3. Parent magma rises to a shallow chamber where it evolves, fractionates, forms a crystal mush but also erupts some of the phenocrysts that are fractionating. The magma recharge does not necessarily stir up the crystal mush, meaning that the phenocrysts found in the picrites are crystals that fractionated from the melt. (This hypothesis is a combination of 1 and 2.)

4. Similar to hypothesis 3, the parent magma rises, fractionates, and erupts a melt containing both phenocrysts and potentially inherited cumulates from a melt of a previous batch. Instead of rising to a shallow chamber, however, it is proposed that these chambers are overlapping columns of rising magma and mush. As such,

the plumbing system of the complex is characterized by a number of overlapping magma mush columns. The inherited phenocrysts in any one eruption could then be the product of both a previous batch, or from another overlapping magma mush column.

Hypothesis One: Continuous Evolution and Ascent

According to this hypothesis, the parent magma rises to a shallow chamber, where it then fractionates, evolves, and erupts in a continuous fashion. As such, the picrite flows would fractionate to their observed crystallinity, and then erupt with their respective phenocrysts. Likewise, the residual, un-erupted liquid would continue to evolve to the hawaiite, mugearite, and benmoreite flows.

Under this hypothesis, the successive flows would be related by fractional crystallization. Past studies (Price and Taylor, 1980), as well as the parallel trends within the bulk rock geochemistry data, support fractional crystallization as a dominant process acting upon magma evolution. Parallel trends in REE patterns (**Figures 5.8**, **5.9)**, along with the linear trends between rock types (excluding the nephelinites) in the Harker diagrams plotted by rock type (**Figures 6.2**, **6.3**) support fractional crystallization relating the flows within individual batches.

The microprobe data, plotted by rock type (**Figures 5.16**, **5.17**, **5.18**) also supports continuous evolution to eruption between batches. Each phenocryst reflects the geochemistry of the flow in which it is contained. Picrites contain higher concentrations in anorthite (**Figure 5.16**) and iron (**Figure 5.17**), and lower concentrations of silica and potassium (**Figure 5.18**). Phenocrysts found in hawaiites, mugearites, and benmoreites each represent more evolved magma (lower anorthite and iron, higher sodium and

potassium) respectively. Phenocrysts within the hawaiites overlap with the three picrite flows LLB21, MBBP07, and LAWBP2 (**Figure 6.9**). This geochemical overlap suggests that the hawaiite could have directly fractionated from the more evolved picrite magma within the shallow chambers. Unfortunately, data are not available from the picrite flow located underneath the analyzed hawaiite flow LAV10EA, and therefore definitive relationships cannot be ascertained.

As mentioned in Chapter 4, predominantly zoned, sieved, and resorbed textures are found within many of the phenocrysts. Viccaro et al. (2010) suggests that sieved and resorbed textures are indicative of the introduction of a new hot melt pushing the phenocrysts out of equilibrium (**Figure 4.3**). This implies that phenocrysts within flows experienced processes outside the continuous fractionation, evolution, and eruption sequence put forth by Hypothesis One. These textures could have also been formed by decompression upon eruption, rather than through the introduction of a new hot magma. If these textures were formed by decompression, then the continuous magma ascent posed by Hypothesis One is not challenged. The overall aphyric characteristic of the hawaiite, mugearite, and benmoreite flows, however, suggest that the crystals fractionating out of the evolving melt are not included in the erupted magma. Again, some process other than continuous evolution and ascent, such as crystal separation, must be occurring to produce the evolved aphyric flows.

Microprobe mineral transects also suggest processes outside a continuous evolution and ascent of the magma. Reverse zoning patterns seen between individual microprobe analyses points on mineral transects from rim to core imply a more complex history for the phenocrysts contained within the flows. Reverse zoning could be formed
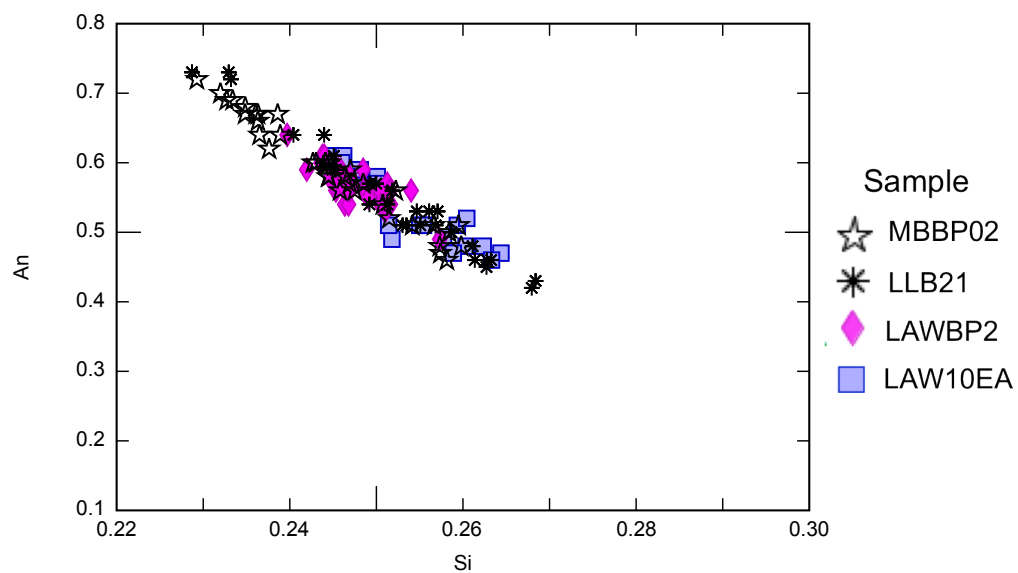
Figure 6.9: An vs Si (wt%) plotted by bay for the overlapping picrite flows LLB21, MBBP07, and LAWBP2 and hawaiite flow LAW10EA.

by the introduction or recharge of a melt with a more primitive composition compared to the original, fractionating melt. As such, the plagioclase phenocrysts experienced recharge events, recording various histories of melt evolution in their oscillatory zoning (**Figure 6.10**, **Figure 6.11**). Note in **Figure 6.11** how LAVC-12 records three separate oscillations that can be interpreted as recharge events. This phenocryst suggests a complex melt history of multiple recharge events affecting the flow's chemistry and phenocryst population.

Hypothesis Two: Crystal Mush

In order to account for textural and mineral geochemical data noted above, Hypothesis Two postulates that the phenocrysts contained within the highly crystalline picrite flows are the remains of a crystal mush that formed through fractionation and crystal settling during the previous batches' evolution. Similar to Hypothesis One, a recharge event would supply a shallow chamber with parent magma, and this magma would fractionate, evolve, and erupt into the observed rock types. However, unlike Hypothesis One, the fractionating phenocrysts would separate from the liquid forming a crystal mush, while the more evolved liquid erupts aphyrically. Upon a rejuvenation event, the crystal mush would be stirred up and erupted with a more primitive picrite magma, thus starting the new batch (**Figure 6.12**).

If this hypothesis is correct, then the picrite flows are essentially cumulates in that they contain crystals that were fractionated from previous melts. As such, the results from the bulk rock data contain the geochemical input of phenocrysts from hawaiite, mugearite, and benmoreite flows. The sieved and resorbed plagioclase textures supports the magma mush hypothesis in that these textures imply the introduction of a new, hotter
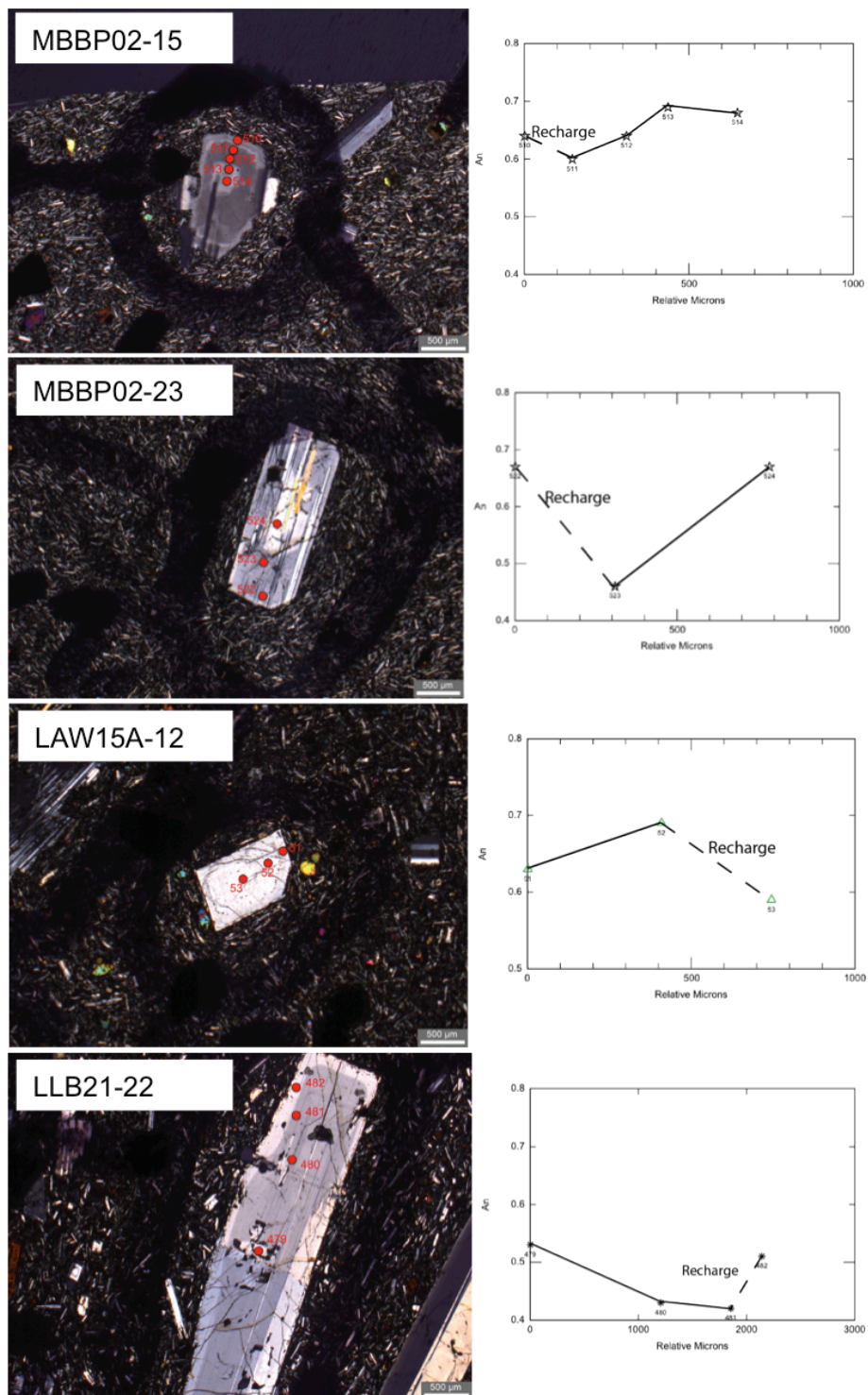
Figure 6.10: Microprobe mineral transects with suggested recharge events where
reverse zoning patterns are observed. Recharge events are marked by a dashed line, and
identified by increases in anorthite moving from the core to the rim.
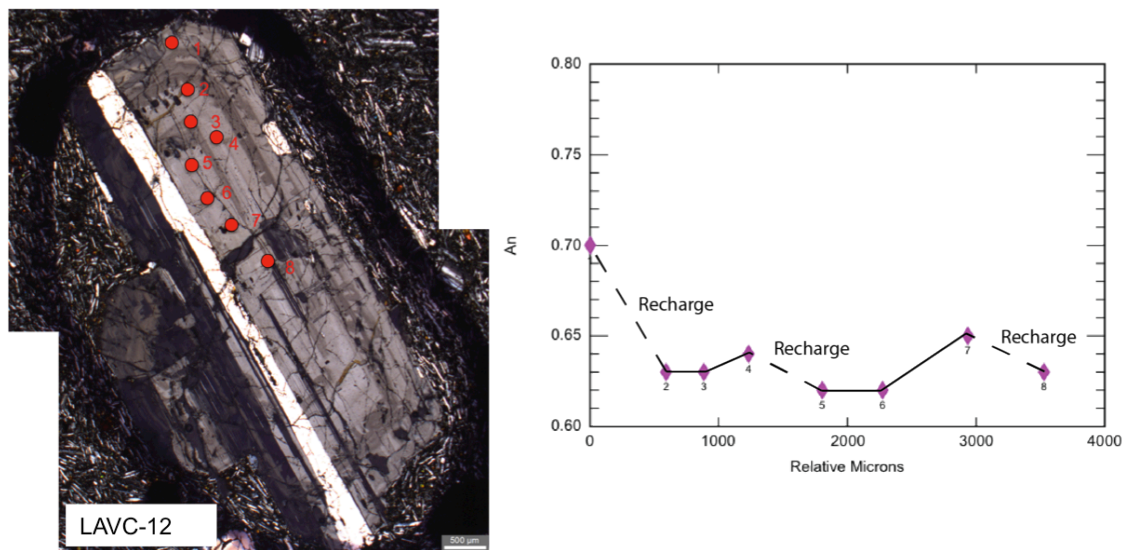
Figure 6.11: Microprobe mineral transect of crystal LAVC-12 with suggested recharge events where reverse zoning patterns are observed. Recharge events are marked by a dashed line, and identified by increases in anorthite moving from the core to the rim.
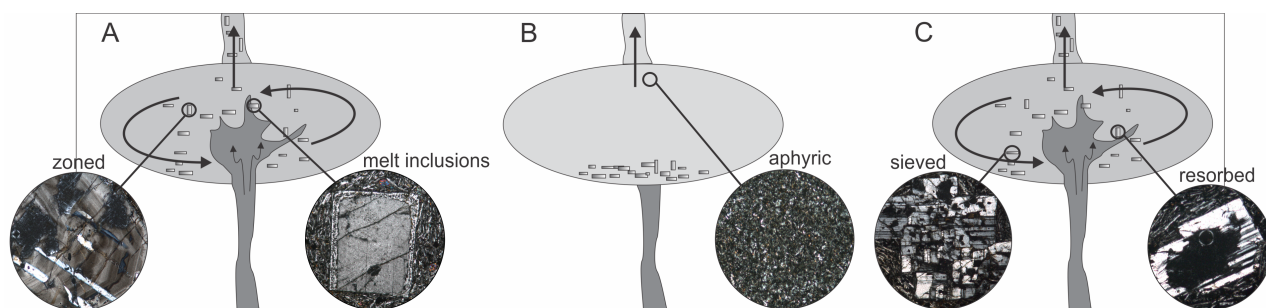
Figure 6.12: A) Magma recharge starts a new batch. The magma recharge stirs up any cumulates that have settled, causing magma mixing and eruption of porphyritic flow. Sieved and resorbed textures support magma recharge; zoned textures support magma mixing. Melt inclusions suggest fast crystallization rates. **B)** Evolution of the magma batch. Eruptions of the evolving magma record the rock type evolution of the batch. Erupted aphyric lava flows suggest very little magma mixing and separation of phenocrysts and liquid, forming a magma mush out of the phenocrysts. **C)** Magma recharge ends the development of the previous batch with the introduction of new, primitive magma. Cumulates from the previous batch are stirred up and erupted. Like **A**, sieved, resorbed, and zoned textures, along with melt inclusions, are observed, suggesting magma recharge of a new hot melt, and fast crystallization rates.

melt causing disequilibrium. Under this hypothesis, it is assumed that the textures are not decompression-induced, but rather caused by the introduction of the new melt in the recharge event. It is possible that the textures were caused by decompression, however the geochemical oscillations recorded in the individual plagioclase crystals (**Figure 6.10**, **6.11**) reflect exposure to a melt of different chemistry thus causing disequilibrium textures. Furthermore, the crystallinity trends of more crystalline picrite flows to aphyric hawaiite, mugearite, and benmoreite flows would be explained by the crystal separation of the evolved flows, and the incorporation of the crystal mush in the picrites. The geochemistry of the parent magma, under this assumption, would have to be more primitive than the observed picrite flows in order to remain of picritic composition with the input of the phenocrysts from more evolved flows. Potentially the necessity of a more primitive parent melt could be indicative of a parent melt closer to the nephelinite flows found elsewhere in Stony Bay. These nephelinite flows may have erupted without incorporating the hypothesized evolved crystal mush, thus preserving the primitive parent magma composition.

The microprobe mineral transects showing reverse zoning patterns also support Hypothesis Two in that from the mineral transects it is clear that the crystals have witnessed the introduction of a more primitive melt during their fractionation history. Jumps from lower to higher anorthite concentration in core to rim plagioclase transects suggest that a magma recharge event occurred during the crystals formation (**Figures 6.10**, **6.11**). Crystal separation of phenocrysts fractionating from more evolved magma, and the following replenishment event reverting the bulk rock geochemistry back to a more primitive rock type, thus creating the observed reverse zoning. Furthermore,

individual crystals that show reverse zoning patterns are all contained within flows that correspond to the first flow in a batch defined by the bulk rock geochemical stratigraphic sections (**Figures 6.13**, **6.14**, **6.15**, **6.16**). As such, these plagioclase crystals could be inherited from the crystal much of the prior batch. It should be noted, however, is that there is no clear way to differentiate whether these crystals are recording the same recharge event of the bulk rock data. For example, the microprobe data for LAVC-12 records several recharge events, while the bulk rock data can only show one recharge event (**Figure 6.16**). As such, these crystals may be recording events that occurred after the new batch started, but prior to the eruption of the first flow. To differentiate whether these plagioclase transects are recording the same event, probe analysis should be conducted on phenocrysts contained within two successive flows from different batches. Through detailed probe work cataloguing the different populations of plagioclase, similarities and differences between the two flows can be investigated.

The implications of the microprobe data, however, present a problem in that clear distinctions can be seen in the plagioclase crystals analyzed in picrites, hawaiites, mugearites, and benmoreites (**Figures 5.16**, **5.17**, **5.18**). Each crystal reflects the geochemistry of the flow in which it is contained, implying that the crystals formed in their host flow (supporting Hypothesis One). If the crystals contained within the picrite flows were inherited from a crystal much from a prior batch, then some of the crystal chemistry should reflect a more evolved composition relative to true picrite phenocrysts. These phenocrysts could potentially be inherited from a picrite basalt melt from a previous batch, however the lack of any geochemical record of a more evolved melt makes this seem unlikely. The only mineral geochemistry overlap observed with evolved
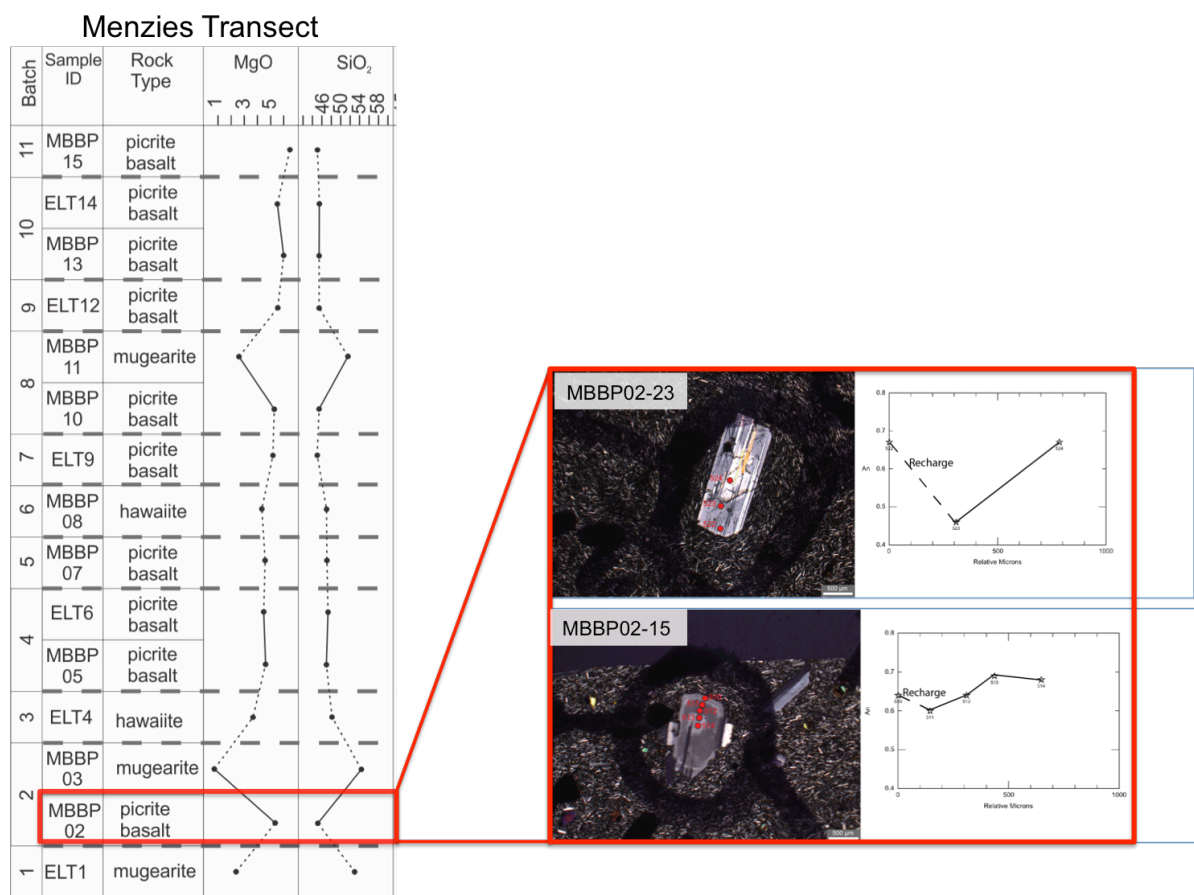
Figure 6.13: Bulk rock geochemistry stratigraphic section for Menzies Bay with its corresponding microprobe geochemical mineral transects. Note how probe analyses MBBP02-15 and MBBP02-23 are both contained within the first flow of batch 2, MBBP02, following the recharge event ending batch 1.
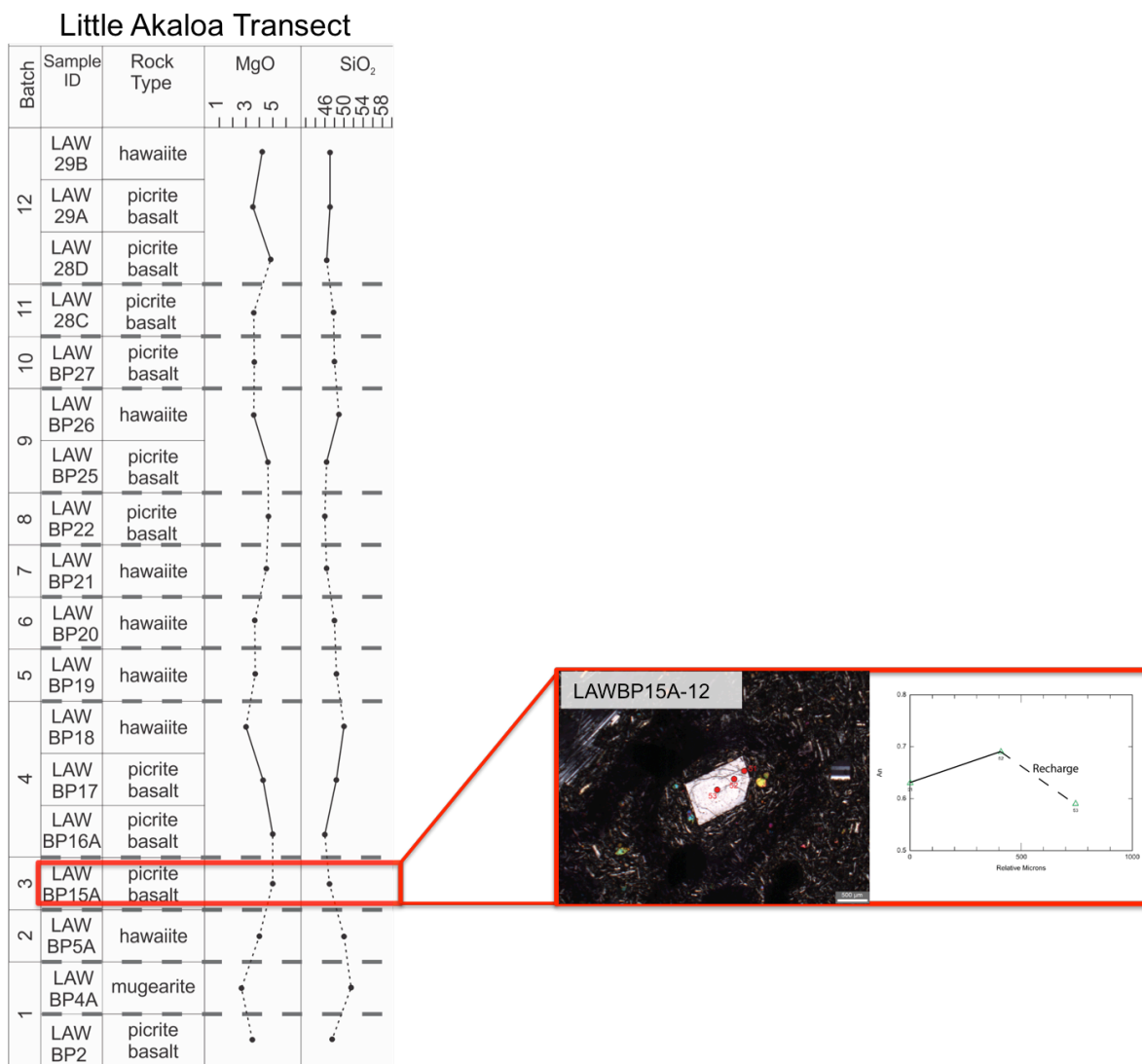
Figure 6.14: Bulk rock geochemistry stratigraphic section for Little Akaloa with its corresponding microprobe geochemical mineral transect. Note how probe analyses LAWBP15A-12 is contained within the first flow of batch 3, LAWBP15A, following the recharge event ending batch 2.
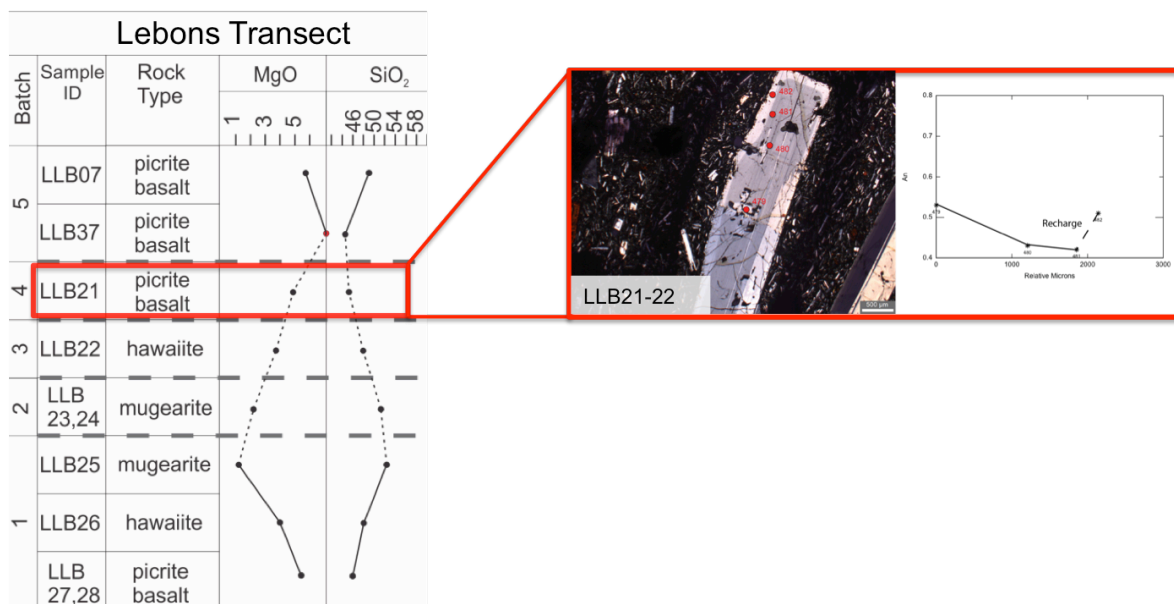
Figure 6.15: Bulk rock geochemistry stratigraphic section for Lebons Bay with its corresponding microprobe geochemical mineral transect. Note how probe analyses LLB21-22 is contained within the first flow of batch 4, LLB21, following the recharge event ending batch 3.
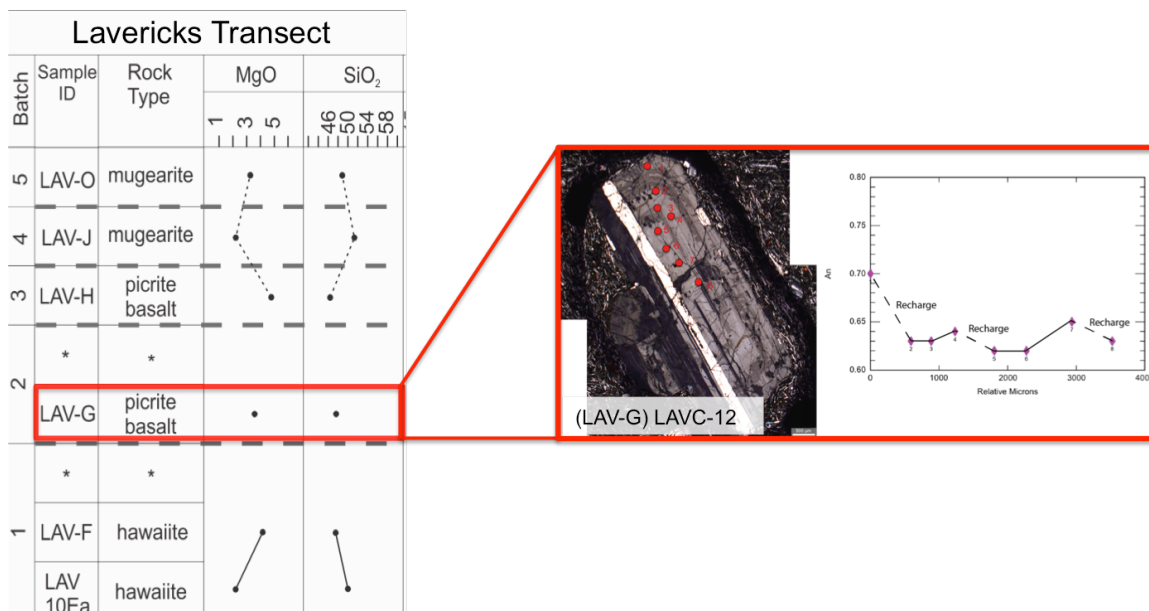
Figure 6.16: Bulk rock geochemistry stratigraphic section for Lavericks Bay with its corresponding microprobe geochemical mineral transect. Note how probe analyses LAVC-12 is contained within the first flow of batch 2, LAV-G, following the recharge event ending batch 1. LAVC-12 records several recharge events, while the bulk rock geochemical data can only record one event between successive flows.

flows is between crystals found in the three picrite flows LAWBP2, LLB21, MBBP02 and the hawaiite phenocrysts of LAV10EA's (**Figure 6.9**). To attain this geochemical overlap, it is possible that a crystal mush derived from a hawaiite melt was incorporated into these three picrite melts, thus producing evolved plagioclase crystals within a more primitive melt. Another possibility is that, as suggested in Hypothesis One, the hawaiite flow was derived directly through the evolution of the picrite melt. As such, with this hawaiite melt, phenocrysts that started to fractionate within a picrite composition simply continued to fractionate as the melt evolved into a hawaiite. To differentiate between these two models, detailed microprobe analyses on mineral transects should be conducted on several of the phenocrysts within these overlapping flows. If there are oscillations from more evolved to primitive compositions, then the phenocrysts may have been inherited. If there are no oscillations, then the phenocrysts may be the product of continuous evolution.

Within **Figure 5.28**, the overlapping hawaiite sample (LAV10EA) displays two separate populations of plagioclase, a more primitive group and a more evolved group. Since there is a distinct gap between the two groups, probably there was not continuous fractionation occurring between the two geochemistries represented; there must have either been an inherited population of plagioclase, or a time gap in which plagioclase was not fractionating. Another cause for the gap could be a sample bias. If, however, the more evolved population was inherited from a crystal mush left behind from a more evolved melt in a previous batch, the inherited population could have changed the bulk rock geochemistry away from the original melt composition. Potentially the hawaiite

LAW10EA was once of picrite composition, however due to the amount of inherited plagioclase crystals, the bulk rock geochemistry was altered to a hawaiite.

In order to investigate the two populations of plagioclase in sample LAW10EA further, the crystals within the hawaiite were plotted by size (**Figure 6.17**). The more An-rich population is composed both of the largest and smallest crystals, and the more evolved population is composed of intermediate-sized crystals. There is some overlap with the large and intermediate crystals in the more evolved anorthite range. As such, the smaller crystals are likely formed simultaneously with the large phenocrysts, or are the product of quenching induced by a recharge event. Quenching requires the interaction of melts with significantly different temperatures. Recorded temperatures for LAV10EA are similar to the other temperatures in the analyzed flows, suggesting similar temperature ranges between all of the flows. These similar temperatures would not be able to create the observed quenching. This, however, could be a product of sample bias not recording diversity among temperatures. Furthermore, the temperatures provided by the minerals analyzed are not in a temporal context. There is no definitive way in knowing when the crystals fractionated relative to the quenching event. As such, the true temperature of the interacting melts that facilitated the observed quenching could have been vastly different than the recorded temperatures. Further analyses on multiple crystals within the same sample should be undertaken to investigate whether there may be a variety of temperatures recorded within the same sample. Assuming the smaller crystals are a product of quenching, recharge from depth could have caused quenching in the more primitive rising magma upon contact with the more evolved shallow melt. Thus, the observed geochemical gap could be indicative of an inherited population of intermediate-
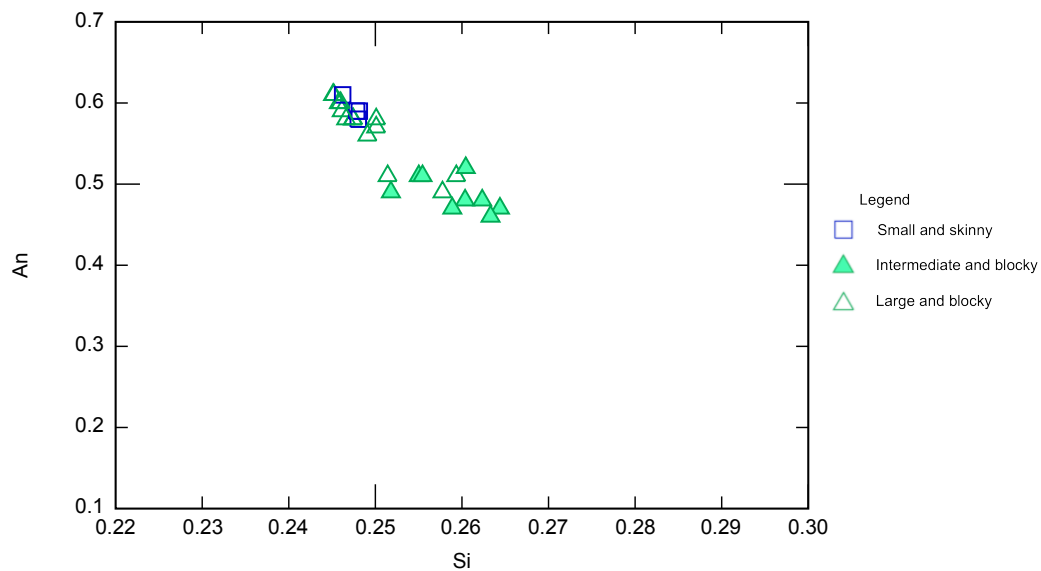
Figure 6.17: An vs Si plotted by size for the hawaiite flow LAW10EA. Sizes of the phenocrysts were determined qualitatively, defined relative to each other.

sized, more evolved plagioclase crystals. The more primitive, large plagioclase population would have then fractionated after the recharge event, recording similar geochemistries to the quenched smaller phenocrysts.

Hypothesis Three: Semi-continuous ascent

This hypothesis is a mixture between Hypothesis One and Hypothesis Two in that the picrite flows would experience the continuous (or near continuous) ascent described in Hypothesis One, and the more evolved flows would experience the crystal separation described in Hypothesis Two to erupt aphyrically. The main difference in this hypothesis relative to the other two hypotheses is that the recharging melt does not necessarily stir up the crystal mush from the previous batch, but instead fractionates to the observed crystallinity within the flow and erupts. As such, this hypothesis describes a melt with semi-continuous ascent. The crystal separation occurring in the more evolved flows could be a result of density differences between the crystal and host melt, from different convection processes occurring within the chamber, or from mechanical separation of the liquid and crystals upon eruption. The resulting crystal mush would remain predominantly underground in the shallow chamber.

Support for this hypothesis comes from the study of phenocryst textures, which, as previously noted, suggests some form of disequilibrium. These textures could be indicative of multiple recharge events occurring early in a batch, before the initial eruption of the first flow setting the geochemical base-line for the following flows in the batch. Another cause for these textures could be a form of crystal settling between successive picrite flows. In many of the bays, batches are composed of one or two picrite flows only. As such, between two picrite flows in different batches, some less extensive

crystal settling could have occurred, and thus upon a recharge event the crystals develope the disequilibrium sieved and resorbed textures. In this way, the crystal geochemistry could match the range of their bulk rock geochemistry even if they were not directly fractionating from their host melt. Both of these scenarios are supported by data from the microprobe mineral transects, recording oscillatory zoning within plagioclase. In both cases, the plagioclase is not fractionating in a closed setting but is interacting with melts of different geochemistry. The grouped bulk rock and microprobe geochemical data (**Figures 6.13**, **6.14**, **6.15**, **6.16**) support both models in that the plagioclase crystals are contained within flows that start a new batch in the bulk rock geochemistry. Again, the textures could also be a result of decompression, however this would not readily explain the oscillatory zoning seen within individual crystals.

Hypothesis Four: Magma mush column

This hypothesis is founded in Hypothesis Three, in that melt is experiencing semi-continuous ascent, fractionation, crystal separation, and the introduction of a new melt causing geochemical cycles in the bulk rock and disequilibrium textures in phenocrysts. While the mechanics producing the observed geochemistry, crystallinity, and mineral textures of this hypothesis are essentially the same as Hypothesis Three, Hypothesis Four is a more realistic scenario than Hypothesis Three in that it attempts to account for the complexities of volcanic plumbing systems. The primary difference of this hypothesis is that the proposed plumbing system is not made up of a number of solitary shallow chambers, but is comprised of overlapping chambers or columns in the forms of dikes and sills (**Figure 6.18**). The occurrence and location of these dikes and sills could be a product of the NE-SW trending faults (Ring and Hampton, 2010). As such, the
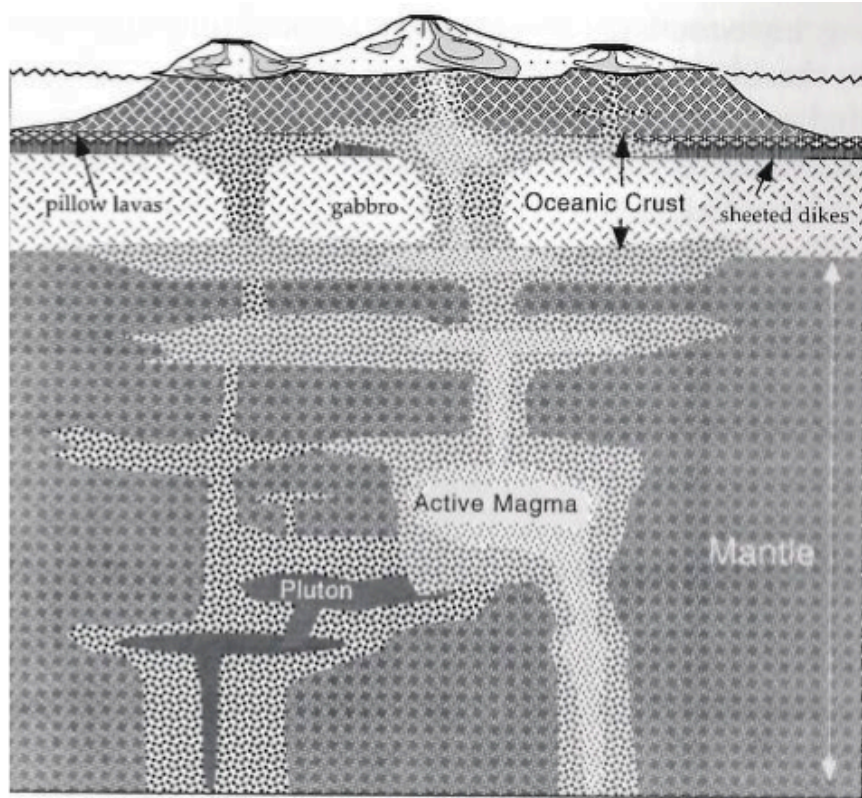
Figure 6.18: Model of proposed magma mush column plumbing system (Marsh, 2006, p. 203-205).

111

interpreted recharge could be both a replenishment event from depth to the specific magma mush column, or more of a mixing event between overlapping magma mush columns. Either way, due to the similar incompatible element ratios (**Figures 6.6**, **6.7**, **6.8**) and bulk rock geochemistry (**Figures 5.10**, **5.11**), the parent melt for the whole system is assumed to be the same. As such, there is no clear way to distinguish between a replenishment event and magma mush column mixing. Both scenarios would produce the bulk rock geochemical cycles seen in **Figure 6.5** for each bay transect, as well as the interpreted recharge events in the mineral geochemistry (**Figures 6.10**, **6.11**).

Due to the close spacing of the bays (less than 5km between bays), it is highly unlikely that each bay has an individual underlying chamber, or that there is one single large chamber that is homogenous in structure underneath the entire Akaroa Volcanic Complex. By incorporating an overlapping magma mush column structure, the heterogeneities of the plumbing system are addressed. These heterogeneities within the plumbing system, when supplied with magma from a common source from depth, would allow for the observed similarities and differences within the geochemistry between bays (**Table 5.8**). Individual magma mush columns could facilitate the specific differences between bay transects, while a common source and magma mush column mixing could create similarities between the bay transects.

It is evident that multiple hypotheses can be developed to explain data from the Akaroa Volcanic Complex. Of the four presented here, Hypothesis Four is favored since it is the most probable. Hypothesis One faces problems with the textural data; the aphyric nature of the more evolved flows, as well as the disequilibrium textures seen in many of the phenocrysts suggests processes outside the continuous evolution and ascent.

Hypothesis Two faces problems with the microprobe data plotted by rock type. The clear distinction between the plagioclase phenocrysts found in each rock type does not allow for crystal separation to be the sole source of picrite crystallinity. Hypothesis Three specifies continuous ascent, fractionation, and eruption to the picrite flows, and the crystal separation to the more evolved flows, thus accounting for the problems of Hypothesis One and Two, but it does not account for the inherent complexities of volcanic plumbing systems.

Chapter VII: Conclusions

The Akaroa Volcanic Complex is a product of intraplate Miocene volcanism. This complex contains an overlapping magmatic system with components that both mixed with each other and were periodically replenished with primitive, potentially nephelinite magma, from depth. These mixing and recharge events caused regionally widespread geochemical cycles, or batches, from picrite to hawaiite, mugearite, and benmoreite lava flows within stratigraphic sections (**Figure 6.5**). Geothermal barometry data from olivine and clinopyroxene phenocrysts indicate that parent magma is fractionating both at depth (under10kbars pressure), and at shallow levels (at 4.7-6.6kbars pressure).

This study postulates that the parent magma rose and evolved in a series of dikes and sills underlying the complex, forming overlapping magma mush columns (Hypothesis Four). Due to the relative crystallinity of the picrite flows, and the consistently primitive mineral chemistries within individual picrite samples, each picrite melt would have stalled in a chamber long enough to develop the observed crystallinity before erupting.

Within single batches, the geochemical overlap of hawaiite phenocrysts (**Figure 6.9**), and similar REE patterns for each rock type (**Figure 5.8**, **5.9**), suggest the more evolved flows are derived from picrite melts. The aphyric characteristic common in most of the hawaiite, mugearite, and benmoreite flows suggest that unlike the picrite flows, crystal separation was occurring upon eruption, leaving a crystal mush in the chamber, while the evolved liquid erupted.

Disequilibrium mineral textures, coupled with microprobe mineral transect data, suggest that the phenocrysts experienced either or both decompression and magma

recharge. Due to the lack of geochemically evolved phenocrysts contained within the primitive picrite flows, however, the crystal mush left behind from the more evolved flows would not have been incorporated into the picrites upon these recharge events. As such, the picrites were evolving and erupting as highly crystalline with their fractionated phenocrysts, and the evolved flows were evolving and erupting predominantly aphyrically, leaving behind a crystal mush.

Future Work

Further testing and refinement of this hypothesis is needed. As a final step more microprobe data from mineral transects on individual crystals is needed. Specifically, multiple microprobe mineral transects on plagioclase should be collected within single samples to correlate recharge events with reverse zoning patterns between crystals. These data could be used to better define whether the observed mineral textures are predominantly decompression or recharge-induced. Moreover, single stratigraphic sections within bays should be focused on microprobe work to define the relationship between stratigraphically related flows and batches. Source depth and temperature should be further investigated through purposefully selecting olivine and clinopyroxene minerals of many different sizes for microprobe analysis.

Additionally, crystal size distribution (CSD) analysis needs to be conducted on these samples in order to investigate magma chamber dynamics, recharge, and crystal populations. Crystal size and morphology will yield more information on various plagioclase populations that are contained within the flows, as well as help define the location of recharge events (Marsh, 1998). Crystal size distribution was attempted in this

study, however to achieve statistically meaningful data, more samples were needed from each flow. As such, extensive sampling of every flow in a single bay's stratigraphic section should be conducted in order to investigate the different crystal populations contained in flows between batches.

Works Cited

Crystal, V., 2013, Understanding the magmatic evolution and processes associated with the formation of the lava flows found in Lavericks Bay, Banks Peninsula, New Zealand. Undergraduate paper. University of Canterbury.

Cashman, K. V., 1993, Relationship between plagioclase crystallization and cooling rate in basaltic melts. Contributions to Mineralogy and Petrology, 113, 126–142. http://doi.org/10.1007/BF00320836

Cox, K.G., Bell, J.D., & Pankhurst, R.J., 1979, The Interpretation of Igneous Rocks, Allen and Unwin, London.

Davies, T., & McSaveney, M., 2007, Natural hazard events and their consequences in Queenstown Lakes and Central Otago. Retrieved November 19, 2015, from http://www.orc.govt.nz/Information-and-Services/Natural-Hazards/Great-Alpine-Fault-Earthquake/

Geology. (2013, November 18). Retrieved November 19, 2015, from https://theaustralianalps.wordpress.com/the-alps-partnership/nature-and-biodiversity/geology/

Hampton, S. J., 2010, Growth, structure and evolution of the Lyttelton Volcanic Complex, Banks Peninsula, New Zealand: A thesis submitted in fulfilment of the requirements for the degree of Doctor of Philosophy in Geology at the University of Canterbury.

Hampton, S. J., & Cole, J. W., 2009, Lyttelton Volcano, Banks Peninsula, New Zealand: Primary volcanic landforms and eruptive centre identification. Geomorphology, 104, 284–298. http://doi.org/10.1016/j.geomorph.2008.09.005

Hoernle, K., White, J., Bogaard, P., Hauff, F., Coombs, D., Werner, R., Timm, C., Garbe-Schönberg, D., Reay, A., Cooper, A. F., 2006, Cenozoic intraplate volcanism on New Zealand: Upwelling induced by lithospheric removal. Earth and Planetary Science Letters, 350-367. doi:10.1016/j.epsl.2006.06.001

Johnson, J., 2012, Insights into the magmatic evolution of Akaroa Volcano from the geochemistry of volcanic deposits in Okains Bay, New Zealand. Undergraduate Paper. University of Canterbury.

Kroner, R., 2016, Composition and rheology of overthickened lava flow units in Banks Peninsula, New Zealand. Undergraduate Thesis. Colorado College.

Marsh, B. D., 1998, On the Interpretation of Crystal Size Distributions in Magmatic Systems. Journal of Petrology, 39(4), 553-599.

Marsh, B., 2006, in Sigurdsson, H., 2000. Encyclopedia of volcanoes. San Diego: Academic Press, 203-205.

Patel, S. C., 2013, On the Subsurface Evolution of Batch Lavas at Stony Bay, Banks Peninsula, New Zealand: A Study in Plagioclase Phenocryst Development. Undergraduate Paper. University of Canterbury.

Pearce, J. A., Gale, G. H., 1977, Identification of ore-deposition environment from trace-element geochemistry of associated igneous host rocks. Volcanic Processes in Ore Genesis, 14-24, Inst. Mining Metallurg., London, United Kingdom.

Perkins, D., & Henke, K., 2004, Minerals in Thin Section (2nd ed.). Upper Saddle River, N.J.: Pearson/Prentice Hall. Print.

Price, R., & Taylor, S., 1980, Petrology and geochemistry of the Banks Peninsula volcanoes, South Island, New Zealand. Contributions to Mineralogy and Petrology, 72, 1-18

Putirka, K. D., Mikaelian, H., Ryerson, F., & Shaw, H., 2003, New clinopyroxene-liquid thermobarometers for mafic, evolved, and volatile-bearing lava compositions, with applications to lavas from Tibet and the Snake River Plain, Idaho. American Mineralogist,88(10), 1542-1554.

Ring, U., & Hampton, S., 2012, Faulting in Banks Peninsula: Tectonic setting and structural controls for late Miocene intraplate volcanism, New Zealand. Journal of the Geological Society, London, 169, 773-785. doi:10.1144/jgs2011-167

Sewell, R.J., 1985, The volcanic geology and geochemistry of central Banks Peninsula and relationships to Lyttelton and Akaroa volcanoes. Unpublished PhD thesis, University of Canterbury.

Sewell, R.J., Weaver, S.D., & Reay, M.B., 1992, Geology of Banks Peninsula. Scale 1:100,000. Institute of Geological and Nuclear Sciences Map 3. Institute of Geological and Nuclear Sciences Ltd, Lower Hutt.

Singer, B. S., Dungan, M. A., & Layne, G. D., 1995, Textures and Sr, Ba, Mg, Fe, K, and Ti compositional profiles in volcanic plagioclase: clues to the dynamics of calc-alkaline magma chambers. American Mineralogist.

Suggate, R., 1978, The Geology of New Zealand (Vol. 1 & 2). Wellington: E.C. Keating, Govt. Print.

Sun S., and W. F. McDonough, 1989, Chemical and isotopic systematics of oceanic basalts: implications for mantle composition and processes. Magmatism in the Ocean Basins, Geological Society Special Publication, 42, 313-345.

Sutherland, R., 1999, Basement geology and tectonic development of the greater New Zealand region: An interpretation from regional magnetic data. Tectonophysics, 308, 341-362.

Timm, C., Hoernle, K., Van Den Bogaard, P., Bindeman, I., & Weaver, S., 2009, Geochemical evolution of intraplate volcanism at Banks Peninsula, New Zealand: Interaction between asthenospheric and lithospheric Melts. Journal of Petrology, 50(6), 989-1023. doi:10.1093/petrology/egp029

Timm, C., Hoernle, K., Werner, R., Hauff, F., Bogaard, P., White, J., Mortimer, N., Garbe-Schönberg, D., 2010, Temporal and geochemical evolution of the Cenozoic intraplate volcanism of Zealandia. Earth-Science Reviews, 98, 38-64. doi:10.1016/j.earscirev.2009.10.002

Viccaro, M., Giacomoni, P. P., Ferlito, C., & Cristofolini, R., 2010, Dynamics of magma supply at Mt. Etna volcano (Southern Italy) as revealed by textural and compositional features of plagioclase phenocrysts. Lithos, 116(1), 77-91

Appendix I: Petrography

Sample ID	Bay	Rock Type	Point Count?
SB-18	Stony	Picrite	Yes
MBBP02	Menzies	Picrite	No (MBBP07 was point counted)
LAWBP28C	Little Akaloa	Picrite	No
LAWBP15A	Little Akaloa	Picrite	Yes
LAWBP2	Little Akaloa	Picrite	No
BRS2	Ducksfoot	Picrite	Yes
LLB21	Lebons	Picrite	Yes
Lav-C	Lavericks	Picrite	Yes
Lav-10EA	Lavericks	Hawaiite	Yes
Lav-J	Lavericks	Mugearite	Yes
SB-34	Stony	Benmoreite	Yes

Table 1A: List of the polished thin sections, noting the nine samples used for modal analysis.

Stony Bay Transect

Flow	Batch	Rock type	Phenocryst %	Mineral Texture
SB-35	7	Picrite	10-15%	Patchy and resorbed core
SB-34	6	Benmorite	6%	Sieved core, resorbed rim and melt inclusions
SB-32	6	Mugearite	10%	Resorbed, patchy, sieved core
SB-31	5	Mugearite	0%	
SB-22	5	Mugearite	No thin section	
SB-21	5	Hawaiite	2%	Patchy and some resorbed core
SB-20	4	Mugearite	<1%	
SB-18	4	Picrite	15-20%	Resorbed and patchy core
SB-17	3	Hawaiite	1%	Some sieved core
SB-16	3	Hawaiite	2%	
SB-15	2	Benmorite	2%	Patchy core, resorbtion
SB-30	2	Hawaiite	<1%	Swallow tail
SB-26	2	Picrite	<1%	(one phenocryst) resorbed rim and melt inclusions
SB-25	2	Picrite	10-15%	Zoned, swallow tail, resorbed rim
SB-28	1	Hawaiite	1%	Melt inclusions, sieved core with some resorbtion

Table 2A: Stratigraphically organized petrographic and bulk rock geochemistry data for the Stony Bay transect. Geochemical data is explored further in Chapter 5.

Menzies Bay Transect

Flow	Batch	Rock type	Phenocryst %	Mineral Texture
MBBP15	11	Picrite	8%	Resorbed rim and core, patchy core, some zoning
ELT14	10	Picrite	12%	Zoned, resorbed and sieved core
MBBP13	10	Picrite	7%	Resorbed rim and cores, melt inclusions
ELT12	9	Picrite	8%	Zoning, swallow tail, resorbed core
MBBP11	8	Mugearite	<1%	Inclusion trains
MBBP10	8	Picrite	2%	Some sieved (not much)
ELT9	7	Picrite	2%	Inclusion trains
MBBP08	6	Hawaiite	1%	Resorbed rims and cores
MBBP07	5	Picrite	15%	Zoned, patchy, sieved, swallow tail
ELT6	4	Picrite	10%	Zoned, sieved and resorbed core, inclusion trains
MBBP05	4	Picrite	7%	Zoned, swallow tail, melt inclusions, resorbtion
ELT4	3	Hawaiite	<1%	
MBBP03	2	Mugearite	<1%	(one phenocryst) swallow tail
MBBP02	2	Picrite	10%	Zoned, sieved core, swallow tail, some melt inclusions
ELT1	1	Mugearite	1%	Rim resorbtion, melt inclusions

Table 3A: Stratigraphically organized petrographic and bulk rock geochemistry data for the Menzies Bay transect. Geochemical data is explored further in Chapter 5.

Little Akaloa Transect

Flow	Batch	Rock type	Phenocryst %	Mineral Texture
LAWBP29B	12	Hawaiite	4%	Sieved core
LAWBP29A	12	Picrite	No thin section	
LAWBP28D	12	Picrite	2%	Swallow tail, melt inclusions
LAWBP28C	11	Picrite	12%	Zoned, sieved core, swallow tail
LAWBP27	10	Picrite	5%	Zoned, sieved core, some resorbtion, melt inclusions
LAWBP26	9	Hawaiite	<1%	(1 plag)
LAWBP25	9	Picrite	8%	Swallow tail, zoned
LAWBP22	8	Picrite	1%	Resorbed rim, inclusion trains
LAWBP21	7	Hawaiite	1%	Some zoning
LAWBP20	6	Hawaiite	<1%	(1 plag) Zoned, resorbed rim
LAWBP19	5	Hawaiite	<1%	
LAWBP18	4	Hawaiite	<1%	(1 plag) Patchy/resorbed core
LAWBP17	4	Picrite	4%	Zoning, swallow tail, some sieved, resorbtion
LAWBP16A	4	Picrite	2%	Sieved core
LAWBP15A	3	Picrite	10%	Sieved core (lots!), zoning (lots), swallow tail
LAWBP5A	2	Hawaiite	20%	Resorbed core (lots!), sieved
LAWBP4A	1	Mugearite	2%	Resorbed rim, swallow tail
LAWBP2	1	Picrite	10%	Zoned, swallow tail

Table 4A: Stratigraphically organized petrographic and bulk rock geochemistry data for the Little Akaloa transect. Geochemical data is explored further in Chapter 5.

Ducksfoot Bay Transect

Flow	Batch	Rock type	Phenocryst %	Mineral Texture
BRS1	5	Mugearite	0%	
PAB32	5	Hawaiite	7%	Rim resorbtion, sieved core, melt inclusions, inclusion trains
BRS2	4	Picrite	1-2%	Swallow tail, some resorbed core, melt inclusions
BRS3	3	Hawaiite	0%	
PAB33	2	Mugearite	<1%	
BRS4	2	Picrite	3%	Sieved core with melt inclusions, resorbed rim
BRS5	1	Hawaiite	<1%	
PAB35	1	Hawaiite	2-3%	Some resorbed and skeletal

Table 5A: Stratigraphically organized petrographic and bulk rock geochemistry data for the Ducksfoot Bay transect. Geochemical data is explored further in Chapter 5.

Lebons Bay Transect

Flow	Batch	Rock type	Phenocryst %	Mineral Texture
LLB20	3	No geochem	<1%	
LLB21	3	Picrite	20%	Sieved, zoned, some resorbtion
LLB22	2	Hawaiite	No thin section	
LLB23, 24	1	Mugearite	0%	
LLB25	1	Mugearite	0%	
LLB26	1	Hawaiite	No thin section	
Placeholder flow	1	No geochem	No thin section	
LLB27, 28	1	Picrite	12%	Inclusion trains, zoned, swallow tail

Table 6A: Stratigraphically organized petrographic and bulk rock geochemistry data for the Lebons Bay transect. Geochemical data is explored further in Chapter 5.

Lavericks Bay Transect

Flow	Batch	Rock type	Phenocryst %	Mineral Texture
Lav-O	5	Mugearite	1%	
Lav-J	4	Mugearite	12%	Sieved and patchy cores, inclusion trains, resorbed rim
Lav-H	3	Picrite	8%	Swallow tail, sieved core with inclusions
Placeholder flow	2	No geochem	No thin section	
Lav-G (Lav-C)	2	Picrite	7%	Zoned, sieved cores, resorbtion and melt inclusions
Placeholder flow	1	No geochem	No thin section	
Lav-F	1	Hawaiite	<1%	(1 plag) swallow tail
Lav-10Ea	1	Hawaiite	25%	Sieved and patchy cores, zoning, melt inclusion, resorbtion

Table 7A: Stratigraphically organized petrographic and bulk rock geochemistry data for

the Lebons Bay transect. Geochemical data is explored further in Chapter 5.

Flow	Bay	Rock type	Phenocryst %	Mineral Texture
SB-35	Stony	Picrite	10-15%	Patchy and resorbed core
SB-18	Stony	Picrite	15-20%	Resorbed and patchy core
SB-26	Stony	Picrite	<1%	(one phenocryst) resorbed rim and melt inclusions
SB-25	Stony	Picrite	10-15%	Zoned, swallow tail, resorbed rim
MBBP15	Menzies	Picrite	8%	Resorbed rim and core, patchy core, some zoning
ELT14	Menzies	Picrite	12%	Zoned, resorbed and sieved core
MBBP13	Menzies	Picrite	7%	Resorbed rim and cores, melt inclusions
ELT12	Menzies	Picrite	8%	Zoning, swallow tail, resorbed core
MBBP10	Menzies	Picrite	2%	Some sieved (not much)
ELT9	Menzies	Picrite	2%	Inclusion trains
MBBP07	Menzies	Picrite	15%	Zoned, patchy, sieved, swallow tail
ELT6	Menzies	Picrite	10%	Zoned, sieved and resorbed core, inclusion trains
MBBP05	Menzies	Picrite	7%	Zoned, swallow tail, melt inclusions, resorbtion
MBBP02	Menzies	Picrite	10%	Zoned, sieved core, swallow tail, some melt inclusions
LAWBP29A	Little Akaloa	Picrite	No thin section	
LAWBP28D	Little Akaloa	Picrite	2%	Swallow tail, melt inclusions
LAWBP28C	Little Akaloa	Picrite	12%	Zoned, sieved core, swallow tail
LAWBP27	Little Akaloa	Picrite	5%	Zoned, sieved core, some resorbtion, melt inclusions
LAWBP25	Little Akaloa	Picrite	8%	Swallow tail, zoned
LAWBP22	Little Akaloa	Picrite	1%	Resorbed rim, inclusion trains
LAWBP17	Little Akaloa	Picrite	4%	Zoning, swallow tail, some sieved, resorbtion
LAWBP16A	Little Akaloa	Picrite	2%	Sieved core
LAWBP15A	Little Akaloa	Picrite	10%	Sieved core (lots!), zoning (lots), swallow tail
LAWBP2	Little Akaloa	Picrite	10%	Zoned, swallow tail
BRS2	Ducksfoot	Picrite	1-2%	Swallow tail, some resorbed core, melt inclusions
BRS4	Ducksfoot	Picrite	3%	Sieved core with melt inclusions, resorbed rim
LLB21	Lebons	Picrite	20%	Sieved, zoned, some resorbtion
LLB27, 28	Lebons	Picrite	12%	Inclusion trains, zoned, swallow tail
Lav-H	Lavericks	Picrite	8%	Swallow tail, sieved core with inclusions
Lav-G (Lav-C)	Lavericks	Picrite	7%	Zoned, sieved, resorbtion, melt inclusions

Table 8A: List of all of the picrite samples observed. Highlighted samples were chosen for polished thin sections.

Flow	Batch	Rock type	Phenocryst %	Mineral Texture
SB-21	Stony	Hawaiite	2%	Patchy and some resorbed core
SB-17	Stony	Hawaiite	1%	Some sieved core
SB-16	Stony	Hawaiite	2%	
SB-30	Stony	Hawaiite	<1%	Swallow tail
SB-28	Stony	Hawaiite	1%	Melt inclusions, sieved core with some resorbtion
MBBP08	Menzies	Hawaiite	1%	Resorbed rims and cores
ELT4	Menzies	Hawaiite	<1%	
LAWBP29B	Little Akaloa	Hawaiite	4%	Sieved core
LAWBP26	Little Akaloa	Hawaiite	<1%	(1 plag)
LAWBP21	Little Akaloa	Hawaiite	1%	Some zoning
LAWBP20	Little Akaloa	Hawaiite	<1%	(1 plag) Zoned, resorbed rim
LAWBP19	Little Akaloa	Hawaiite	<1%	
LAWBP18	Little Akaloa	Hawaiite	<1%	(1 plag) Patchy/resorbed core
LAWBP5A	Little Akaloa	Hawaiite	20%	Resorbed core (lots!), sieved
PAB32	Ducksfoot	Hawaiite	7%	Rim resorbtion, sieved core, melt inclusions, inclusion trains
BRS3	Ducksfoot	Hawaiite	0%	
BRS5	Ducksfoot	Hawaiite	<1%	
PAB35	Ducksfoot	Hawaiite	2-3%	Some resorbed and skeletal
LLB22	Lebons	Hawaiite	No thin section	
LLB26	Lebons	Hawaiite	No thin section	
Lav-F	Lavericks	Hawaiite	<1%	(1 plag) swallow tail
Lav-10Ea	Lavericks	Hawaiite	25%	Sieved and patchy cores, zoning, melt inclusion, resorbtion

Table 9A: List of all of the hawaiite samples observed. Highlighted samples were chosen for polished thin sections.

Flow	Bay	Rock type	Phenocryst %	Mineral Texture
SB-32	Stony	Mugearite	10%	Resorbed, patchy, sieved core
SB-31	Stony	Mugearite	0%	
SB-22	Stony	Mugearite	No thin section	
SB-20	Stony	Mugearite	<1%	
MBBP11	Menzies	Mugearite	<1%	Inclusion trains
MBBP03	Menzies	Mugearite	<1%	(one phenocryst) swallow tail
ELT1	Menzies	Mugearite	1%	Rim resorbtion, melt inclusions
LAWBP4A	Little Akaloa	Mugearite	2%	Resorbed rim, swallow tail
BRS1	Ducksfoot	Mugearite	0%	
PAB33	Ducksfoot	Mugearite	<1%	
LLB23, 24	Lebons	Mugearite	0%	
LLB25	Lebons	Mugearite	0%	
Lav-O	Lavericks	Mugearite	1%	
Lav-J	Lavericks	Mugearite	12%	Sieved and patchy cores, inclusion trains, resorbed rim

Table 10A: List of all of the mugearite samples observed. Highlighted samples were chosen for polished thin sections.

Flow	Bay	Rock type	Phenocryst %	Mineral Texture
SB-34	Stony	Benmorite	6%	Sieved core, resorbed rim and melt inclusions
SB-15	Stony	Benmorite	2%	Patchy core, resorbtion

Table 11A: List of all of the benmoreite samples observed. Highlighted samples were chosen for polished thin sections.

Appendix II: Geochemistry

Standards for Rock Trace	
Standard name	**Standard description**
(full calibration)	
AC-E	Microgranite (GIT-IWG)
AGV-1	Andesite (USGS)
AL-1	Albite (GIT-IWG)
AN-G	Anorthosite (GIT-IWG)
BE-N	Basalt (GIT-IWG)
BIR-1	Basalt (USGS)
DNC-1	Diabase (USGS)
DR-N	Diorite (ANRT(GIT-IWG))
DT-N	Kyanite (ANRT(GIT-IWG))
DTS-1	Dunite (USGS)
FK-N	Feldspar (ANRT(GIT-IWG))
G-2	Granite (USGS)
GS-N	Granite (ANRT(GIT-IWG))
GSP-1	Granodiorite (USGS)
IF-G	Iron Formation (GIT-IWG)
JA-2	Andesite (GSJ)
JB-3	High Alumina Basalt (GSJ)
JF-1	Feldspar (GSJ)
JF-2	Feldspar (GSJ)
JG-1a	Granodiorite (GSJ)
JG-2	Granite (GSJ)
JLk-1	Lake Sediment (GSJ)
JLs-1	Limestone (GSJ)
JR-2	Rhyolite (GSJ)
JSd-1	Stream Sediment (GSJ)
JSl-1	Slate (GSJ)
JSl-2	Slate (GSJ)
MA-N	Granite (GIT-IWG)
MAG-1	Marine Mud (USGS)
MRG-1	Gabbro (CCRMP)
NIM-D	Dunite (SABS)
NIM-G	Granite (SABS)
NIM-L	Lujavrite (SABS)
NIM-N	Norite (SABS)
NIM-P	Pyroxenite (SABS)
NIM-S	Syenite (SABS)
PCC-1	Peridotite (USGS)
QLO-1	Quartz Latite (USGS)
RGM-1	Rhyolite (USGS)
SARM39	Kimberlite (SACCRM)
SARM41	Carbonaceous Shale (SACCRM)
SARM44	Sillimanite Schist (SACCRM)
SARM45	Kinzingite (SACCRM)
SARM47	Serpentinite (SACCRM)
SARM48	Fluorspar Granite (SACCRM)
SARM50	Dolerite (SACCRM)
SCo-1	Cody Shale (USGS)
SDC-1	Mica Schist (USGS)
SDO-1	Devonian Ohio Shale (USGS)

Table 1B: List of the standards used on the University of Canterbury XRF.

Colorado College XRF Standards
G-2
PCC-1
DTS-1
SY-4
AGB-1
JSD-2
JSD-3
JLK-1
JH-1
BHVO2
W2
STM1
QLO1
JSP2
BIR1
DTS2
AGB2
BCR2

Table 2B: List of the standards used on the Colorado College XRF.

Standards for Microprobe analysis	
Element	Standard Description
Na, Al	Monash An49
Ca	Diopside, NY NMNH 11733
Si, Fe	Fayalite syn - CalTech - Rossman
Cr	Cr2O3 synthetic
Mg	Kilbourne Olivine
Ti	TiO2 synthetic
Mn	Rhodonite-Evans - LGM P
Ni	NiO synthetic

Table 3B: List of the standards used on the University of Wisconsin-Madison Microprobe.

Feldspar Error	
Element	**Error**
Na, Ca, Al, Si	<1.5% (An error +/- 0.09)
K, Fe	<15%

Table 4B: Microprobe error for each element analyzed in plagioclase samples.

Pyroxene Error	
Element	**Error**
Ti, Mg, Si, Al, Ca	<3.0%
Mn, Na	<20%
Cr, Ni	>100%

Table 5B: Microprobe error for each element analyzed in pyroxene samples.

Olivine Error	
Element	**Error**
Si, Fe, Mg	<1.5%
Al, Ti, Mn, Ni, Cr	<50%
Na	~100%

Table 6B: Microprobe error for each element analyzed in olivine samples.

Table 7B (below): Microprobe analyses for all plagioclase samples. Spot analyses are labeled as "Un *# Sample ID-phenocryst number*". Each phenocrysts (denoted by the number after the dash) contains several spot analyses, which are shown and numbered under each Sample ID-Probe Spot heading. Analyses that fell outside the acceptable error range are in red, and were not used in the data analysis.

Sample ID-Probe Spot	Na2O	K2O	CaO	Al2O3	SiO2	FeO	Oxide Totals
Un 3 LAW15A-5-rr							
26	3.98	0.26	13.43	31.26	51.21	0.37	100.51
27	4.07	0.31	13.22	30.53	51.58	0.33	100.03
28	3.94	0.27	13.36	30.85	51.29	0.45	100.15
29	3.54	0.18	14.09	31.75	50.11	0.37	100.05
30	3.89	0.15	13.80	31.55	50.56	0.41	100.37
31	3.57	0.17	14.32	31.56	49.66	0.41	99.68
32	4.25	0.21	12.93	30.81	51.90	0.39	100.49
Un 4 LAW15A-7							
33	4.06	0.26	13.04	31.25	51.69	0.41	100.71
34	4.16	0.20	12.87	30.97	52.22	0.45	100.86
35	3.06	0.18	15.38	32.68	49.79	0.44	101.52
36	3.55	0.15	13.95	31.19	50.38	0.51	99.74
Un 5 LAW15A-8							
37	3.98	0.21	13.04	31.22	51.17	0.40	100.03
38	0.74	0.01	20.30	7.20	45.33	8.73	82.32
39	4.10	0.19	13.54	31.63	51.90	0.35	101.71
Un 6 LAW15A-9							
40	3.62	0.18	13.87	31.50	50.44	0.36	99.97
41	3.22	0.19	14.50	32.56	50.23	0.41	101.11
42	3.63	0.17	14.03	32.07	51.09	0.42	101.41
43	3.82	0.20	13.69	31.66	51.20	0.38	100.95
Un 7 LAW15A-10							
44	4.38	0.24	12.71	30.39	53.00	0.43	101.14
45	4.54	0.25	12.49	30.11	52.71	0.37	100.47
46	3.02	0.14	15.28	32.56	49.13	0.40	100.53
47	2.55	0.11	15.85	33.23	48.63	0.46	100.83
Un 8 LAW15A-11							
48	3.91	0.19	13.55	31.50	50.86	0.30	100.30
49	4.20	0.28	13.08	31.01	52.18	0.44	101.18
50	4.15	0.27	12.86	31.13	51.14	0.41	99.96
Un 9 LAW15A-12							
51	4.12	0.28	13.10	31.20	51.53	0.51	100.74

52	3.28	0.29	14.28	32.34	48.47	1.22	99.87
53	4.60	0.27	12.32	29.93	52.40	0.45	99.98
Un 10 LAW15A-13							
54	3.36	0.20	14.46	31.96	49.44	0.43	99.84
55	3.52	0.15	14.70	32.14	49.88	0.38	100.78
56	3.31	0.19	14.23	32.05	49.18	0.42	99.38
57	4.25	0.24	12.72	30.42	51.52	0.40	99.56
Un 11 LAW15A-14							
58	2.67	0.13	15.44	32.76	47.34	0.36	98.70
59	3.18	0.16	14.65	32.32	48.90	0.36	99.57
Un 12 LAW15A-15							
60	3.68	0.17	13.92	31.83	50.50	0.39	100.49
61	3.49	0.22	14.27	31.89	49.15	0.43	99.45
62	3.50	0.18	14.27	31.45	49.17	0.48	99.05
63	4.23	0.22	13.13	30.43	51.36	0.46	99.83
Un 13 LAW15A-16							
64	2.65	0.11	15.65	33.07	48.17	0.36	100.00
65	3.09	0.13	15.12	32.33	48.89	0.36	99.91
66	4.44	0.27	12.45	29.73	52.01	0.61	99.51
Un 14 LAW15A-17							
67	4.26	0.25	12.74	30.55	50.62	0.46	98.88
68	4.06	0.18	13.01	30.91	50.65	0.41	99.22
69	4.36	0.29	12.56	30.14	51.15	0.54	99.02
Un 15 LAW15A-18							
70	3.77	0.23	13.47	31.34	50.14	0.51	99.47
71	2.66	0.08	15.57	32.94	47.59	0.44	99.28
72	4.05	0.22	13.02	30.54	50.81	0.40	99.04
Un 16 LAW15A-20							
73	2.68	0.11	15.65	33.02	48.45	0.39	100.31
74	4.40	0.25	12.64	30.21	52.64	0.42	100.56
75	4.46	0.29	12.40	29.94	52.87	0.42	100.39
Un 17 LAW15A-22							
76	4.58	0.27	12.12	29.55	51.71	0.48	98.72
77	3.78	0.20	13.67	31.32	49.63	0.39	98.99
78	3.53	0.16	14.19	31.21	49.46	0.35	98.90
Un 18 LAW15A-25							
79	4.40	0.28	12.51	29.82	50.43	0.56	97.99
80	4.24	0.18	12.26	29.49	50.40	0.42	96.99
81	3.40	0.20	14.23	31.36	49.17	0.36	98.71
Un 19 BRS2-1							
82	4.40	0.28	12.63	30.26	50.47	0.45	98.49
83	4.25	0.23	13.08	30.38	50.49	0.49	98.92
84	4.66	0.30	11.94	29.66	50.84	0.56	97.96
Un 20 BRS2-4							

85	4.32	0.23	12.50	30.46	51.21	0.40	99.12
86	4.49	0.25	12.49	30.50	50.64	0.34	98.72
87	4.28	0.25	12.42	30.35	50.34	0.38	98.01
Un 21 BRS2-5							
88	4.13	0.25	12.49	30.16	48.93	0.37	96.32
89	4.91	0.28	11.38	28.52	49.64	0.42	95.16
Un 22 BRS2-6microlite							
90	6.16	0.44	9.24	27.52	54.24	0.61	98.21
91	6.20	0.46	9.16	27.05	54.58	0.78	98.23
Un 23 BRS2-7							
92	4.47	0.25	12.35	29.59	50.46	0.43	97.56
93	4.58	0.22	12.03	29.71	50.62	0.39	97.55
Un 24 BRS2-8micro							
94	6.13	0.66	8.92	26.33	54.08	1.02	97.14
95	5.41	0.35	10.22	28.00	52.25	0.90	97.13
Un 25 BRS2-9							
96	5.48	0.38	10.49	27.97	52.34	0.62	97.28
97	4.59	0.24	11.97	29.82	51.01	0.36	98.00
98	4.46	0.22	12.31	29.26	50.34	0.45	97.04
99	4.54	0.20	12.21	30.12	50.16	0.43	97.66
Un 26 BRS2-10							
100	4.17	0.17	12.51	30.09	50.39	0.37	97.69
101	4.45	0.24	12.48	29.97	49.93	0.37	97.44
Un 27 BRS2-11							
102	4.46	0.25	12.07	29.06	48.57	0.43	94.83
103	4.36	0.25	12.33	29.29	48.95	0.37	95.55
104	4.60	0.30	11.90	28.76	50.35	0.58	96.49
105	4.56	0.26	12.13	29.16	50.08	0.40	96.60
Un 28 BRS2-12							
106	6.35	0.58	8.86	25.93	53.30	0.59	95.60
Un 29 BRS2-14							
107	4.94	0.22	11.29	29.10	50.96	0.38	96.89
108	4.30	0.15	12.14	29.52	49.04	0.40	95.55
Un 30 SB18-1							
109	4.28	0.19	12.43	29.62	49.57	0.60	96.69
110	4.27	0.22	12.51	28.95	48.42	0.43	94.80
111	3.83	0.22	13.17	30.68	49.53	0.46	97.88
112	4.20	0.22	12.61	29.88	48.85	0.49	96.24
113	4.14	0.18	13.10	29.85	48.09	0.50	95.86
Un 31 SB18-3							
114	4.84	0.28	11.59	28.99	50.31	0.58	96.59
115	4.25	0.24	12.46	30.23	49.51	0.42	97.11
Un 32 SB18-5							
116	6.43	0.50	8.18	27.23	54.76	0.27	97.37

117	6.55	0.44	8.71	26.91	54.33	0.28	97.23
Un 33 SB18-6							
118	3.43	0.15	13.74	31.44	47.79	0.43	96.98
119	4.13	0.24	12.65	29.93	49.42	0.42	96.79
120	4.11	0.24	12.82	29.84	49.40	0.50	96.90
121	3.85	0.24	12.98	30.50	49.04	0.39	97.00
Un 34 SB18-7							
122	4.14	0.21	13.21	30.28	49.53	0.35	97.72
123	4.22	0.27	12.28	30.06	50.85	0.61	98.29
Un 35 SB18-8							
124	3.42	0.12	14.19	31.56	48.41	0.50	98.21
125	4.04	0.21	11.86	28.20	47.75	0.50	92.56
Un 36 SB18-9							
126	4.20	0.21	12.45	29.51	49.36	0.54	96.26
127	4.59	0.22	11.84	29.23	49.49	0.45	95.82
128	3.82	0.14	13.18	30.41	48.00	0.51	96.06
Un 37 SB18-10							
129	4.19	0.27	12.87	30.29	49.81	0.48	97.90
130	5.08	0.31	11.04	28.40	52.48	0.56	97.87
Un 38 SB18-11							
131	4.52	0.22	11.97	29.39	50.35	0.47	96.92
132	4.31	0.25	12.46	30.03	50.10	0.45	97.59
133	5.13	0.33	11.30	29.32	52.84	0.54	99.47
Un 39 SB18-15							
134	3.98	0.16	12.98	30.41	49.56	0.45	97.54
135	4.02	0.20	13.18	30.22	49.14	0.52	97.29
136	3.21	0.12	14.25	32.16	48.71	0.47	98.92
137	3.27	0.14	14.42	31.96	47.63	0.42	97.85
138	3.84	0.15	13.23	31.07	49.66	0.51	98.48
Un 40 SB18-29							
139	4.25	0.11	12.62	30.32	50.06	0.51	97.87
140	4.21	0.23	12.44	30.33	50.28	0.42	97.92
141	4.33	0.21	12.94	31.21	51.66	0.63	100.99
142	4.78	0.29	11.35	29.60	52.17	0.44	98.63
Un 47 LAW10EA-3							
243	4.67	0.26	11.94	30.19	53.50	0.40	100.95
244	4.70	0.30	11.89	30.36	53.50	0.43	101.17
Un 50 LAW10EA-3							
245	4.68	0.27	12.04	29.38	52.94	0.41	99.71
246	4.76	0.29	12.13	30.77	52.93	0.31	101.19
Un 51 LAW10EA-4							
247	4.69	0.28	12.22	29.67	53.06	0.39	100.31
248	4.53	0.28	12.48	30.60	53.09	0.35	101.32
249	5.37	0.37	10.74	29.08	54.56	0.40	100.52

250	5.41	0.34	9.91	28.38	53.87	0.44	98.34
Un 52 LAW10EA-5							
251	4.41	0.21	12.81	30.52	52.45	0.37	100.78
252	4.43	0.28	12.68	30.30	52.58	0.36	100.64
Un 53 LAW10EA-6							
253	5.57	0.31	10.85	28.73	55.48	0.34	101.29
254	5.47	0.36	10.66	28.82	53.79	0.39	99.49
Un 54 LAW10EA-7							
255	4.62	0.25	12.45	30.37	52.65	0.45	100.80
Un 56 LAW10EA-7							
256	4.75	0.24	12.34	30.46	53.35	0.40	101.54
257	4.81	0.29	12.27	30.22	54.24	0.36	102.19
Un 57 LAW10EA-9							
258	5.02	0.33	11.93	29.92	54.06	0.33	101.60
259	4.34	0.24	12.94	31.22	52.44	0.32	101.49
Un 58 LAW10EA-10							
260	5.74	0.34	10.58	28.93	56.01	0.33	101.94
261	5.72	0.38	10.35	28.70	56.27	0.32	101.75
Un 59 LAW10EA-11							
262	4.47	0.23	12.84	30.69	52.67	0.35	101.25
263	4.57	0.31	12.23	30.01	53.02	0.35	100.49
Un 60 LAW10EA-12							
264	5.51	0.33	10.89	28.94	54.65	0.33	100.64
265	5.80	0.35	10.22	28.19	56.12	0.33	101.01
Un 61 LAW10EA-13							
266	4.61	0.25	12.69	30.43	53.08	0.50	101.57
267	4.94	0.24	11.69	29.91	53.29	0.36	100.44
Un 62 LAW10EA-14							
268	5.26	0.29	11.05	29.86	54.85	0.29	101.59
269	5.47	0.29	10.97	28.67	55.72	0.37	101.49
Un 64 LAW10EA-15							
270	5.67	0.32	10.40	28.60	56.48	0.34	101.81
271	5.65	0.35	10.36	28.94	55.14	0.40	100.85
272	5.86	0.41	9.69	27.86	56.56	0.32	100.70
273	5.93	0.35	10.13	28.58	55.70	0.38	101.06
Un 65 LAW10EA-16							
274	4.63	0.30	12.17	30.43	52.76	0.36	100.66
275	4.56	0.22	12.89	30.51	52.62	0.39	101.18
Un 66 LAW10EA-18							
276	5.85	0.36	9.78	28.09	55.38	0.34	99.80
277	6.07	0.41	9.92	28.45	56.33	0.32	101.50
Un 67 LAVJ-2							
278	7.26	0.84	7.29	26.07	59.55	0.34	101.36
279	7.30	0.70	7.39	26.37	59.00	0.23	100.98

280	7.87	1.06	5.91	24.68	60.34	0.24	100.10
281	7.79	1.01	5.54	24.84	61.49	0.22	100.88
Un 68 LAVJ-3							
282	5.55	0.37	10.60	28.59	55.48	0.33	100.92
283	5.55	0.36	11.09	29.38	54.83	0.35	101.55
Un 69 LAVJ-5							
284	5.45	0.30	10.79	29.57	55.59	0.33	102.03
285	5.62	0.33	10.71	29.19	55.11	0.39	101.34
Un 70 LAVJ-7							
286	7.70	1.13	5.56	25.29	61.83	0.25	101.76
287	8.07	1.33	5.22	24.22	62.00	0.21	101.04
Un 71 LAVJ-8							
288	8.08	1.05	5.74	24.83	61.65	0.26	101.61
289	8.15	1.43	5.00	24.15	61.49	0.25	100.45
Un 72 LAVJ-10							
290	7.62	1.27	6.14	24.77	60.58	0.16	100.54
291	7.79	1.17	5.69	24.41	60.89	0.20	100.15
Un 73 LAVJ-13							
292	7.90	1.34	5.50	24.73	61.16	0.25	100.89
293	7.95	1.13	5.42	24.48	61.41	0.18	100.58
294	7.90	1.20	5.59	24.54	61.81	0.29	101.33
295	7.97	1.54	5.19	24.00	61.46	0.26	100.42
Un 74 LAVJ-15							
296	7.91	1.22	5.66	24.62	60.56	0.22	100.19
297	6.52	0.62	8.96	27.13	56.48	0.29	99.99
298	7.45	0.90	7.00	25.67	59.19	0.28	100.50
299	7.79	1.30	5.51	24.77	61.27	0.28	100.90
Un 75 LAVJ-18							
300	8.15	1.29	5.00	23.96	61.71	0.17	100.28
301	7.99	1.28	5.60	24.33	60.84	0.20	100.24
Un 76 LAVJ-19							
302	6.73	0.57	8.24	26.40	57.76	0.36	100.05
303	6.68	0.59	8.42	27.52	58.47	0.35	102.04
Un 77 LAVJ-20							
304	8.21	1.33	5.02	24.53	62.76	0.21	102.06
305	7.90	1.32	5.84	25.07	61.28	0.24	101.65
306	7.84	1.21	5.74	24.44	61.12	0.17	100.52
Un 78 LAVJ-23							
307	8.08	1.79	4.74	23.86	62.75	0.22	101.44
308	7.00	0.84	7.83	26.85	58.56	0.18	101.26
Un 83 LAWBP2-1							
314	4.65	0.24	11.89	30.50	52.35	0.44	100.08
315	4.75	0.24	11.54	29.71	53.75	0.42	100.41
Un 84 LAWBP2-2							

316	4.60	0.23	11.82	30.54	52.52	0.47	100.17
317	4.52	0.23	12.21	30.46	52.54	0.44	100.40
Un 85 LAWBP2-3							
318	4.47	0.22	11.84	29.89	53.16	0.45	100.03
319	4.71	0.23	11.86	30.17	52.85	0.34	100.16
320	4.77	0.24	11.39	30.06	52.48	0.43	99.37
Un 86 LAWBP2-5							
321	5.62	0.30	10.09	28.79	55.05	0.38	100.22
322	5.62	0.33	10.33	29.31	55.86	0.34	101.79
Un 87 LAWBP2-6							
323	4.51	0.22	12.01	30.19	52.53	0.37	99.82
324	3.95	0.18	13.01	31.12	51.28	0.39	99.93
Un 88 LAWBP2-7							
325	4.83	0.26	11.39	29.69	53.17	0.39	99.74
326	4.96	0.31	11.06	30.12	52.70	0.34	99.49
327	4.71	0.27	12.15	30.21	52.83	0.38	100.54
Un 89 LAWBP2-8							
328	4.83	0.23	11.34	30.04	53.82	0.37	100.64
329	4.34	0.18	12.40	30.54	52.15	0.38	99.98
330	4.31	0.22	12.00	30.39	52.12	0.39	99.42
Un 90 LAWBP2-9							
331	4.65	0.28	11.36	29.98	54.34	0.41	101.02
332	4.35	0.18	12.43	30.60	52.20	0.42	100.18
Un 91 LAWBP2-10							
333	5.09	0.29	11.34	29.09	53.77	0.39	99.97
334	5.11	0.28	11.30	29.58	53.83	0.38	100.48
Un 92 LAWBP2-11							
335	4.87	0.24	11.56	29.69	53.24	0.43	100.03
336	5.04	0.30	10.87	29.22	53.70	0.42	99.54
Un 93 LAWBP2-13							
337	4.44	0.24	12.20	30.19	51.76	0.45	99.28
338	4.94	0.23	11.43	29.62	53.29	0.46	99.97
Un 94 LAWBP2-14							
339	5.01	0.22	11.01	29.10	52.79	0.41	98.54
340	4.75	0.24	11.44	29.75	53.57	0.38	100.13
341	5.02	0.28	11.08	29.32	53.59	0.41	99.71
Un 95 LAWBP2-15							
342	5.01	0.25	11.08	29.44	53.80	0.44	100.01
343	4.74	0.27	11.52	29.53	52.82	0.35	99.23
344	4.49	0.21	12.04	30.29	52.60	0.36	99.98
Un 96 LAWBP2-17							
345	4.70	0.26	11.75	29.90	52.63	0.48	99.71
346	4.65	0.22	11.66	29.87	52.42	0.43	99.25
347	4.74	0.22	11.52	29.78	52.88	0.42	99.57

Un 97 SB34-1							
348	7.72	0.77	6.43	25.98	59.90	0.27	101.07
349	7.78	0.76	6.07	25.64	60.66	0.27	101.18
350	7.70	0.78	6.04	25.42	60.70	0.22	100.87
Un 98 SB34-2							
351	8.50	2.06	3.33	22.19	63.13	0.21	99.43
352	8.45	2.40	3.08	22.48	63.23	0.27	99.91
353	7.24	0.64	7.21	25.95	59.04	0.30	100.38
Un 99 SB34-3							
354	7.30	0.57	7.22	25.92	59.21	0.30	100.52
355	7.77	0.63	6.63	25.32	59.82	0.28	100.44
356	7.86	0.75	5.97	24.98	60.81	0.22	100.58
Un 100 SB34-4							
357	8.39	1.12	4.79	24.86	62.09	0.24	101.49
358	8.41	1.26	4.39	23.74	63.19	0.19	101.18
359	8.47	1.48	3.73	23.20	63.23	0.50	100.60
Un 101 SB34-5							
360	8.67	1.60	3.91	23.29	63.54	0.28	101.29
361	8.39	1.44	4.33	23.46	63.45	0.19	101.27
362	8.38	1.71	3.99	23.29	63.40	0.19	100.96
Un 102 SB34-7							
363	7.02	0.62	7.29	26.46	58.43	0.29	100.11
364	7.41	0.70	6.82	25.96	59.39	0.25	100.52
365	7.89	0.81	5.64	25.44	61.56	0.21	101.56
366	7.88	0.83	5.85	24.86	60.78	0.23	100.43
Un 103 SB34-10							
367	7.65	0.85	6.32	25.22	59.57	0.23	99.83
368	7.76	0.87	5.85	24.87	61.01	0.24	100.60
369	7.71	0.83	5.90	24.88	60.47	0.20	100.00
Un 104 SB34-11							
370	7.76	0.81	5.82	24.79	60.19	0.29	99.65
371	8.07	0.99	5.09	24.32	61.35	0.20	100.02
372	8.05	0.98	5.05	24.06	61.72	0.18	100.04
Un 105 SB34-14							
373	7.73	0.83	6.12	25.51	59.93	0.22	100.33
374	8.10	0.85	5.80	24.28	58.90	0.20	98.14
375	8.08	0.90	5.53	24.39	60.74	0.19	99.83
Un 106 LAW28c_2							
376	4.51	0.25	12.26	30.05	51.73	0.42	99.22
377	3.12	0.12	14.79	32.49	49.40	0.52	100.44
378	3.96	0.24	12.77	31.02	51.82	0.52	100.34
Un 107 LAW28c-3							
379	3.93	0.29	12.68	30.67	50.95	0.47	98.99
380	4.51	0.26	12.24	30.90	51.90	0.36	100.18

Un 108 LAW28c-9							
381	4.31	0.23	12.52	30.71	51.65	0.48	99.90
382	3.67	0.29	14.14	30.83	47.74	1.91	98.58
383	3.45	0.12	13.74	31.99	49.52	0.55	99.37
384	3.95	0.25	12.86	30.82	51.23	0.52	99.62
385	3.73	0.18	13.30	31.21	50.45	0.50	99.38
386	3.42	0.17	13.79	31.84	49.93	0.56	99.71
Un 109 LAW28c-10							
387	2.90	0.11	15.04	32.70	48.50	0.57	99.81
388	3.27	0.15	14.29	32.05	49.49	0.50	99.73
389	3.81	0.16	13.13	31.39	50.61	0.38	99.48
390	4.12	0.30	12.84	30.92	51.18	0.48	99.83
391	3.73	0.27	13.39	31.17	50.74	0.58	99.88
Un 110 LAW28c-11							
392	4.03	0.14	12.91	31.04	51.25	0.48	99.84
393	4.55	0.19	11.96	30.54	53.43	0.40	101.07
394	5.08	0.30	11.11	29.50	53.01	0.43	99.42
Un 111 LAW28c-12							
395	3.89	0.19	13.40	31.38	51.09	0.51	100.46
396	4.08	0.21	12.73	30.90	51.06	0.44	99.41
397	3.58	0.18	13.51	31.75	50.78	0.49	100.29
398	3.88	0.19	13.24	31.52	51.69	0.53	101.04
Un 112 LAW28c-13							
399	4.39	0.19	12.00	30.53	52.11	0.35	99.58
Un 113 LAW28c-14							
400	6.55	0.50	8.52	27.29	57.69	0.38	100.92
Un 114 LAW28c-15							
401	3.28	0.17	14.13	32.22	48.89	0.57	99.25
402	4.36	0.23	12.48	30.24	52.24	0.36	99.90
Un 115 LAW28c-16							
403	4.17	0.22	12.49	30.70	52.61	0.56	100.75
404	3.54	0.19	13.56	31.20	51.26	0.40	100.16
405	3.87	0.20	13.61	31.41	51.81	0.43	101.32
406	3.44	0.16	13.95	32.22	50.40	0.39	100.57
Un 116 LAW28c-18							
407	4.29	0.28	12.27	30.51	52.32	0.64	100.31
408	4.30	0.30	12.22	30.58	51.98	0.38	99.77
Un 117 LAW28c-21							
409	0.05	0.17	13.92	20.25	28.64	0.45	63.49
410	4.68	0.33	11.62	29.58	52.58	0.44	99.22
Un 118 LAW28c-22							
411	3.30	0.19	14.13	32.07	49.34	0.47	99.51
412	4.03	0.20	13.24	31.11	51.01	0.44	100.03
413	3.96	0.20	12.99	30.73	51.49	0.48	99.85

Un 119 LAW28c-23							
414	4.02	0.22	12.49	30.87	51.01	0.69	99.29
415	4.06	0.22	12.86	30.99	51.27	0.45	99.85
416	4.77	0.24	11.60	29.45	52.70	0.43	99.19
417	4.09	0.24	12.65	30.84	50.14	0.59	98.55
Un 120 LAW28c-24							
418	3.64	0.17	13.38	31.11	50.97	0.48	99.76
419	4.08	0.19	12.64	31.00	51.91	0.51	100.33
Un 121 LAVC-1							
435	3.17	0.15	14.13	31.81	50.32	0.41	99.99
436	3.25	0.11	14.64	32.04	49.53	0.44	100.01
Un 122 LAVC-4							
437	3.97	0.18	13.07	31.00	51.66	0.45	100.34
438	4.00	0.19	12.73	30.89	51.66	0.49	99.96
439	3.79	0.18	13.94	30.99	51.23	0.48	100.60
440	2.77	0.14	15.24	33.32	49.05	0.46	100.99
441	4.19	0.25	12.54	30.59	52.23	0.42	100.23
Un 123 LAVC-5							
442	4.09	0.22	13.12	31.20	51.92	0.44	101.00
443	3.92	0.20	13.12	31.02	51.49	0.43	100.18
444	3.50	0.17	14.22	31.76	50.47	0.43	100.55
445	2.75	0.12	15.70	32.57	48.96	0.42	100.51
Un 124 LAVC-7							
446	3.40	0.14	14.23	31.20	49.39	0.43	98.78
447	4.27	0.22	13.15	30.74	51.89	0.39	100.67
Un 125 LAVC-11							
448	3.12	0.11	14.92	32.61	50.11	0.46	101.34
449	3.11	0.13	14.77	32.12	49.69	0.40	100.22
450	2.96	0.12	14.88	33.22	49.06	0.44	100.68
Un 126 LAVC-12							
451	3.34	0.12	14.59	32.26	50.32	0.47	101.10
452	3.95	0.20	12.82	30.80	51.86	0.45	100.09
453	3.99	0.21	12.87	30.39	51.63	0.47	99.57
454	4.00	0.18	13.27	30.56	51.94	0.40	100.36
455	4.23	0.18	12.67	30.73	52.53	0.47	100.82
456	4.23	0.17	12.81	30.74	52.07	0.41	100.43
457	3.88	0.20	13.20	31.18	51.39	0.44	100.30
458	4.04	0.20	13.13	31.21	51.70	0.44	100.74
Un 127 LAVC-14							
459	4.03	0.20	12.77	30.39	51.13	0.52	99.03
460	4.00	0.27	13.27	30.98	51.27	0.39	100.17
Un 128 LAVC-17							
461	3.79	0.21	13.63	31.98	51.43	0.48	101.52
Un 129 LAVC-18							

	462	3.75	0.19	13.69	30.98	51.23	0.53	100.37
	463	2.94	0.13	15.06	32.61	49.47	0.38	100.59
Un 130 LAVC-19								
	464	3.80	0.18	13.64	31.22	51.32	0.56	100.70
	465	2.98	0.11	14.97	32.61	49.39	0.43	100.48
Un 131 LLB21								
	466	4.44	0.22	12.67	30.07	52.16	0.56	100.11
	467	4.29	0.20	12.28	30.02	52.43	0.51	99.73
Un 132 LLB21-3								
	468	5.17	0.27	11.36	29.03	53.31	0.44	99.58
	469	5.70	0.39	9.79	28.19	55.86	0.42	100.36
Un 133 LLB21-8								
	470	3.88	0.17	13.02	30.88	52.19	0.50	100.64
	471	3.95	0.21	13.37	30.54	51.43	0.55	100.05
	472	4.77	0.28	11.80	29.45	53.32	0.50	100.11
Un 134 LLB21-9								
	473	5.21	0.34	11.24	29.04	55.00	0.48	101.32
	474	5.37	0.32	10.72	28.50	54.13	0.44	99.48
Un 135 LLB21-15								
	475	5.18	0.34	11.08	28.84	54.79	0.46	100.68
Un 136 LLB21-16								
	476	5.08	0.26	11.26	29.65	53.76	0.36	100.37
	477	5.36	0.29	10.58	28.86	54.23	0.45	99.76
	478	5.42	0.32	10.57	28.84	54.57	0.43	100.15
Un 137 LLB21-22								
	479	5.19	0.35	11.02	29.31	54.48	0.31	100.66
	480	6.36	0.42	8.96	27.70	57.42	0.30	101.16
	481	6.49	0.44	8.73	27.43	57.32	0.30	100.71
	482	5.38	0.31	10.72	29.02	54.95	0.36	100.73
Un 138 LLB21-23								
	483	5.68	0.35	10.57	28.54	55.34	0.31	100.78
	484	6.09	0.40	9.62	28.24	56.32	0.29	100.97
	485	5.87	0.42	9.45	28.27	56.22	0.25	100.48
	486	5.98	0.37	9.44	28.22	55.91	0.23	100.16
	487	6.16	0.47	9.40	28.02	56.20	0.24	100.49
Un 139 LLB21-25								
	488	4.79	0.29	11.75	29.53	53.48	0.42	100.24
Un 140 LLB21-28								
	489	4.91	0.24	11.81	29.97	53.88	0.40	101.21
	490	2.95	0.15	15.05	33.18	48.93	0.54	100.80
Un 141 LLB21-30								
	491	3.02	0.14	14.98	32.23	49.83	0.51	100.71
	492	3.15	0.15	14.81	32.28	49.89	0.47	100.75
Un 142 LLB21-33								

493	4.67	0.24	12.36	29.71	52.48	0.46	99.92
494	4.53	0.26	12.19	30.39	52.40	0.44	100.21
Un 143 MBBP02-1							
495	3.61	0.19	13.57	30.86	51.04	0.53	99.80
496	5.39	0.30	10.59	28.98	54.37	0.48	100.10
Un 144 MBBP02-2							
497	4.35	0.25	12.37	30.21	52.22	0.39	99.79
498	4.53	0.26	11.78	30.04	52.31	0.36	99.28
Un 145 MBBP02-3							
499	4.39	0.26	12.52	30.56	52.33	0.43	100.49
500	4.51	0.23	12.09	30.35	52.84	0.41	100.42
Un 146 MBBP02-4							
501	4.74	0.23	12.07	30.28	52.72	0.40	100.43
502	4.73	0.24	11.87	29.63	52.83	0.45	99.74
Un 147 MBBP02-5							
503	5.36	0.33	10.64	29.51	54.91	0.35	101.10
504	5.41	0.34	10.80	29.01	55.51	0.34	101.42
Un 148 MBBP02-6							
505	4.91	0.26	11.88	29.50	53.96	0.40	100.91
Un 149 MBBP02-13							
506	5.30	0.41	10.85	28.90	53.80	0.37	99.62
507	5.20	0.32	11.39	29.62	53.64	0.33	100.50
508	5.92	0.39	10.02	28.21	55.06	0.39	100.00
509	4.63	0.31	12.05	30.29	52.29	0.47	100.02
Un 150 MBBP02-15							
510	3.98	0.23	13.34	31.12	51.11	0.41	100.19
511	4.25	0.26	11.86	29.94	51.99	0.84	99.15
512	3.96	0.20	13.43	31.57	50.60	0.47	100.23
513	3.47	0.15	14.05	31.58	49.93	0.41	99.59
514	3.59	0.17	14.05	32.04	50.24	0.45	100.54
Un 151 MBBP02-18							
515	5.58	0.36	10.33	28.63	55.28	0.38	100.55
516	5.96	0.38	10.19	28.21	55.58	0.39	100.70
Un 152 MBBP02-20							
517	4.86	0.30	11.56	29.89	52.58	0.29	99.49
518	4.49	0.21	12.34	30.68	51.91	0.29	99.92
519	4.43	0.19	12.59	31.01	52.22	0.31	100.75
Un 153 MBBP02-22							
520	3.65	0.19	13.70	31.93	50.24	0.60	100.31
521	3.31	0.13	14.27	32.72	49.63	0.48	100.53
Un 154 MBBP02-23							
522	3.73	0.21	13.97	31.29	50.56	0.56	100.32
523	5.90	0.41	9.60	28.06	55.23	0.37	99.57
524	3.63	0.16	13.99	31.94	50.50	0.34	100.55

Un 155 MBBP02-24							
525	4.20	0.25	13.00	30.78	50.83	0.57	99.63
526	5.85	0.40	10.11	28.63	55.05	0.34	100.38
Un 156 MBBP02-25							
527	4.70	0.24	11.62	30.26	53.16	0.43	100.41
528	4.82	0.30	11.49	29.49	52.95	0.51	99.57
Un 157 MBBP02-26							
529	3.06	0.14	14.40	32.58	49.05	0.41	99.65
Un 158 MBBP02-27							
530	3.63	0.22	13.48	31.35	50.56	0.51	99.75
531	3.46	0.17	14.12	32.37	49.78	0.40	100.31